Synthetic Studies of Labelled Antimicrobial and Metal Peptides

Written by Michael Dewar-Oldis

A thesis submitted in total fulfilment of the requirement for the degree of Master of Science by Research

November 2020

Collage of Science, Health and Engineering
Department of Chemistry and Physics
La Trobe Institute for Molecular Science
La Trobe University
Victoria, Australia

Table of Contents

Statements of Authorship and Ethics

Statement of Authorship

Except where reference is made in the text of the thesis, this thesis contains no material published elsewhere or extracted in whole or in part from a thesis accepted for the award of any other degree or diploma. No other person's work has been used without due acknowledgment in the main text of the thesis. This thesis has not been submitted for the award of any degree or diploma in any other tertiary institution.

Ethics

None of the research undertaken in connection with this thesis required approval by a University Ethics Committee Safety Committee or authorised officer.

Michael Dewar-Oldis **12th November 2020**

Name of Author (s): Michael Dewar-Oldis

Designation: Master of Science by Research Candidate

Affiliated Institution: La Trobe University

Title of the paper: Synthetic Studies of Labelled Antimicrobial and Metal Chelating Peptides

Acknowledgements

I would like to thank my supervisors' Dr Peter Barnard and Professor Adam Mechler who provided me with mentorship, guidance and support throughout my studies. They have been excellent mentors and I have the highest respect and appreciation for their contributions.

I would like to thank La Trobe University and La Trobe Institute for Molecular Science for giving me the opportunity to undertake my research project with the use of their facilities.

I would like to thank Pria Ramkissoon for synthesising the series of iridium complexes that were used extensively for this project and for conducting the fluorescent spectroscopic measurements of the iridium complexes and the labelled antimicrobial peptides.

I would like to thank Ahmed Houri for preparing the labelled liposomes that were used in the microscopy studies.

I would like to thank all the members within my research groups for their support (Dr. Barnard & A. Prof. Mechler Laboratories) and specifically thank several individuals personally for their additional support throughout the year.

I would like to thank the following people for their scientific contributions to my research project:

Ahmed Houri

Alessandria Ottonello

Claire Buchanan

Joel Mather

Nuchareenat Wiratpruk

Pria Ramkissoon

Tahmineh Hashemzadeh

I would like to thank my fiancée Sharon Snow, my two daughters Charlotte and Lily and other family members for their support throughout my studies.

I would like to thank the Australian Government, as this work was supported by an Australian Government Research Training Program Scholarship.

Abbreviations

Chemicals

4MP – 4-Methylpiperidine

AA – Amino acid

AMP – Antimicrobial peptide

Boc_2O – Di-*tert*-butyl decarbonate

BOP – Benzotriazol-1-yloxytris(dimethylamino)phosphonium

CD_3OD – Deuterated methanol

DCM – Dichloromethane

Diox – 1,4-Dioxane

DIPEA – *N,N*-Diisopropylethylamine

DMAP – 4-Dimethylaminopyridine

DMF – *N,N*-Dimethylformamide

DMPC – 1,2-Dimyristoyl-sn-glycero-3-phosphocholine

DMPE – 1,2-Dimyristoyl-sn-glycero-3-phosphoethanolamine

DMSO – Dimethylsulfoxide

DOTA – Tetraxetan, 1,4,7,10-Tetraazacyclododecane-1,4,7,10-tetraacetic acid

EtOAc – Ethyl acetate

EtOH – Ethanol

Fmoc-Cl – 9-Fluorenylmethyl chloroformate

HATU – Hexafluorophosphate azabenzotriazole tetramethyl uronium

HBTU – Hexafluorophosphate benzotriazole tetramethyl uronium

HCTU – 1-[Bis(dimethylamino)methylene]-5-chloro-1H-benzotriazolium 3-oxide hexafluorophosphate

HOBt – 1-Hydroxybenzotrizole

IF – Immunofluorescence

IPA, iPrOH – Isopropyl alcohol

MeOH – Methanol

NMP – 1-Methyl-2-pyrrolidinone

PPR – Piperidine

PyBOP – Benzotriazol-1-yloxytripyrrolidinophosphonium hexafluorophosphate

PZ - Piperazine

t-BuOK – Potassium tertbutoxide

TBTU – 1-[Bis(dimethylamino)methylene]-1H-benzotriazolium 3-oxide tetrafluoroborate

TEA – Triethylamine

TFA – Trifluoroacetic acid

TIPS – Triisopropylsilane

TMP – 2,2,6,6-Tetramethylpiperidine

Amino Acids

Alanine – Ala, A

Arginine – Arg, R

Asparagine – Asn, N

Aspartic Acid – Asp, D

Cysteine – Cys, C

Glutamic Acid – Glu, E

Glutamine – Gln, Q

Glycine – Gly, G

Histidine – His, H

Isoleucine – Ile, I

Leucine – Leu, L

Lysine – Lys, K

Methionine – Met, M

Phenylalanine – Phe, F

Proline – Pro, P

Serine – Ser, S

Threonine – Thr, T

Tryptophan – Trp, W

Tyrosine – Tyr, Y

Valine – Val, V

Hydroxamic amino acid – HAA

Terminology

(D, +) – Dextrorotary

(L, -) – Levorotatory

DFT - Density functional theory

HOMO – Highest occupied molecular orbital

HSAB theory – Hard soft acid base theory

LUMO – Lowest unoccupied molecular orbital

RBF – Round Bottom Flask (1N, 2N, 3N – 1, 2, or 3 neck)

Equipment

HPLC – High performance liquid chromatography

HRMS – High resolution mass spectrometer

NMR – Nuclear magnetic resonance spectrometer

RP-HPLC – Reverse phase high performance liquid chromatography

SSPS – Solid phase peptide synthesis

Figures

Tables

Schemes

Abstract

Peptides are an important class of molecules that are involved in countless biological processes.[1] Antimicrobial peptides (AMPs) are biosynthesised by many organisms as a natural antimicrobial defensive system. Short-chain AMPs are known to disrupt biological membranes in two ways, pore forming and carpet binding. The latter is not well understood and was investigated herein using labelled AMPs and fluorescent microscopy.

An optimised peptide synthesis and purification protocol has been developed to allow the efficient synthesis of the antimicrobial peptides Aurein 1.2 and Citropin 1.1 using standard Fmoc solid phase peptide synthesis (SPPS) and a Biotage automated synthesiser. Once synthesised the Aurein 1.2 peptide was conjugated via amide coupling to a series of three carboxylic acid functionalised luminescent iridium complexes. The spectroscopic properties of the iridium complexes and the peptide-conjugates were recorded. The length of the linker group between the complex and the peptide was found to have a notable effect on the spectroscopic properties of the complexes. The binding of the labelled AMP to a liposome membrane was then investigated using fluorescence microscopy. Images from the fluorescence microscopy studies show an interaction between the labelled AMP and the liposome membrane.

Chelating molecules and radioactive metal ions are commonly used as radiopharmaceutical compounds for medical imaging and therapies. Therefore improvements in the chemistry involving the chelator molecule is an area of great interest both academically and clinically.

The synthesis of a hydroxamic amino acid for use on an automated peptide synthesiser is reported. The unnatural amino acid is intended to be incorporated into a peptide segment for use as a hexadentate chelator of hard metals. The chelating peptide framework was analysed using computational modelling to determine an optimised geometry for the ligand and complex. The energetics involving the chelation of gallium(III) were calculated and found to be favourable.

Chapter 1. Introduction

Peptides are polymeric molecules that are constructed from twenty common naturally occurring α-amino acids. The short sequences of amino acids are usually between two and fifty residues in length, however an exact point whereby the peptide is classified as a protein can be ambiguous. Proteins are generally greater than fifty residues and tend to have more complex structures and confirmations.[4]

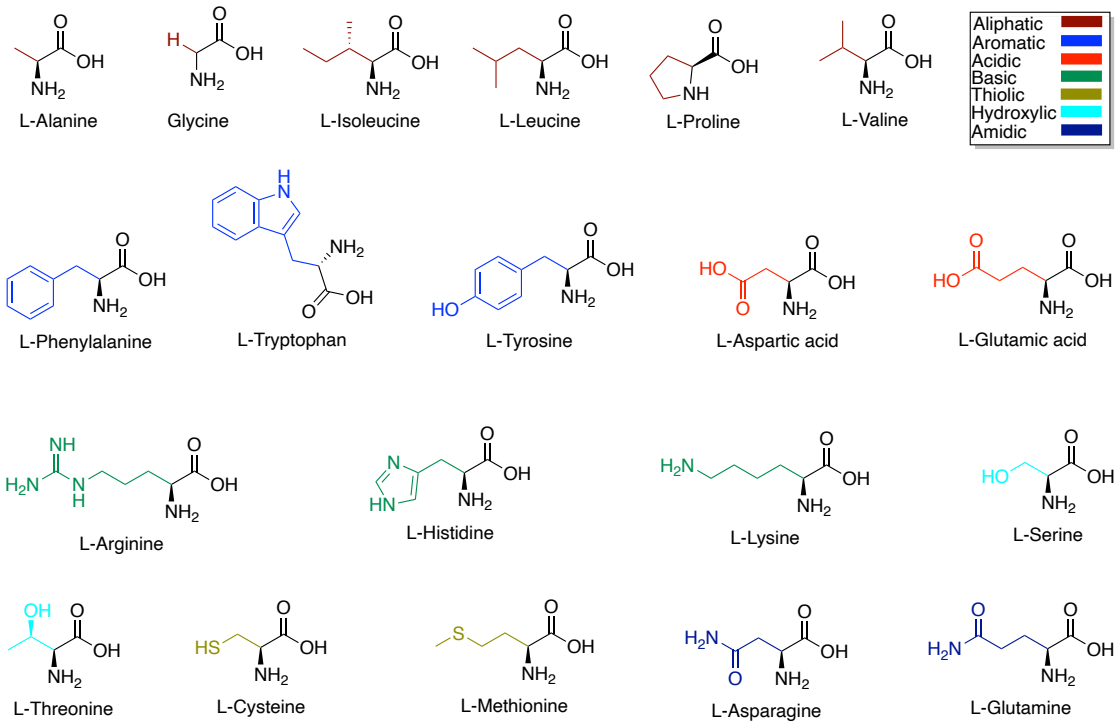

Figure 1 – Structures of proteogenic amino acids showing colour-coded sidechain groups

The modular nature of amino acids is due to amine and carboxylic acid functional groups being amenable to amide bond formation. The structural complexity of peptides and proteins is driven by the variation in sidechain groups of amino acids, as shown in *Figure 1*. Molecules or synthetic amino acids that contain amine and carboxylic acid functionality can be utilised as a monomeric unit within a peptide, or added at the terminal positions by amide linkage, enabling additional functionality to be incorporated into a peptide structure. The modularity and biocompatibility of peptides situate them as an ideal framework for modification, allowing the design of useful molecular probes and therapeutic compounds.[5]

Part 1 - Antimicrobial Peptides

Antimicrobial peptides (AMPs) are deployed in nature by several organisms as a defence against unwanted pathogenic invaders.[2] Most commonly AMPs are linear peptides that form α-helical secondary structures, but in some cases β-sheets or a mixture of both α-helices and β-sheets are

formed. In all cases the antimicrobial properties appear to be due to the AMPs binding to the microbial membrane and disrupting it, resulting in cellular lysis.[3, 6]

Table 1 – Primary sequences of peptides isolated from several Australian native frog species with the highly active AMPs Aurein 1.2 and Citropin 1.1 highlighted in bold

Aurein (Australian Bell Frog – *Litoria raniformis*)		**Citropin** (Blue Mountains Tree Frog – *Litoria citropa*)	
1.1.0	GLFDIIKKIAESI-NH_2	1.1.0	**GLFDVIKKVASVI GGL-NH_2**
1.2.0	**GLFDIIKKIAESF-NH_2**	1.1.1	FDVIKKVASVI GGL-NH_2
2.1.0	GLLDIVKKVVGAFGSL-NH_2	1.1.2	DVIKKVASVI GGL-NH_2
2.1.1	LDIVKKVVGAFGSL-NH_2	1.1.3	GLFDVIKKVASVI GLASP-OH
2.5.0	GLFDIVKKVVGAFGSL-NH_2	1.1.4	GLFDVIKKVASVI GLASQ-OH
2.6.0	GLFDIAKKVIGVIGSL-NH_2	1.2.0	GLFDIIKKVASVVGGL-NH_2
3.1.0	GLFDIVKKIAGHIAGSI-NH_2	1.2.1	FDIIKKVASVVGGL-NH_2
3.1.1	GLFDIVKKIAGHIA-OH	1.2.2	DIIKKVASVVGGL-NH_2
3.1.2	FDIVKKIAGHIAGSI-NH_2	1.2.3	GLFDIIKKVAS-NH_2
3.2.0	GLFDIVKKIAGHIASSI-NH_2	1.2.4	GLFDIIKKVASVVGLASP-OH
3.3.0	GLFDIVKKIAGHIVSSI-NH_2	1.2.5	GLFDIIKKVASVVGLASQ-OH
3.3.1	FDIVKKIAGHIVSSI-NH_2	1.3	GLFDIIKKVASVI GGL-NH_2
4.2.0	GLLQTIKEKLKEFAGGVVTGVQS-OH	2.1	GLIGSIGKALGGLLVDVLKPKL-OH
4.4.0	GLLQTIKEKLKELATGLVIGVQS-OH	2.1.1	GLIGSIGKALGGLLVDVLKPKLQ-OH
5.1.0	GLLDIVTGLLGNLIVDVLKPKTPAS-OH	2.1.2	GLIGSIGKALGGLLVDVLKPKLQAA-OH
5.2.0	GLMSSIGKALGGLIVDVLKPKTPAS-OH	2.1.3	GLIGSIGKALGGLLVDVLKPKLQAAS-OH
		3.1.0	DLFQVIKEKLKELTGGVIEGIQ-OH
		3.1.1	DLFQVIKEKLKELTGGVIEGIQG-OH
		3.1.2	DLFQVIKEKLKELTGGVIEGIQGV-OH

A large variety of AMPs have been isolated from various species of Australian native frogs of the genus *Litoria* (*Table 1)*[5, 7, 8] The numbered designation for each peptide represents variation in the primary sequence, with each variant exhibiting differing antimicrobial properties, however only a small number of the isolated peptides have been shown to be highly active broad spectrum antimicrobial agents.[5, 7, 8] Citropin 1.1 and Aurein 1.2 are among the most active antimicrobial peptides that have been studied to date, however, mechanistically their mode of action is not fully understood.[5, 7, 8]

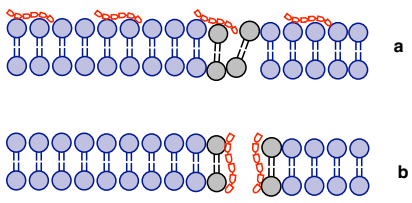

*Figure 2 – (**a**) Carpet binding and (**b**) pore forming mechanism of membrane disruption caused by AMPs*

AMPs disrupt microbial membranes by binding to them via one of two distinctive mechanisms with these being carpet binding (*Figure 2* - ***a***) or pore forming (*Figure 2* - **b**).[9] It is generally accepted that AMPs that are larger than 20 residues in length are long enough to span a lipid membrane and form pores, resulting in cellular lysis. Smaller peptides (less than 20 amino acid

residues) are more likely to bind to the surface of a lipid membrane in a "carpet binding mechanism".[2, 3, 9] However, it has been suggested that AMPs reaching a critical concentration on the surface of the membrane may induce pore formation.[3, 6]

Aurein 1.2

The peptide Aurein 1.2 (GLFDIIKKIAESF-NH_2) is secreted by the Australian Bell frog (*L. aurea, L.raniformis*) and has been shown to be an effective broad-spectrum antibiotic and exhibit anti-cancer properties *in vitro*.[5]

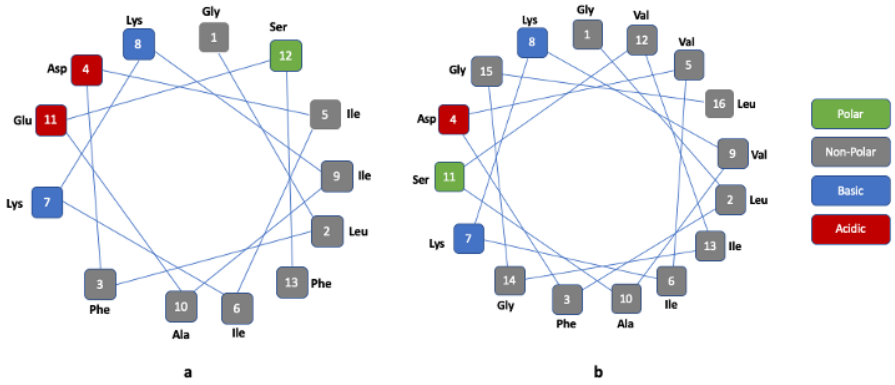

*Figure 3 – Edmundson projection of (**a**) Aurein 1.2 and (**b**) Citropin 1.1 showing the hydrophobic and hydrophilic faces of the helical structure*

It has been suggested the structure of Aurein 1.2 is α-helical with an amphipathic nature due to the discrete hydrophobic and hydrophilic faces along the length of the α-helix (*Figure 3 – **a***).[5, 9, 10] The antimicrobial activity of Aurein 1.2 can be significantly reduced when the primary sequence is altered. The loss of activity is likely due to disrupting the congregation of polar or non-polar amino acids on faces of the helix. Therefore, conservation of the primary sequence appears to be essential to preserve the high antimicrobial activity.[2, 3, 5, 8] The helical wheel projections shown in *Figure 3* can be used as a model to predict the discrete faces of an α-helix by highlighting the gathering of amino acid residues of a particular type (polar, non-polar, acid or basic) in the secondary structure. The helical wheel projections can be useful models to reveal how changes made to the primary sequence alter the alignment of amino acids in the secondary structure.[5, 9]

Citropin 1.1

Citropin 1.1 (GLFDVIKKVASVIGGL-NH_2) is an AMP isolated from the Blue Mountains Tree Frog (*Litoria citropa*). Citropin 1.1 is a wide-spectrum antimicrobial peptide with well-defined hydrophobic and hydrophilic regions in its secondary α-helical structure (*Figure 3 - **b***). These well-defined regions are a shared feature between Citropin 1.1 and Aurein 1.2 and are likely to be the defining characteristic in terms of their high antimicrobial activity.[8] The wild-type form of Aurein 1.2 and Citropin 1.1 additionally feature an amidated C-terminus, a trait that is

commonly seen among the Aurein and Citropin AMPs (*Table 1*). It has been suggested that C-terminus amidation may prevent the peptide from aggregating and as a consequence influence membrane disruption, therefore may be an important component of the AMPs antimicrobial activity.[10] Similarly to Aurein 1.2, Citropin 1.1 is thought to adopt an α-helical secondary structure, however due to both primary sequences being less than 20 residues in length these AMPs are unlikely to be large enough to span a lipid bilayer. Therefore, the mode of interaction with the microbial membrane is thought to be the "carpet binding mechanism" in this case.[8]

Regarding membrane disruption, the carpet binding mechanism is not well understood and presents itself as an interesting area of investigation.[9, 11] Therefore, the preparation of Aurein 1.2 and Citropin 1.1, labelled with luminescent molecules is of interest to assist in directly observing their membrane interactions using fluorescence microscopy.

Luminescence

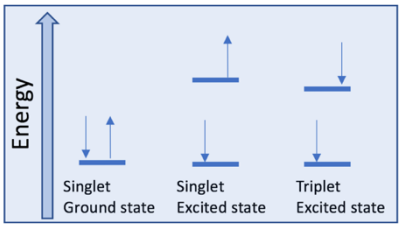

Figure 4 - Singlet and triplet states of an excited electron

Luminescence is a light emitting process that occurs when electrons in a molecule absorb energy and enter an excited state. Upon relaxation to their ground state, the energy is emitted as a photon of light, at a wavelength corresponding to the transition energy.[12] Luminescence can be divided into two different processes, fluorescence and phosphorescence.[12] The radiative processes in fluorescence occur on a fast time scale (10^{-9} to 10^{-6} seconds) whereas phosphorescent light emission occurs more slowly (10^{-3} to 100 seconds).[12-14] The slower rate of the radiative process observed in phosphorescence is due to the excited electron being in a triplet state (*Figure 4*). This results in a slower relaxation process as the transition to the ground state is quantum mechanically forbidden, in accordance with the Pauli exclusion principle.[12]

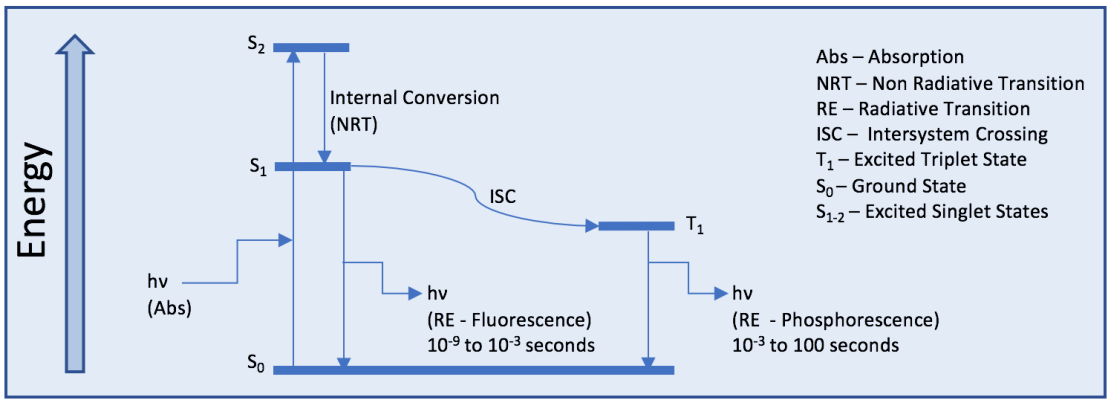

Figure 5 - Jablonski diagram showing fluorescence and phosphorescence radiative transmissions

A simplified Jablonski diagram is shown in *Figure 5,* which is useful to visualise the excitation and emission processes that occur during luminescence. Initially the electron is excited to the S_2 excited state and rapid energy loss occurs via internal conversion to give the S_1 state. Intersystem

crossing can then occur to produce the triplet excited state (both internal conversion and intersystem crossing are non-radiative processes). Radiative emissions occur when a photon of light is released, either through fluorescence (from the S_1 excited state) or phosphorescence processes (from the T_1 excited state). The light is emitted at a lower energy than absorbed due to some energy being lost in non-radiative processes.[12]

Biological Applications of Luminophores

Biological molecules conjugated to luminophores are commonly used to facilitate the study of biochemical processes that would otherwise be difficult to visualise using light microscopy.[15] Bio-conjugates can be molecules that directly contribute or perturb a cellular activity, are passively present, or are a structural component of the process.[15] Biological molecules such as amino acids, lipids, peptides, DNA, carbohydrates and antibodies are routinely labelled with fluorophores to assist in studying their biochemistry using fluorescence microscopy.[16] The last decade of research has produced a large selection of fluorophores, many of which are currently available commercially.[17, 18]

Immunofluorescence (IF) is an example of a labelling method used in cellular biology involving a fluorophore being conjugated to an antibody that can bind with high specificity to a molecular target.[19] There are two common variations of this technique. In the first variation the antibody-luminophore conjugate binds directly to its target and can be visualised using fluorescence microscopy. However, a limitation of this method is that only a single antibody-luminophore conjugate can bind to its target. In the second approach two separate antibodies are used, the primary antibody is used to bind to the cellular target, and the secondary antibody-luminophore conjugate (anti-antibody) binds to the primary antibody.[19] Secondary IF is more sensitive due to multiple secondary antibodies being able to bind to the primary antibody, and hence carry a higher number of fluorophores to the molecular target.[19] Green fluorescent protein (GFP) is another excellent fluorophore that is commonly utilised in the labelling biological molecules and is available in large range of colours. GFP has gained much interest due to the ability to integrate its genetic code into a sequence of a targeted biomolecule and be co-expressed during protein synthesis.[20] The use of GFP is generally only practical when co-expressed with large proteins due to its native size (238 amino acid residues).[21] Therefore it is impractical to conjugate GFP to small molecules or peptides, as its presence would likely perturb any natural behaviour that was intended to be studied.[20]

There are a wide variety of small organic molecules available for use as luminophores, and these are usually based on aromatic or conjugated systems with their own characteristic emission wavelengths. Small organic molecules that contain fluorophores are often suitable when designing a bio-luminophore conjugate, however they can be unstable when exposed to prolonged UV light.[16, 17, 19] Luminescent transition metal complexes have been growing in

popularity due to their relatively small molecular size, their high photo-stability and the large range of emission wavelengths available.[17, 18]

When selecting a fluorescent label for a biomolecule, it is important to take several factors into consideration. These include the size of the fluorophore relative to the analyte, meaning the fluorophore should not be so large that the natural behaviour of the biomolecule to be studied is perturbed. The fluorescent label should be chemically and photo-chemically stable, to allow it to tolerate exposure to UV light for long periods of time to enable studies using florescence microscopy. It should produce high quantum efficiency, meaning the losses in energy transitions are minimal and most of the absorbed energy is converted to light output. And finally, if used with other luminescent molecules their colours should be contrasting, so each bioluminescent conjugate can be easily identified.[15-17]

Labelling With Luminescent Iridium Complexes

The use of iridium complexes as luminophores for biological studies have several advantages over other commonly used organic fluorescent labels.[13, 18] Many organic fluorescent labels are molecules comprised of conjugated or aromatic components, or mixtures of both, and are therefore often rigid and bulky structures that can be problematic when linked to small biomolecules, such as functional peptides (e.g. AMPs).[18] Considering the objective of labelling AMPs with luminophores is to study their natural interactions with lipid membranes, any perturbation of that behaviour would be undesirable. Therefore, iridium metal complexes are a suitable choice for AMP labelling as they are less likely to perturb the measurement. Further advantages of using iridium complexes as fluorescent labels is their ability exhibit properties of both fluorescence and phosphorescence due to efficient intersystem crossing (*Figure 5*).[14, 22] Additionally, the emission wavelength of iridium complexes can be tuned by modifying the electron donating or withdrawing nature of the ligand substituents. These modifications alter the energy of the ligand orbitals, and therefore the energy of the radiative emission resulting in variation of the emission wavelength.[14, 22] For these reasons, luminescent iridium complexes are highly suitable for the labelling of AMPs to enable fluorescent microscopy studies.

Part 2 - Metal Chelating Amino Acid

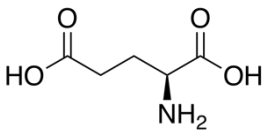

Figure 6 – Glutamic Acid

Radiopharmaceuticals are compounds that contain a radioactive isotope within their structure and are routinely used for medical imaging and as therapeutic drugs for the treatment of many types of cancers. Several radioactive isotopes are hard metal cations, and therefore can be chelated by an organic molecule with the appropriate binding groups, such as hydroxamates. Galium-68(III) is a hard metal cation and has clinical relevance as a radioisotope for targeted medical imaging and therapies. Therefore, any developments in the chemistry involving the chelator molecule has meaningful implications both academically and clinically. An additional objective of this project is aimed at synthesising an unnatural amino acid that can add metal chelating functionality to a peptide segment. The modified metal chelating peptide could potentially be used to develop compounds for use in medical imaging and targeted therapies. Glutamic acid (*Figure 6*) is an ideal candidate for modification due to the sidechain containing a carboxylic acid group that can be chemically altered to form a hydroxamic acid. Additionally, the two methylene groups connecting the carboxylic acid to the α-carbon allow free rotation around their bonds, a feature that is known to be important for enabling effective chelation of a metal.[23] In nature molecules that commonly contain hydroxamic acid moieties within their structures are biosynthesised by microbes and fungi to chelate hard metals such as iron(III) for their metabolic requirements. The naturally occurring molecules can provide inspiration when considering the design of an unnatural amino acid with analogous properties.[24-26]

Siderophores

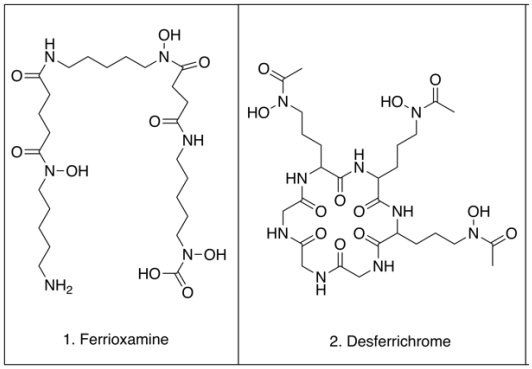

*Figure 7 - Examples of natural siderophores (**1**) Ferrioxamine, (**2**) Desferrichrome*

Iron is an essential nutrient for life that cells require in an available form for use in biochemical processes.[25] The balance of iron availability is critical due to its incorporation in a range of biological compounds that are involved in important cellular processes, such as cell signalling, oxygen transport and DNA synthesis.[27, 28] In contrast, free iron is catalytically active in free radical reactions that can cause cellular damage.[25] Therefore, the bioavailability of iron is tightly regulated to achieve the correct balance in cells.[25] Although iron is generally abundant, it readily oxidises to form an insoluble ferric oxyhydroxide rendering it highly biologically unavailable.[24, 25] In the microbial world, biosynthetic pathways produce a wide variety of iron chelator molecules that are collectively referred to as siderophores. These

pathways have evolved due to selective pressures that are applied to microbes to secure an iron supply for their biochemical requirements.[24, 25, 27] The naturally occurring siderophores desferrichrome and ferrioxamine as shown in *Figure 7* are known to be excellent chelators of iron. These siderophores are equipped with hydroxamic acid moieties and linked by long alkyl chains allowing a high degree of flexibility in their structures. Siderophores can be classified into distinct groups depending on the chemical moieties present within the molecule, these being catecholates, phenolates, polycarboxylates, hydroxamic acids and mixtures of all types. These chemical moieties found in siderophores all have a high affinity for chelating hard metals such as iron(III) and are highly soluble in aqueous environments.[23, 24] The biosynthesis of siderophores can be regulated by the availability of iron within the microbial environment, however conditions such as temperature, pH and the other metals present can be contributing factors.[24]

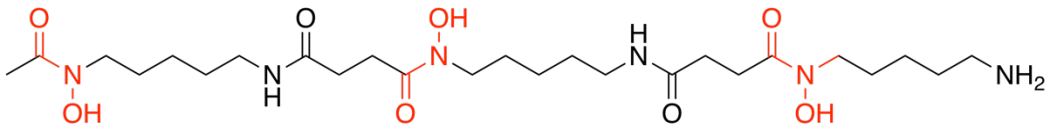

Figure 8 - The structure of a desferoxamine molecule with the hydroxamic acid moieties highlighted in red.

Hydroxamic Acids

The outstanding chelating abilities of hydroxamic acid moieties have not only enabled microbes access to an iron supply from their environment, but have also facilitated the application of siderophores containing these functional groups as therapeutics. Desferoxamine (*Figure 8)* is a siderophore that is used to treat hemochromatosis (iron accumulation) and aluminium toxicity due to its excellent metal chelating properties.[29, 30] Desferoxamine readily binds to iron and allows the complex to be easily excreted, providing a highly effective treatment in iron overload diseases.[30]

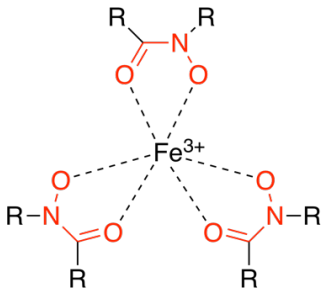

Figure 9 – Iron complex showing hydroxamate moieties in red

A generic hydroxamate complex incorporating an Fe^{3+} cation is shown in *Figure 9,* however other hard metals can be chelated with similar high affinity.[23, 31] Naturally occurring siderophores incorporate a high level of flexibility into their molecular scaffolds and is a structural feature that appears to be necessary for effective chelation to occur.[23, 24, 27, 31]

The natural siderophores excellent ability to sequester iron from their environment can serve as a source of inspiration in the design of peptide based chelators that have a high affinity for radioisotopes such as ^{68}Ga(III), that are commonly utilised in diagnostic imaging and radiotherapies.[23, 31]

Radiopharmaceuticals

The gallium-68 isotope (^{68}Ga) has been successfully used as a radiolabel in many types of compounds such as biological, peptide-based and small molecules for radiopharmaceutical applications.[32-34] The use of the radioisotope ^{68}Ga in Positron Emission Tomography (PET) imaging offers advantages over other commonly deployed radioisotopes such as ^{18}Fluorine (^{18}F). In particular, a key advantage of ^{68}Ga is the ability to produce the isotope via a radioactive decay process using a gallium-68 generator.[32] Many radioisotopes including ^{18}F are synthesised by a particle accelerator known as a cyclotron, in the case of ^{18}F, the synthesis occurs by the bombardment of a natural stable isotope of oxygen (^{18}O) with protons (^{1}H) to produce the fluorine radioisotope (^{18}F). ^{18}Fluorine can then undergo standard nucleophilic chemistry to label a molecule that can be used as a radiotracer.[35]

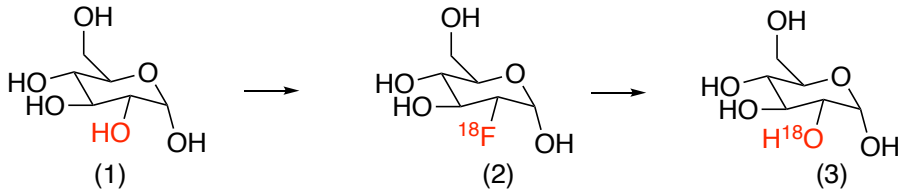

*Scheme 1 – Fluorodeoxyglucose (FDG) flowchart showing the starting glucose molecule, the FDG radiotracer and the final decay product (**1** – glucose, **2** – ^{18}FDG, **3** – heavy oxygen (^{18}O) decay product)*

This method has been utilised to label a range of molecules, for example ^{18}Fluorodeoxyglucose (*Scheme 1* - ***2***) is used in Positron Emission Tomography (PET) imaging routinely as a diagnostic tool in the staging of many types of delocalised cancers.[36-38] However due to the half-life ($t_{1/2}$) of ^{18}F being 109.7 minutes, labelling chemistry must occur quickly and directly before the imaging procedure in order to retain its viability as a radiotracer.[35] As a result ^{18}F imaging is restricted to facilities that are equipped with an expensive array of equipment including a cyclotron and the technical staff that are required for its operation.[35] In contrast, the radioisotope ^{68}Ga is produced via the radioactive decay of germanium-68 (^{68}Ge). The parent ^{68}Ge isotope has a $t_{1/2}$ of 270.95 days, allowing ample time for transport of a gallium-68 generator to locations practically anywhere in the world. The long half-life of ^{68}Ge facilitates the ongoing production of the ^{68}Ga isotope directly onsite as it is needed for the synthesis of medical radioisotopes, therefore circumventing the need for an expensive cyclotron installation.[32, 39]

The half-life of the ^{68}Ga isotope is 68 minutes allowing sufficient time for the rapid assembly of a metal-chelate complex that can be utilised for an imaging or therapy procedure while retaining

its radioactive potency, without remaining radioactive for an unnecessary duration.[40] Additionally, the use of the ^{68}Ga isotope in medical imaging is known to produce high resolution images due to the characteristic physical properties of its positron emission.[32, 39, 41]

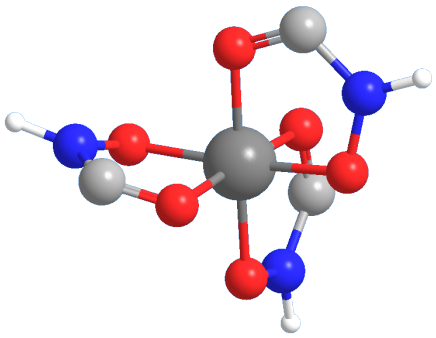

Figure 10 – 3D Structure highlighting the octahedral geometry of Ga(III) chelated by three bidentate hydroxamate ligands

The ^{68}Ga(III) cation is produced by the gallium generator allowing for labelling chemistry to occur with hexadentate ligands that are able to suitably bind in an octahedral geometry as shown in *Figure 10*.[32, 39, 42] Since the eluent from the Ga-68 generator retains a persisting trace concentration of other unwanted metal ions (e.g. Zn, ^{68}Ge), a chelator molecule that has a high specificity for ^{68}Ga(III) is advantageous to further aid the purification process of ^{68}Ga. Such a molecule with a high affinity for its substrate (^{68}Ga) over other metal ions present in the eluent will require less ligand and increase the specific radioactivity of the complex.[32, 39, 41] The stability of the chelate-metal complex will be highly dependent on the ion size, oxidation state and the overall charge to surface area ratio, in accordance with HSAB theory.[32, 39] Additionally, a chelator that is hexadentate, rather than three individual bidentate ligands will form a more stable complex in accordance with the chelate effect.[43] Due to these properties it is possible to attempt to design a chelator molecule with a high level of specificity for the ^{68}gallium(III) isotope.

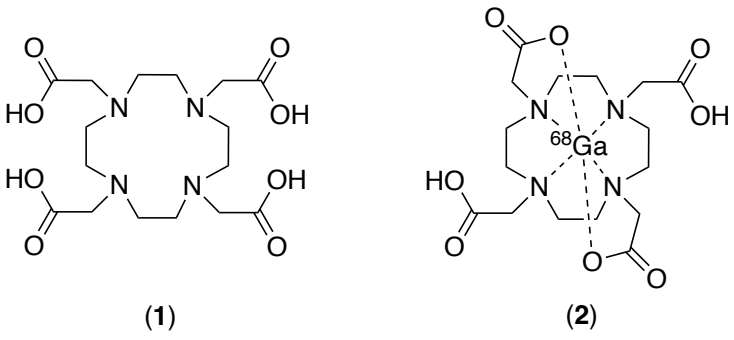

*Figure 11 – DOTA, a common chelator used for ^{68}Ga radioisotope chemistry (**1** – H_4DOTA, **2** – DOTA-^{68}Ga Complex)*

There are currently an immense range of chelators available for use with ^{68}Ga, and the available selection is consistently increasing as further research into this area develops.[44] One of the most widely used ^{68}Ga chelators is the DOTA macrocycle (*Figure 11 - **1***). DOTA is a highly versatile ligand and can form multiple geometries by binding in hexadentate or octadentate fashion

depending on the binding sites available on the host metal.[45] This versatility is due to four tertiary nitrogen atoms and four carboxylates being able coordinate to a metal, as shown in *Figure 11 - **2***.[45] DOTA can be easily conjugated to other compounds (such as targeting segments) by condensing a carboxylic acid group with an amine group on a targeting molecule.[46-50] While DOTA is generally a versatile chelator, there are inherent disadvantages. Generally, the synthesis of DOTA - ^{68}Ga complexes (*Figure 11 – **2***) is achieved by applying heat at 95 °C for ~ 5 minutes, and as a consequence these conditions can lead to the decomposition of heat sensitive conjugates.[51] It is therefore highly desirable to have a coordination chemistry in place that is able to rapidly chelate ^{68}Ga under mild conditions to enable the largest scope of applications for the radiopharmaceutical complex.

Furthermore, the stability of a chelator-radioisotope complex is key to reducing off-target exposure to radiation for the duration of the therapy. The complex must be able to withstand physiological conditions such as the unwanted chelation of commonly found ions in the body (Mg^{2+} and Ca^{2+}) that may compete with a radioisotope ion for binding sites. Unwanted chelation of common ions in the body will subsequentially displace the radioisotope, decreasing the effectiveness of the treatment and generate unwanted off target exposure to radiation. Therefore the chelator molecule must have a much greater affinity for the radioisotope than other potentially competitive ions that will be present under physiological conditions.[52]

Investigations into the use of siderophores for the chelation of radioisotopes remains a continuing area of research.[41, 53] The ongoing effort toward improving the end-use chemistry that facilitates the rapid, reliable and effective chelation of a radioisotope that is stable under physiological conditions for use in medical imaging and therapy is an exciting area of study. Certainly synthetic siderophore inspired hydroxamate containing peptides are a promising and worthy inclusion in this avenue of investigation.

Project Aim

Optimisation of the solid phase peptide synthesis (SPPS) process is key to success in efficiently and reproducibly generating peptides using an automated synthesiser. Automated peptide synthesis gives the impression of a "plug and play" system in which a sequence is entered and a peptide is then automatically synthesised. However, the configuration process is technical and needs a great amount of fine tuning that requires experimentation to determine the values for optimal output in each synthetic case. These optimised programming parameters are required to ensure an efficient, reproducible and high yielding synthesis result is achieved, and therefore is a key objective of the project. Furthermore, the development of a purification procedure is critical to achieving pure peptide samples. Due to the nature of SPPS being a multistep synthesis on the surface of a solid resin, many unwanted products are formed. Purifying the complex mixture requires the use of a HPLC equipped with specialised column pairs (analytical and semi-preparatory) and individual method development in each synthetic case. Therefore, an important aspect of this project is the development of purification techniques using HPLC to optimise the final purified yield of the peptides. The optimised SPPS and purification methods can then be implemented to synthesise antimicrobial peptides (AMPs).

This project aims to investigate and develop the synthetic methodology needed to allow the conjugation of luminescent organometallic complexes to selected AMPs. The AMPs to be studied are thought to bind to biological membranes according to the "carpet binding mechanism". The peptide-luminophore conjugates will then be used as molecular probes for allowing the preliminary study of their membrane interactions using fluorescence microscopy. This will aid in developing the understanding of their "carpet binding mechanism".

A further objective of this project is to synthesise an unnatural amino acid with a hydroxamic acid moiety. The unnatural amino acid will be designed to be incorporated into a peptide sequence allowing the structure to chelate a hard metal, such as gallium-68. To achieve this, the synthetic amino acid will be equipped with Fmoc-protection to allow compatibility with standard Fmoc SPPS. The synthetic amino acid can then be programmed into a peptide sequence and automatically synthesised using a Biotage automated peptide synthesiser. This work may lead to the development of improved peptide-chelating radiopharmaceuticals for use in medical diagnosis and therapy.

Chapter 2. Peptide Synthesis and Labelling

Peptide synthesis

Method development and optimisation in solid state peptide synthesis (SSPS) is critical to achieving efficient and reproducible results. SSPS occurs on the surface of a resin where each amino acid is added sequentially to produce the desired peptide sequence. The SPPS process allows excess reagents to be washed from the resin surface, thereby eliminating the need for a workup after each coupling step and enabling automation of the peptide synthesis process. Upon completion of the synthesis, the final product is liberated from the resin affording the desired peptide. Amino acids and coupling reagents are added in large excess to drive each coupling step as close to completion as possible. Efficient coupling at each step of the synthesis is key to achieving good yields. For example, if each coupling step achieves an 80% yield and the peptide is 10 residues in length, the overall maximum yield achievable can be calculated by multiplying the yield of each coupling step, e.g., $0.8^{10} = 0.107$, 11%. The effect of the SPPS efficiency on the overall yield in a hypothetical 10 step synthesis is shown in *Table 2*. Subsequently, as the peptide length increases, the effect of diminishing yield increases as a function of the coupling efficiency. It is also important to note, the material initially liberated from the resin will contain the desired product and all other polymeric artefacts from the synthesis. Therefore, the final yield can be stated as a crude yield (the material that is initially cleaved from the resin) and a purified yield (the isolated peptide of interest).

Table 2 - Maximum peptide yield calculations according to coupling efficiency

Efficiency	Residues	Yield
80%	10	11%
85%	10	20%
90%	10	34%
95%	10	60%

Figure 12 – Stages of the peptide synthesis process

Automated Peptide Synthesis

Analogous to traditional organic synthesis, many variations in reaction conditions are possible when programming an automated peptide synthesiser, such as coupling reagent selection, duration for coupling and deprotection steps, concentrations (coupling reagents, amino acids and bases) and heating specifications. There is essentially no limit to the different combinations of parameters that are possible when designing a synthesis on an automated peptide synthesiser, and often experimental work is required to establish a working protocol.

*Table 3 – (**a**) Original method / programming for SPPS on the Biotage peptide synthesiser, (**b**) Modified original method using HCTU as the primary coupling reagent, (**c**) Improved method implemented on the Biotage peptide synthesiser*

Chemical	Eq.	Conc. (M)
Fmoc-AA	3	0.7
HBTU	3	0.5
HOBt	3	0.5
DIPEA	6	0.5
Piperidine	72	2

a

Chemical	Eq.	Conc. (M)
Fmoc-AA	3	0.7
HCTU	3	0.5
HOBt	3	0.5
DIPEA	6	0.5
Piperidine	72	2

b

Chemical	Eq.	Conc. (M)
Fmoc-AA	4	0.5
HCTU	4	0.5
HOBt	4	2
DIPEA	6	0.2
Piperidine	72	2

c

Initial attempts at synthesising Citropin 1.1 using the general procedure for Peptide Synthesis with the variations shown in Table 3 – **a**, failed to yield any compound containing peaks when inspecting both crude and HPLC fractionated samples by mass spectrometry. Due to the many possible points of failure during peptide synthesis (*Figure 12*), a troubleshooting process was undertaken. The first potential problem identified was with completely solubilising phenylalanine in DMF for the duration of the peptide synthesis, approximately 30 hours. It was noticed that upon the completion of the attempted synthesis, a solid had formed in the reagent vessel containing the phenylalanine in DMF solution, indicating that the Fmoc-phenylalanine had recrystallised during the synthesis. After consulting the manufacturers specifications for Fmoc-phenylalanine it became apparent that stated solubility in DMF was slightly below the concentrations required for the Biotage peptide synthesiser.[54] Considering that the Fmoc-amino acids are added in multiple equivalents, it is possible that the synthesis may have been successful regardless of this problem, however maintaining solubility of the reagents is important when attempting to optimise the peptide synthesis process and therefore a resolution was required. As per the Biotage specifications, the solvent *N*-methylpyrrolidone (NMP) can be used for more non-polar reagents such as Fmoc-phenylalanine. The synthesis of Citropin 1.1 was repeated using NMP to dissolve Fmoc-phenylalanine and DMF was used for all other reagents. The Fmoc-phenylalanine remained solubilised throughout the synthesis, however, the modified method failed to yield desired peptide. To confirm the problem was not intrinsic to Citropin 1.1 the synthesis was repeated for the shorter peptide Aurein 1.2 using the general method for peptide synthesis, with variations as shown in *Table* 3 – **a**. However, the synthesis of Aurein 1.2 was also unsuccessful using this method.

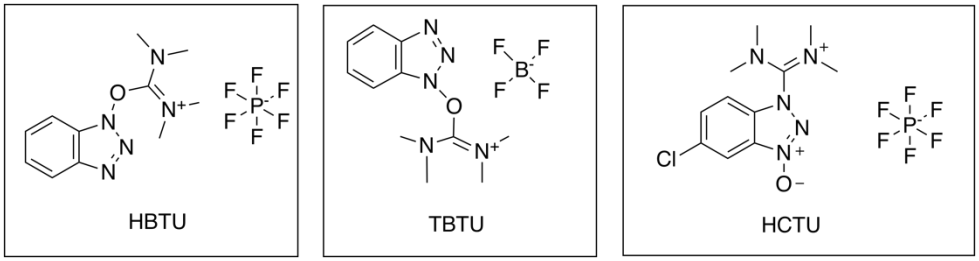

Figure 13 – Peptide coupling reagents (Uronium salts)

Considering both AMPs could not be synthesised, it was a logical next step to attempt to synthesise a peptide with less complexity in the sequence. The sequence of AGAG was selected for synthesis to eliminate the possibility of sidechain interference and therefore directly test the method in *Table* 3 – **a**. However, the synthesis failed to yield even this small peptide segment. To identify the problem initial scrutiny was directed toward the coupling reagent HBTU. The coupling reagents TBTU and HCTU (*Figure 13*) were available for use and were both sequentially tested to attempt to synthesise the peptide sequence AGAG (**1**). Synthesis attempts of **1** using TBTU and HCTU in two separate instances using the general procedure and variations shown in *Table* 3 - **b** were both successful and produced **1** in crude yields 93% and 99% respectively, both syntheses were confirmed by mass spectrometry (*Appendix **1***). This result indicated the initial problem with synthesis was likely to be the chemical HBTU having lost activity, as that was the sole commonality among all failed peptide synthesis attempts. No further purification was attempted in the case of **1** as it was synthesised purely for diagnostic purposes.

The synthesis of Aurein 1.2 (**2**) was then attempted using the general procedure for Peptide Synthesis with the variations as shown in *Table* 3 - **b**, and was successfully synthesised with a yield of 17%. Several excellent reviews comparing coupling reagent efficiency in automated peptide synthesis have been published and provide some useful insight into reagent selection and optimising method protocols, these reviews guided the selection of the modified parameters shown in *Table* 3 – **c** that were used for subsequent syntheses.[55, 56]

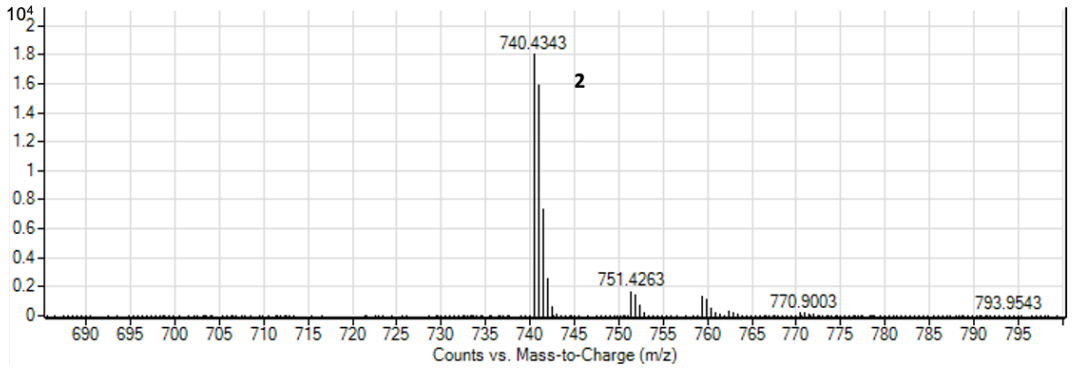

*Figure 14 - HRMS (positive mode) of Aurein 1.2 (Compound **2**), (Calcd. for $C_{71}H_{114}N_{16}O_{18}$: 1478.8497) $[M]^{2+}$ 740.4343*

Using the updated method shown in *Table* 3 – **c**, **2** was successfully synthesised and a purified yield of 62% was obtained, confirmed by mass spectrometry as shown in *Figure 14*. As detailed in *Table 2,* the efficiency of the SPPS process appeared to be satisfactorily optimised allowing the effective preparation of the AMPs Aurein 1.2 (**2**) and Citropin 1.1 (**3**) that was necessary to for further experimentation with conjugating iridium-based luminophores to commence.

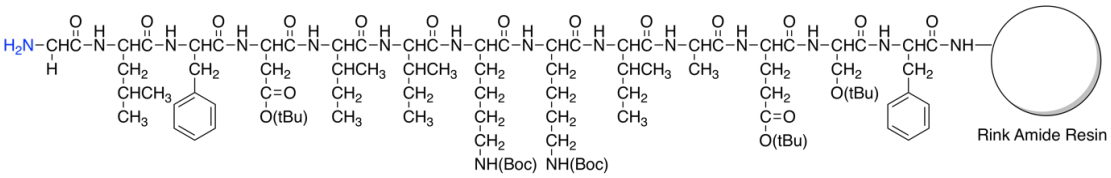

*Figure 15 – Aurein 1.2 (Compound **2**) with sidechain protection remaining and attached to the resin, showing the de-protected primary amine group in blue*

Aurein 1.2 (**2**) (300 mg scale) and Citropin 1.1 (**3**) (200 mg scale) were prepared according to the general procedure for Peptide Synthesis using the parameters shown in *Table* 3 - **c**, however in this case the finished peptides were retained on the resin. This allowed the terminal amine group to be solely de-protected creating the exposure of a single reactive site on the molecule while leaving all sidechain functionality protection intact as can be seen in *Figure 15*. This approach enabled several options for further conjugation of the peptide to the iridium complex luminophores, either using the Biotage peptide synthesiser, or using a manual approach. The peptides **2** and **3** remaining attached to the resin were dried under reduced pressure and weighed to determine a conversion factor based on the theoretical yield in each case. The theoretical yields of 300 mg for compound **2** and 200 mg for compound **3** were used per total mass of dried resin, thereby allowing reagent equivalents to be determined for the subsequent coupling reactions. The reasoning for this calculation is due to the true yield only being possible to calculate upon cleavage of the peptide from the resin and subsequent removal of the protection groups, in which case no further chemistry such as labelling would be possible due to the many sites of reactivity being present on the deprotected peptide. Leaving a single site of reactivity is important to enable the labelling of the *N*-terminus exclusively, as shown in *Figure 15*.

Peptide Iridium-Complex Conjugation

The single site of reactivity left exposed on the AMPs **2** and **3** allows the conjugation with a molecule containing a compatible functional group such as a carboxylic acid. The carboxylic acid and amine groups can be condensed to form an amide bond, facilitating the conjugation between the AMP and luminescent iridium complex.

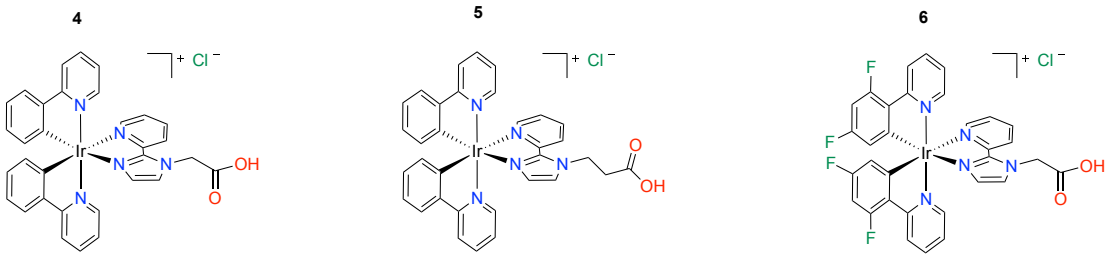

*Figure 16 – Luminescent Iridium complex series, (**4**) Single methylene linkage, (**5**) Double methylene linkage, (**6**) Single methylene linkage with fluorine substituents*

A series of luminescent iridium(III) complexes functionalised with carboxylic acid groups to allow for coupling to the *N*-terminus of the AMPs **2** and **3** were prepared by PhD Candidate Pria Ramkissoon as seen in *Figure 16*. Initially, it was envisioned that the iridium complex could be coupled to the final amino acid residue of the peptide sequence using an automated peptide synthesiser, however it became apparent that the iridium complexes **4** and **5** could not be solubilised in DMF or NMP at appropriate concentrations for automated SPPS (0.4 – 0.7 M), with the lowest possible concentration available for programming on the Biotage peptide synthesiser being 0.1 M.[57] The iridium complex **4** was able to be dissolved in DMF at a 0.1 M concentration after overnight stirring with heating, however this concentration is not within the recommended range for use on the Biotage peptide synthesiser.

The coupling of AMP **2** with iridium complex **4** was however attempted on the Biotage peptide synthesiser at a concentration of 0.1 M, and was successful, although a poor yield of 2% was obtained. Therefore, it was deemed impractical to use the automated synthesiser for coupling the iridium complexes **4** and **5** to the AMPs due to their difficult solubility in DMF. Iridium complex **6** was synthesised after the initial conjugation experiments with complexes **4** and **5** and was found to have higher solubility in DMF, likely as a result of the polarising nature of the fluorine substituents. Due to time constraints, the coupling of **2** or **3** with **6** has not been attempted using the Biotage peptide synthesiser, however the outstanding solubility of **6** in DMF suggests this complex is an ideal candidate for automated synthesis.

Another consideration that was made in the design of the iridium complex series was the length of the alkyl chain between the iridium complex and the carboxylic acid functionality. It was hypothesised that a single methylene group may not be long enough to allow enough steric freedom for effective coupling between the terminal amine of the large peptide molecule attached to the resin and the carboxylic acid group on the iridium complexes. Therefore, it was

reasoned that the longer linker of complex **5** (*Figure 16 -* **5**) may result in a higher yield of the conjugate due to improved steric factors.

(7): Coupling Aurein 1.2 with (4)

The synthesis of **7** was carried out as per the general procedure for Peptide Labelling with Luminescent Iridium Complexes on a 25 mg scale (**2** – 25 mg, 0.017 mmol, 1 eq.), (**4** – 50 mg, 0.068 mmol, 4 eq.) and produced **7** in a purified yield of 2.8 mg (8%).

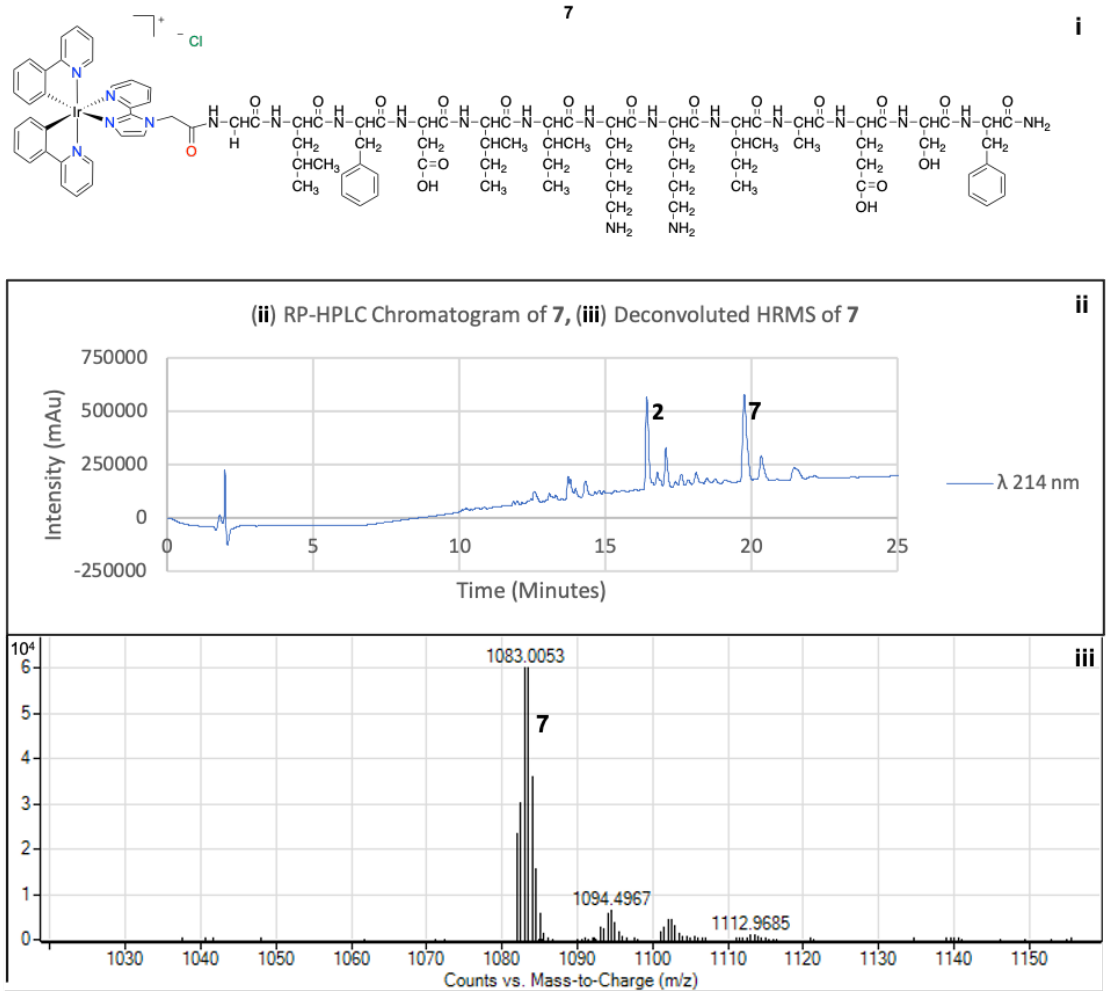

*Figure 17 – **(i)** Compound (**7**) - Aurein 1.2 (**2**) coupled to iridium complex (**4**). **(ii)** Reverse phase HPLC chromatogram at λ 214 nm showing two main peaks corresponding to compounds **2** and **7**. **(iii)** HRMS of compound **7** (Calcd. $C_{103}H_{137}IrN_{21}O_{19}$+ : 2166.0057), $[M]^{2+}$ 1083.0053*

While the coupling was successful as confirmed by HRMS (Figure 17 – **iii**), the yield of the reaction was low. Several factors that may have contributed to the low yield can be addressed to help improve the efficiency of future reactions. The poor solubility of **4** in DMF (50 mg, in 500 µL; 0.14 M) may have been a contributing factor to the low yield, as the concentration is below the recommended range for SPPS (0.4 – 0.7 M).[57, 58] Another consideration is the compatibility of the coupling reagent HCTU that was used in all cases, therefore studies with a range of coupling reagents would be useful to determine if the coupling inefficiency in this case is

intrinsic to HCTU. Heating with microwave energy has been suggested to improve the coupling of sterically difficult reactions and would also be an interesting avenue of investigation for future studies.[59] It is evident from the HPLC chromatogram as shown in *Figure 17* – **ii** that the coupling between **2** and **7** was incomplete as both peaks are clearly visible in the chromatogram and identified using HRMS (**2** – rt = 16.5 mins, **7** – rt = 19.5 mins).

(8): Coupling Aurein 1.2 with (5)

The synthesis of **8** was carried out according to the general procedure for Peptide Labelling with Luminescent Iridium Complexes on a 25 mg scale (**2** – 25 mg, 0.017 mmol, 1 eq.), (**5** – 51 mg, 0.068 mmol, 4 eq.) producing a purified yield of 2.0 mg (5%).

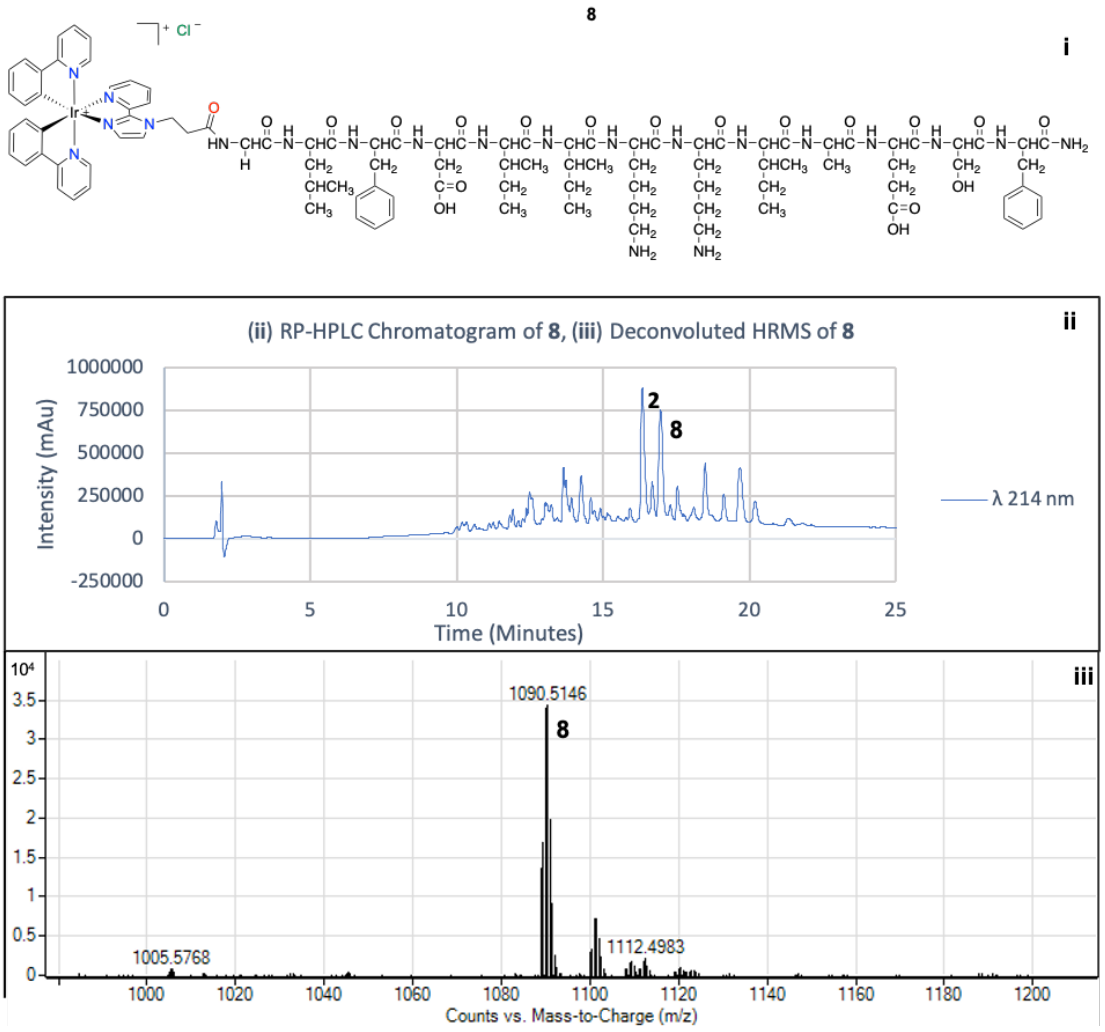

*Figure 18 – **(i)** Compound (**8**) - Aurein 1.2 (**2**) coupled to iridium complex (**5**). **(ii)** Reverse phase HPLC chromatogram at λ 214 nm showing two main peaks corresponding to compounds **2** and **8**. **(iii)** HRMS of compound **8** (Calcd. $C_{104}H_{139}IrN_{21}O_{19}$+ : 2180.0213) $[M+H]^{2+}$ 1090.5146*

The coupling of **2** with **8** was successful confirmed by HRMS as shown in *Figure 18* – **iii**, however in low yield. The solubility of the iridium complex **5** in DMF was significantly lower than **4**, requiring 5 mL of DMF for **5** to become fully solubilised, resulting in a final

concentration of 0.014 M. It is possible that any benefit gained by the addition of the longer linker between the complex and the carboxylic acid group was negated by the amount of solvent required to achieve full solubility. Due to the variation in solubility between **4** and **5** it is difficult to directly compare their coupling efficiencies. The HPLC chromatogram as seen in *Figure 18* – **ii** shows two distinct peaks for **2** and **8**, indicating that the coupling between the AMP and luminescent label remained incomplete. **(2** – rt = 16.5 mins, **8** – rt = 17.0 mins).

(9): Coupling Aurein 1.2 with (6)

The synthesis of (**9**) was carried out as per the general procedure for Peptide Labelling with Luminescent Iridium Complexes on a 25 mg scale (**2** – 25 mg, 0.017 mmol, 1 eq.), (**6** – 55 mg, 0.068 mmol, 4 eq.) producing a purified yield of 0.5 mg (1%).

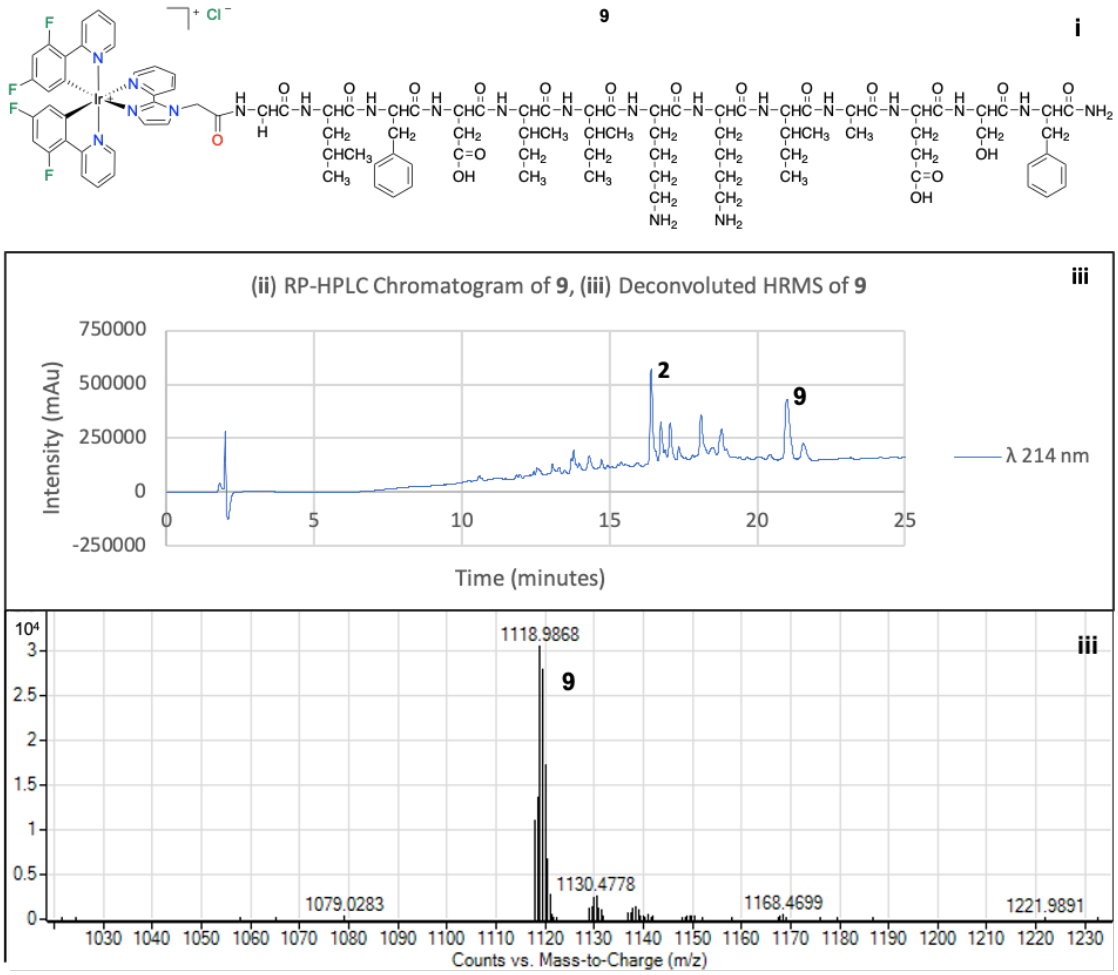

*Figure 19 – (**i**) Compound (**9**) - Aurein 1.2 coupled to iridium complex (**6**). (**ii**) Reverse phase HPLC chromatogram at λ 214 nm showing two main peaks corresponding to compounds **2** and **9**. (**iii**) HRMS of compound **9** (Calcd. $C_{103}H_{133}F_4IrN_{21}O_{19}$+ : 2237.9680) $[M]^{2+}$ 1118.9868*

The coupling of **2** with **9** was successfully confirmed by HRMS as shown in *Figure 19* – **ii**, however in low yield. The HPLC chromatogram shown in *Figure* 19 – **ii** shows two distinct peaks for **2** and **9** indicating incomplete coupling between the peptide and the iridium complex

(**2** – rt = 16.5 mins, **9** – rt = 21.5 mins). The solubility of complex **6** was excellent, dissolving immediately in 500 µL of DMF (0.14 M), and could potentially be solubilised at higher concentrations. Considering the extremely low yield of **9**, and the low yields of conjugates **7** and **8**, it is possible that the coupling reagent HTCU may be inefficient for these sterically difficult conjugation reactions. Another possibility worthy of consideration is the AMP peptides **2** and **3** may undergo an internal aggregation while held on the resin and create a sterically challenging environment for effective coupling to occur. In all cases it would be extremely interesting to utilise microwave heating to determine if this indeed would reduce or inhibit any potential internal aggregation and therefore result in a higher level of steric availability for coupling.

Microwave Assisted Peptide Synthesis

The formation of amide bonds to generate peptide sequences using SPPS is generally undertaken at room temperature using one of the many common amide coupling reagents, such as HBTU, HCTU or TBTU. In peptide elongation using SPPS, each coupling step is given between 45 minutes to 1 hour for completion, and in some cases difficult couplings may need to be repeated multiple times. This process can ultimately end up being extremely time consuming and depending on the length of the target peptide sequence, a single syntheses of a peptide between 10 to 12 amino acids can span multiple days. Using microwave heating has been investigated in many studies and shown in some cases to be beneficial for reducing the reaction time and increasing the overall purity of the crude peptide.[59-62] Generally, with some exceptions that will be further discussed here, these studies have demonstrated when using microwave heating at ~ 60 °C the crude peptide purity was higher, and the reaction time per coupling step is significantly reduced to between 2 – 6 minutes.[59-62] Several studies have suggested there is no significant difference in conventional heating and microwave irradiation, and therefore reasoned that the improved results in coupling and purity are caused by increased temperature rather than an intrinsic effect generated by microwave radiation.[59-61] However, it has been suggested that the high dipole moment of an amide bond may interact with the magnetic field generated by microwave irradiation and as a result lead to a de-aggregation of the elongating peptide while held on a solid resin surface, therefore freeing it sterically and enhancing its availability for chemical reactivity.[62]

Whether microwave heating aids in achieving a higher yield and purity of the crude product is still an area of active research and is highly dependent on the primary sequence and reaction conditions. Reports of internal aggregation during the peptide synthesis occurring at approximately the 5th residue of the elongation process indicate that heating could be beneficial for any SPPS that is planned to be greater than 5 amino acid residues in length.[62] Furthermore, it is well known that increasing the temperature will certainly increase the rate of reaction as described by the Arrhenius equation, however this could potentially lead to unwanted side

reactions, and a decrease in the purity of the crude product.[61] It is therefore imperative that several considerations be taken into account for the design of the peptide synthesis parameters when utilising heating, whether it be microwave or conventional. Such considerations include the primary sequence of the target peptide, the solvent choice, the steps involved in the synthesis (elongation, amine deprotection, sidechain deprotection) and the type of resin used. Since the possible array of unwanted by-products in a peptide synthesis and the variation in possible reaction conditions is large, only relevant side reactions that are known to occur with the use of microwave heating will be discussed here.

Peptide Racemisation

There are 19 proteogenic amino acids that contain a chiral centre at the α-carbon and are commonly referred to as either levorotatory (L, -) or dextrorotary (D, +). On earth nature utilises the (L) configuration for life as we know it and as a consequence the preservation of the chirality of amino acids during protein synthesis is critical.[63] Due to the nature of chirality, these configurations must be conserved in order for a secondary peptide structures (e.g. α-helix) to retain their natural function.[64] Therefore, to conserve the chirality of amino acids during SPPS, any conditions that promote racemisation must be avoided. There are numerous pathways that have been described regarding racemisation, such as direct α-proton abstraction and aspartimide formation.[58, 65-68]

Direct α-Proton Abstraction

The carbon and hydrogen atoms directly adjacent to a carbonyl moiety are commonly referred to as alpha (α) and are often more reactive due to their proximity to the δ^+ carbonyl carbon. Due to this property the protons attached to the α-carbon are more acidic than a C-H bond that is not located in an alpha position to a carbonyl.[69] In a study investigating the acidity of the α-hydrogen in various amino acids, the pKa values in the compounds examined were found to range between 14.9 and 17.0, and therefore many amino acids could potentially undergo direct α-proton abstraction under certain conditions during SPPS, such as microwave heating, with some residues being more susceptible than others.[69]

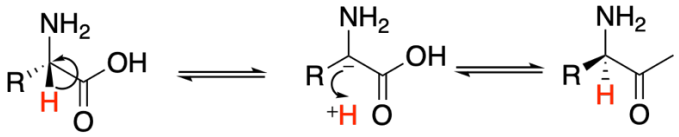

Scheme 2 - Direct abstraction of the acidic α-proton in an amino acid resulting in a change in chirality

Due to the acidity of the α-proton, care must be taken when using microwave heating during a peptide synthesis to avoid promoting direct α-proton abstraction as shown in *Scheme 2.* Studies have shown that in some cases microwave heating to over 100 °C can result in significant increases in racemisation, however when heating is sustained at 65 °C the effect is not apparent, suggesting a temperature range of 60 – 65 °C is optimal for increased yield and purity, while generally minimising racemisation. [59-62]

Susceptible Amino Acids

The amino acids Aspartic Acid (Asp), Cysteine (Cys) and Histidine (His) are commonly reported to be highly susceptible to racemisation during SPPS and generally should be omitted from microwave heating conditions. However, there are some possible counter measures that can be implemented when incorporating these residues into a peptide if microwave heating is necessary.

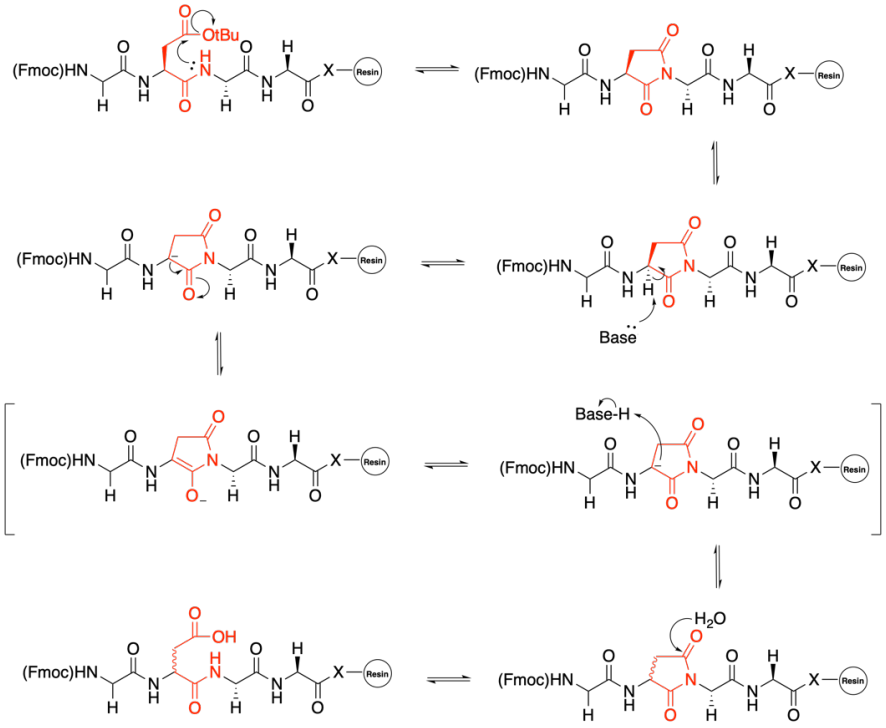

Scheme 3 – Mechanism describing the formation of aspartimide and subsequent racemisation in a aspartic acid residue during SPPS

Aspartic acid (Asp) is well documented to form aspartimide during the *N*-deprotection step when exposed to microwave heating, as detailed in *Scheme 3*. Changing the deprotecting amine to piperazine dramatically lowers the formation of aspartimide and subsequent racemisation.[59, 67] However, avoiding microwave heating during aspartic acid coupling and deprotection steps can generally mitigate the formation of aspartimide and therefore ultimately reduce or eliminate any significant level of racemisation.

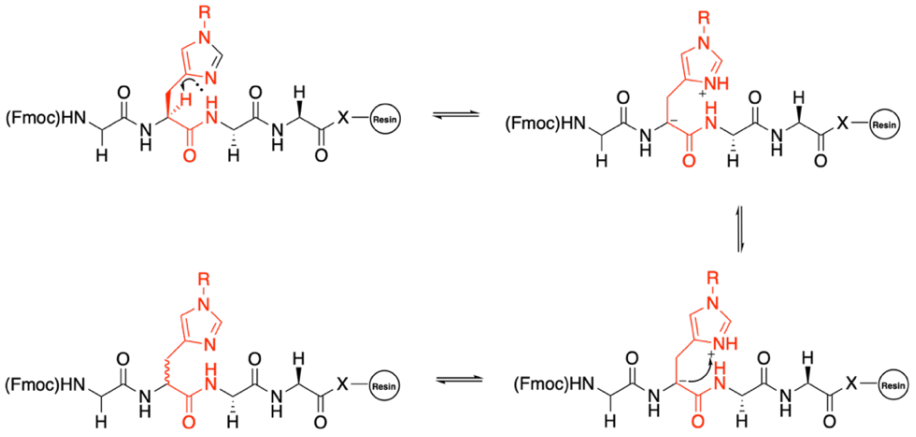

Scheme 4 - Racemisation via Histidine α-proton abstraction pathway

In the case of histidine, microwave heating can lead to an internal proton abstraction that originates from the nitrogen present on the imidazole sidechain of the amino acid, as shown in *Scheme 4*. Several studies have shown that microwave heating during the coupling and *N*-deprotection steps of SPPS involving His residues results in significant increases in racemisation, however the effect can be reduced dramatically by minimising the concentration of the base used during the deprotecting step.[59, 60, 70, 71] Cysteine is considered to be the most prone to suffering racemisation during peptide synthesis due to the high tendency for direct proton abstraction to occur in the presence of a base (*Scheme 2*).[59-62, 70, 71] Furthermore, cysteine has been reported to undergo high levels of racemisation when directly anchored to a hydroxyl-based resin.[66, 68, 72]

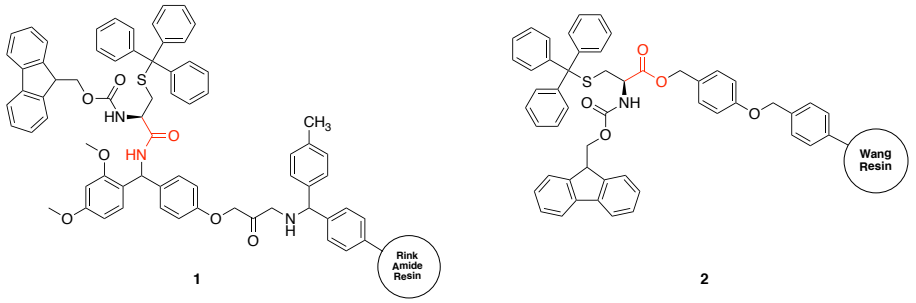

*Figure 20 – Fmoc protected cysteine moiety attached to (**1**) Rink Amide resin and (**2**) Wang resin highlighting the differences in covalent bonds used to anchor the residue to the resin*

When cysteine is directly anchored to a hydroxyl-based resin (*Figure 20– **2***), the racemisation effect significantly is increased.[68, 73] In contrast there is no apparent racemisation increase during the repeated α-*N* deprotecting step in a peptide synthesis when cysteine is anchored to a resin that utilises an amide linkage, such as a Rink Amide resin (*Figure 20 - **1***), or incorporated into a peptide sequence further in the elongation process.[66, 68] Due to cysteine having such a high susceptibility to racemisation microwave heating is not recommended in any case.[66] Interestingly, significant racemisation in all amino acids with the exception of cystine can be generally mitigated in by switching to an aprotic solvent mixture of DMSO and toluene (1:3) when using microwave SPPS at 60 °C.[59]

Deprotection

The most commonly used protection strategy in modern day SPPS is the Fmoc/tBu combination, whereby the terminal amine (R-NH_2) is protected by the base labile group Fmoc and the amino acid sidechains are protected by acid labile groups, such as Boc and t-Butyl esters. This protection strategy limits chemical reactivity to the amine and carboxylic acid allowing the two groups to form an amide linkage resulting in the elongation of the peptide sequence. Deprotection of the amine is carried out with a base, usually a secondary amine such as piperidine, with the deprotection step generally lasting from 10 to 20 minutes and constituting a significant portion of the reaction time.[74]

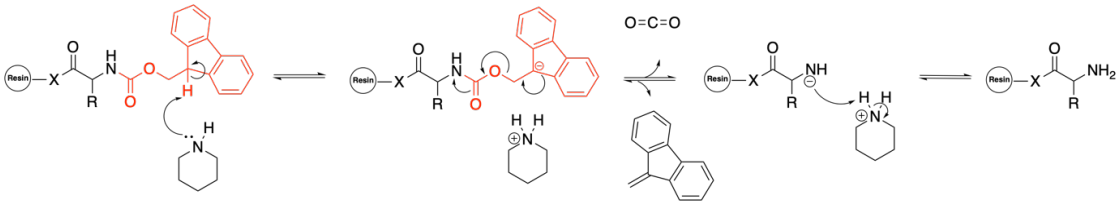

Scheme 5 – α-N deprotection reaction scheme highlighting the Fmoc moiety in red

The use of microwave heating for the Fmoc deprotection step (*Scheme 5*) in SPPS has been investigated by in many studies and has in some cases been shown to be advantageous in terms of crude yield purity and enhanced reaction times. Microwave heating however, can lead to significant racemisation in susceptible amino acids and via the direct α-proton abstraction mechanism (*Scheme 2*), and as general guideline is not recommended for deprotecting the α-amine nitrogen.[59-62, 72]

With careful considerations in regard to the primary sequence of the target peptide, the use of microwave heating can be beneficial to increase the purity of the crude peptide and decrease reaction time. The use of an aprotic solvent system could further aid the reduction of racemisation during SPPS. Effective mixing has been shown to be critical to achieving improved results when using microwave heating, however magnetic stirring should be avoided as it has been suggested that it may degrade the solid phase resins.[59]

Comparison Synthesis of Aurein 1.2

The peptide Aurein 1.2 (**2**) (*GLFDIIKKIAESF-NH_2*) was selected to compare reaction conditions at room temperature with microwave heating at 60 °C using a Biotage automated peptide synthesiser. Due to the native sequence of Aurein 1.2 not containing any Aspartic Acid (Asp), Cysteine (Cys) or Histidine (His) residues, all coupling steps were subjected to microwave heating. The Biotage automated peptide synthesiser allows the selection of each step in the synthesis to be fully customised with regard to heating and reagent selection. Due to the possibility of increased racemisation, as mentioned in the above introduction, heating was not used during the α-*N* deprotection steps of the synthesis.

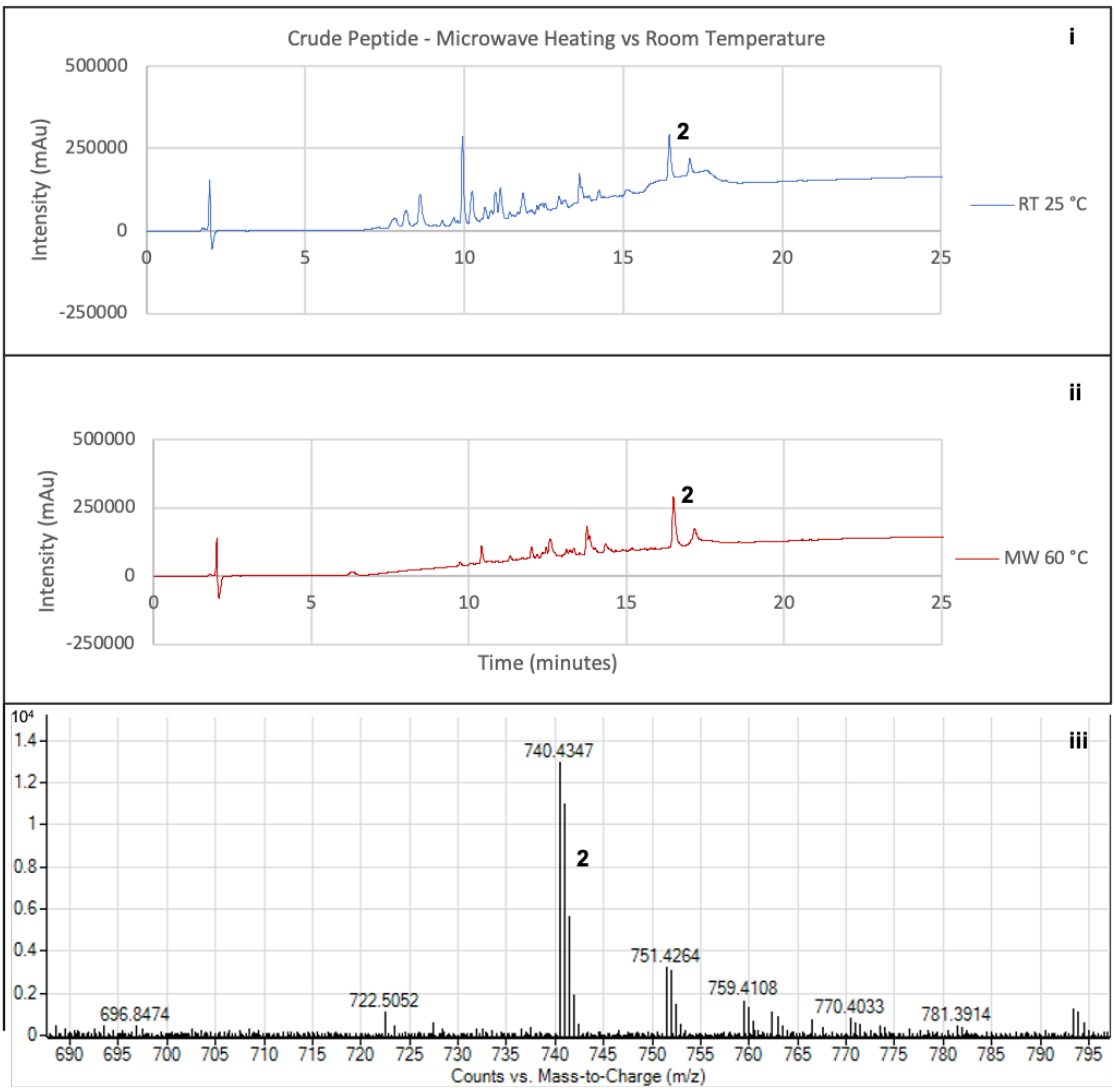

*Figure 21 – **(i)** HPLC Chromatogram (λ 214 nm) of crude peptide mixture containing **2** at room temperature, **(ii)** HPLC chromatogram (λ 214 nm) of crude peptide mixture containing **2** using microwave heating at 60 °C. **(iii)** HRMS spectra of peaks rt = 16.5 mins corresponding to **2** (Calcd. for $C_{71}H_{114}N_{16}O_{18}$: 1478.8497) $[M]^{2+}$ 740.4347*

The HPLC chromatogram measured at 214 nm shown in *Figure 21* compares the crude product from two Aurein 1.2 syntheses using the general method for Peptide Synthesis with the exception of temperature and time. The room temperature chromatogram (*Figure 21*- **i**) appears to have a significantly higher level of impurities and side products comparatively to the microwave synthesis as seen in *Figure 21*- **ii**. Aurein 1.2 (**2**) was confirmed by HRMS (*Figure 21* - **iii**).

Summary

Microwave heating has been shown to be beneficial under certain conditions when careful considerations toward the design of the synthesis are made. The reaction time was greatly reduced and the crude purity of the peptide Aurein 1.2 was increased. Microwave heating could provide a mechanism for internal aggregation reversal and may lead to improved yields when

sterically difficult couplings are attempted. Microwave assisted heating could further improve the atom efficiency of the SPPS due to negating the need for double and triple couplings for difficult residues.

Table 4– Comparison between room temperature and microwave synthesis

Reaction Conditions:	Deprotection	Coupling Time	Reaction Time
Room Temperature	30 mins	60 mins	19.5 hours
Microwave	30 mins	6 mins	7.8 hours

Due to the clearly improved purity of the crude peptide in this experimental comparison as seen in *Figure 21-* ***b*** and the decreased reaction time (*Table 4*) it would appear to be advantageous to consider utilising microwave heating for difficult couplings and peptide segments greater than 5 residues. The crude peptide mixtures from the microwave heating and room temperature syntheses were subjected to analytical HPLC to allow a direct comparison of their relative chromatograms. In this study preparatory HPLC was not carried out to determine final yields of each synthesis due to restricted laboratory access during the year. However the data obtained from the analytical HPLC experiments is sufficient to contrast the two reaction conditions and highlights the improved result of using microwave heating in this case. Future study into the possible benefits of microwave heating to couple luminescent iridium complexes to peptide segments should be investigated, and could provide an elegant solution to the low yields seen in previous attempts at synthesising the AMP-iridium complex conjugates.

HPLC Method Development

HPLC methods were developed for each peptide and conjugate **2**, **3** **7**, **8** and **9**, due to each molecule having unique different properties. The HPLC system used in these studies was equipped with a diode array detector that allowed multiple wavelengths to be monitored simultaneously. Generally, observing high energy wavelengths (200-215 nm) is not useful in HPLC methods due to the large range of compounds (including many solvents) that absorb in this region, therefore determining a discrete peak in this range is often problematic. However, it is known that amide bonds absorb well in this wavelength range, and for multi residue peptides with numerous amide bonds the signal observed in this region can be easily identified providing useful characteristic information.[75, 76]

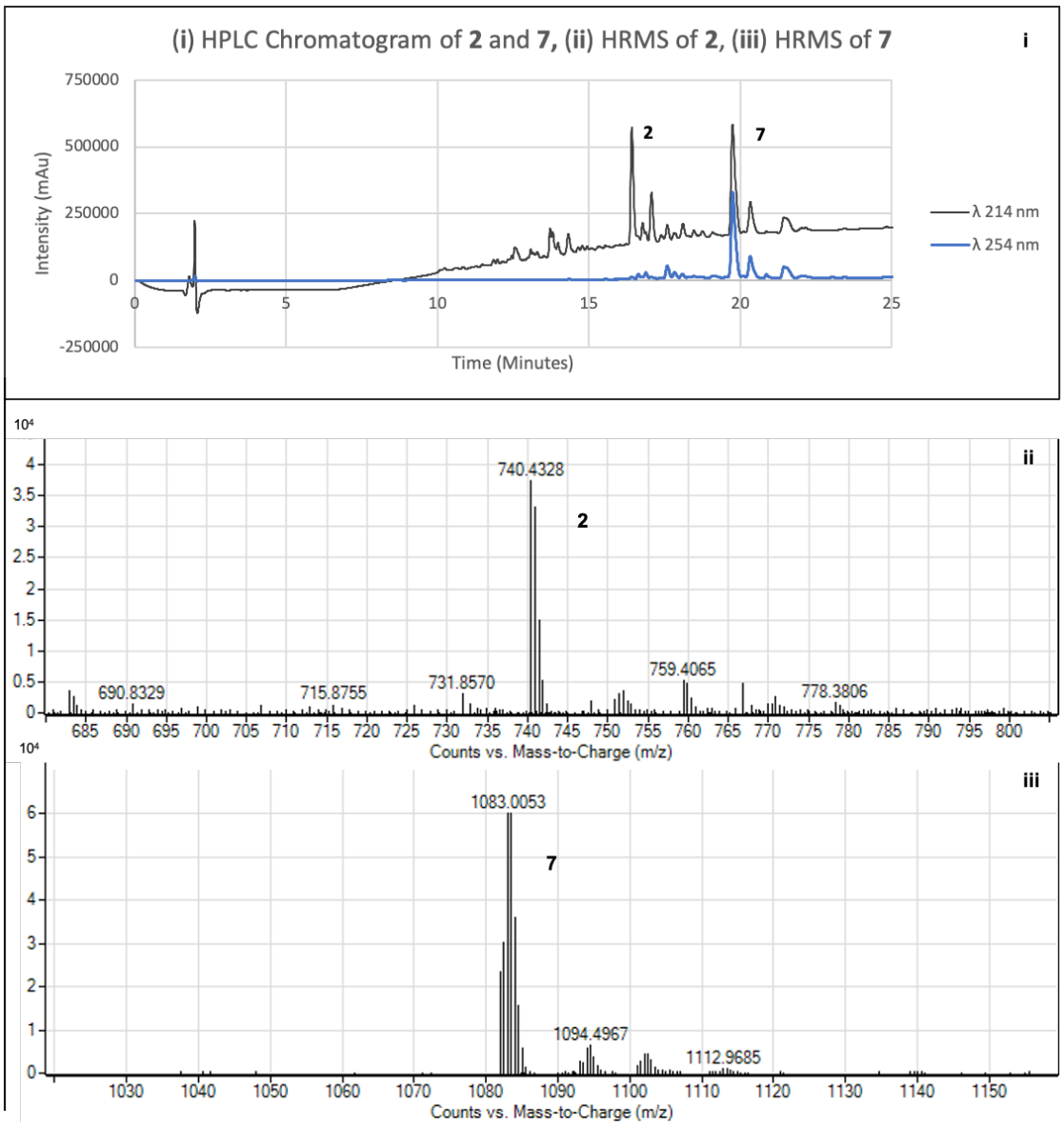

*Figure 22 – **(i)** HPLC Chromatogram of crude peptide mixture (λ 214 and 254 nm) showing peaks for (**2**): rt = 16.5 mins and (**7**): rt = 19.5 mins, **(ii)** HRMS spectra for Aurein 1.2 (**2**) (Calcd. for $C_{71}H_{114}N_{16}O_{18}$: 1479.79) $[M]^{2+}$ 740.4328, **(iii)** HRMS spectra for conjugate (**7**) (Calcd. $C_{103}H_{137}IrN_{21}O_{19}$+ : 2166.0057) $[M]^{2+}$ 1083.0053*

The HPLC chromatogram for the crude peptide mixture containing conjugate **7** is shown in *Figure 22* exhibiting two large peaks, retention time: (peak 1) 16.5 and (peak 2) 19.5 minutes at λ 214 nm. These large peaks seen at λ 214 nm are consistent of molecules with multiple amide bonds. Additionally, the peptide-iridium conjugates have excellent absorbance in the region of 240-280 nm. The presence of a signal (retention time: 19.5 mins) is seen at both wavelengths (recorded at λ = 214 and 254 nm), enabling this peak to be assigned to conjugate **7**. This characteristic peak was present in the all three of the peptide-conjugates that were synthesised and provided an excellent method of predicting the presence of the labelled AMPs in the HPLC chromatogram. This preliminary determination of **7** was then confirmed by mass spectrometry as seen in *Figure 22* – **iii**. Compound **2** was confirmed as the large peak eluting first (λ = 214, rt = 16.5 mins) by HRMS (*Figure 22* – **ii**).

In summary, purification of the crude peptide mixtures containing the labelled AMPs was successful using HPLC. A coalescence of peaks at λ = 214 and 254 nm was a characteristic absorbance of the conjugates that allowed an effective preliminary determination of successful coupling in compounds **7**, **8** and **9** using HPLC.

Fluorescence Spectroscopy

The luminescent iridium complexes and the labelled AMPs fluorescence profiles were compared to investigate if the addition of a peptide to the luminophore would alter the spectroscopic profile. In the case of labelled AMPs a change in the emission profile between the iridium complexes (**4** and **6**) and the conjugated peptide-complexes (**7** and **9**) is seen that is conceivably due to the conjugation of the peptide.

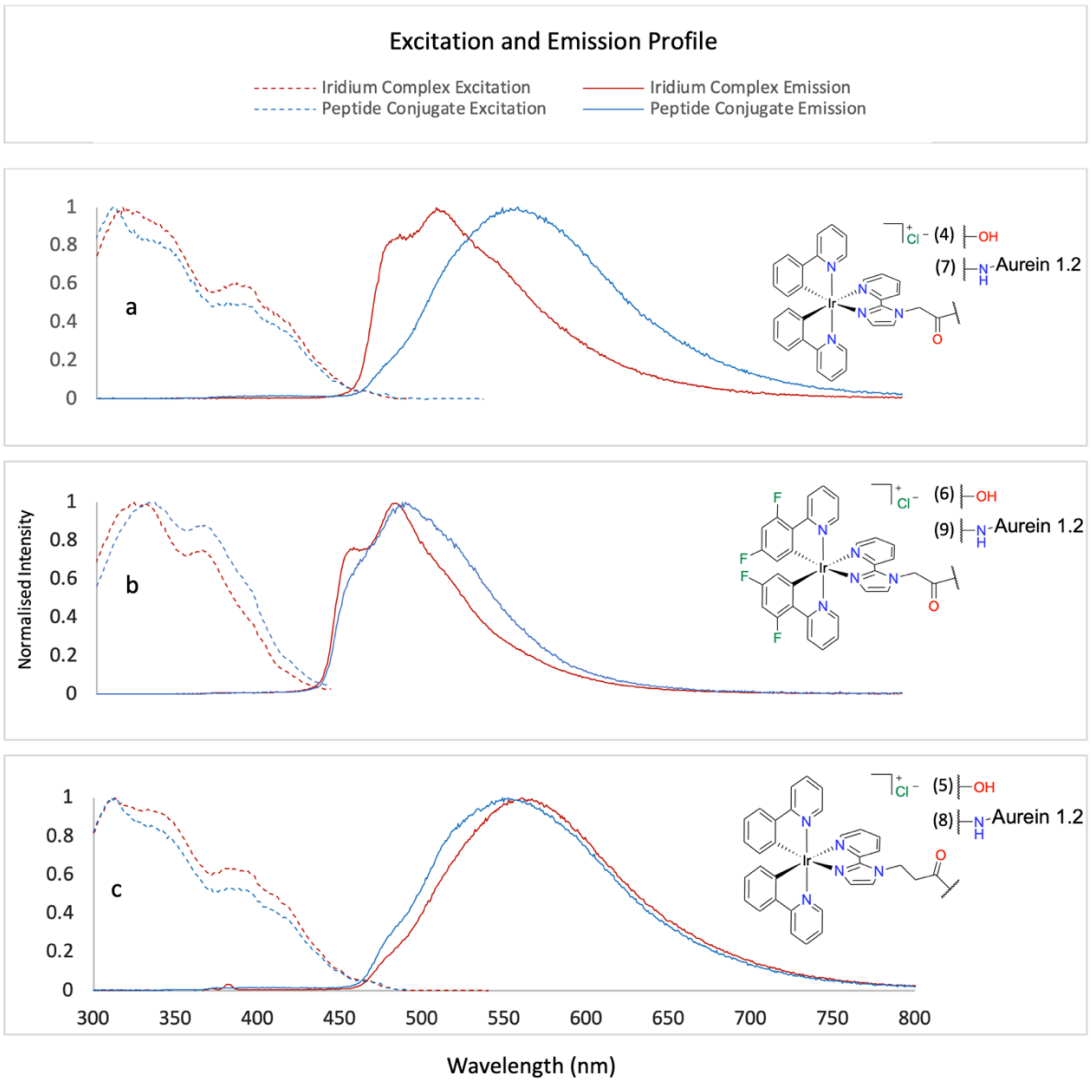

*Figure 23 - Comparison of excitation and emission spectra between the Aurein 1.2-iridium complex conjugates and iridium complexes. Panel (**a**) - Iridium complex **4** and conjugate **7**, (**b**) - Iridium complex **5** and conjugate **8**, (**c**) - Iridium complex **6** and conjugate **9**. Excitation λ: (**4**) – 316 nm, (**5**) – 310 nm, (**6**) – 325 nm, (**7**) – 310 nm, (**8**) – 310 nm, (**9**) – 334 nm. Emission λ: (**4**) – 512 nm, (**5**) – 562 nm, (**6**) – 487 nm, (**7**) – 559 nm, (**8**) – 550 nm, (**9**) – 491 nm.*

A comparison between the iridium complexes **4**, **5** and **6** (red), and the conjugated peptide-complexes **7**, **8** and **9** (blue) is shown in *Figure 23*. In the case of **7**, the emission wavelength has red shifted substantially (47 nm) indicating there is an effect on the emission due to the conjugation to the peptide. The influence of conjugation on the iridium complex emission is similarly apparent in **9,** albeit to a lesser extent (*Figure 23* - ***b***)

The commonality between **7** and **9** is the single methylene group that brings the amide linkage and peptide closer to the iridium complex that may cause a perturbation of the electronic properties of the conjugate, therefore resulting in the observed change in emission spectra of **7** and **9**. Examining the emission profile of **8** in comparison to **5** further supports this hypothesis, as in the case of **8** (*Figure 23* - ***c***), a longer alkyl chain is present and any electronic effects of the conjugated peptide exert a lesser effect on the complex.

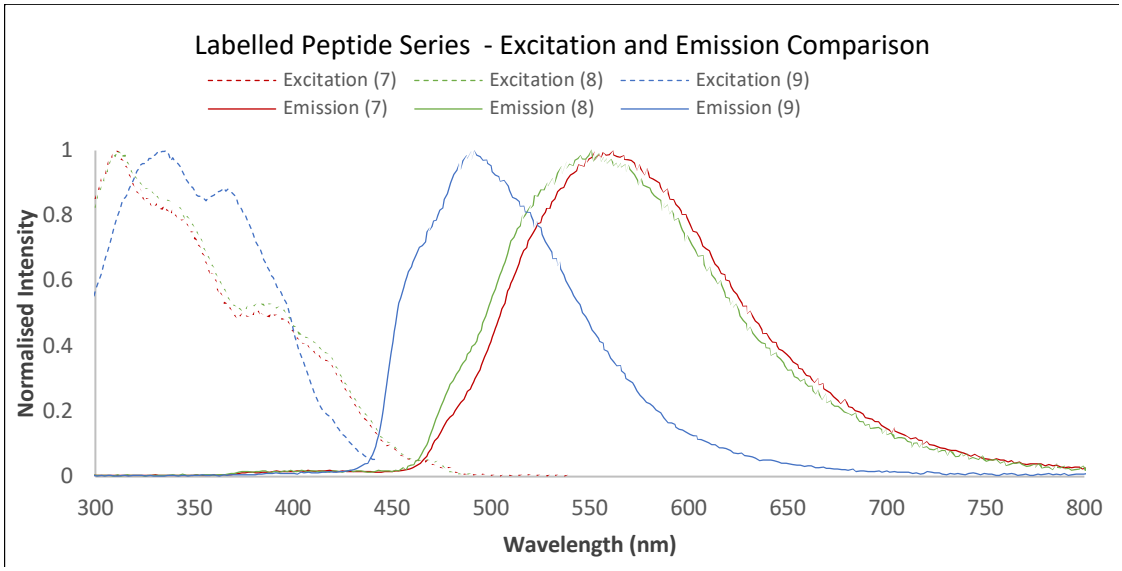

*Figure 24 – Comparison of the excitation and emission profile of the labelled peptide series (**7**), (**8**) and (**9**).*

The comparison of the excitation and emission profiles shown in *Figure 24* for the labelled AMPs highlight the obvious blue shifted emission in **9**. The fluorine groups located on the phenyl ring of the phenyl pyridine ligands of **9** are electron withdrawing groups and are known to cause a blue shift in emission spectra.[77] Iridium complexes are well known for their tuneable emission by functionalising with either electron withdrawing or electron donating groups.[14, 77] The shift in emission toward a shorter wavelength (higher energy), is likely to be due to the electron withdrawing fluorine groups stabilising the HOMO and therefore the energy gap between the HOMO and LUMO is greater, hence a higher energy emission is observed.[78]

Fluorescence Microscopy

Liposomes are self-assembling biological structures that are formed from lipids. The chemical structure of the lipid will determine the type of structure that is spontaneously formed, for example micelles or lipid bilayers.[79]

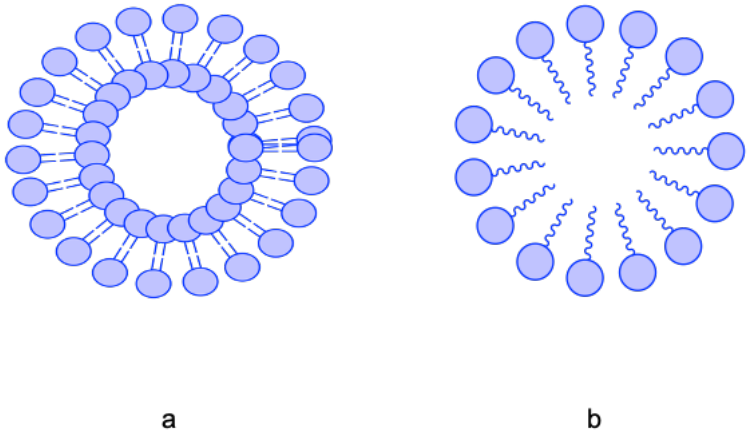

*Figure 25 – (**a**) Model structure of a liposome constructed as a lipid bilayer formed from a phospholipid with two aliphatic chains, (**b**) Structure of a micelle formed from a phospholipid with a single aliphatic chain*

Phospholipids with two aliphatic tails, such as those shown in *Figure 25- **a***, tend to form lipid bilayers, whereas phospholipids with a single aliphatic chain tend to form micelles *Figure 25- **b***.[79] Liposomes are arrangements of lipid bilayers that are organised into spherical shapes with an aqueous environment at their core and outer surface, as seen in *Figure 25- **a***.[79] Therefore, liposomes provide an excellent representation of a biological membrane and can be used as a model to study membrane related processes.[80, 81]

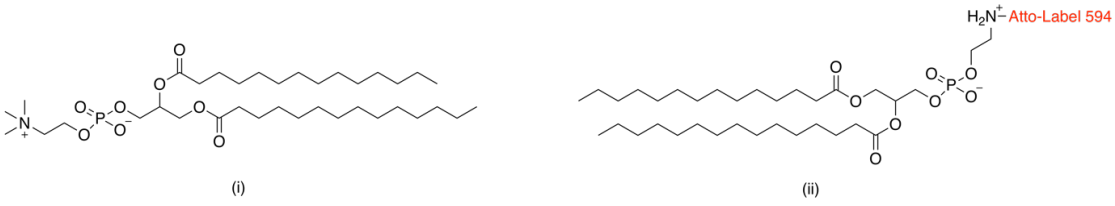

*Figure 26 – Lipid structures, (**i**) DMPC and (**ii**) DMPE-Atto-594 labelled with a red emitting fluorophore*

To study the lipid membrane binding of the labelled AMP **7**, a solution containing luminescent labelled phospholipids was prepared by PhD candidate Ahmed Houri according to the general procedure for Liposome Preparation. The dye "Atto-594", a red emitting fluorophore was selected for this purpose as it offers a contrast in colour to the labelled AMPs allowing both fluorophores to be visualised using fluorescence microscopy. The structures in *Figure 26* show the lipids (**i**) DMPC and (**ii**) DMPE-Atto 594 that were used to form the labelled liposome solution.

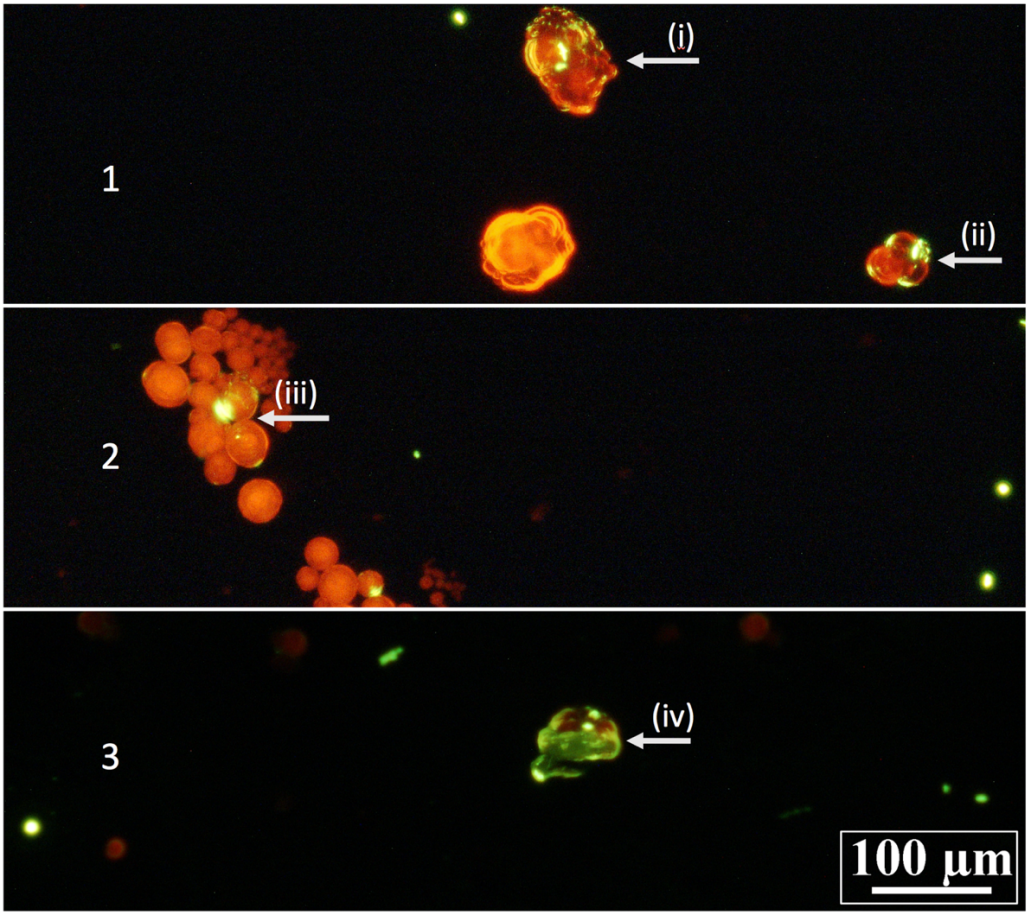

Figure 27 – Fluorescence microscopy composite image of labelled AMP and labelled liposome at 10x magnification. Panels 1, 2 and 3 represent different images taken at the same magnification.

An aqueous solution of the labelled AMP **7** (1 µl, 10 µM) was added to the microscope slide containing the labelled liposome solution and several images were recorded using a fluorescent microscope. The composite diagram in *Figure 27* shows an image taken after both fluorophores were added to the microscope slide (AMP – green, liposome – red). The panels in *Figure 27* will be referred to as *Panel 1, 2* and *3* for reference. *Panel 1* shows two liposome structures (**i**, **ii**) where labelled AMP is clearly visible adhering to the membrane surface. In *panel 1*, structure (**i**) appears to be deformed, which may be due to the slide dehydrating. Another example of the labelled AMP binding to the surface of the liposome can be seen for liposome structure (**ii**). The image shows several liposomes, possibly two or three stacked on top of each other, with the labelled AMP appearing to assume the shape of the membrane. The individual liposome structures are spherical in nature, and in this image it appears that the AMP is covering the surface of the sphere. *Panel 2* shows similar images, with two liposomes seen in (**iii**) showing the AMP spread over the surface area of the liposome structure. In *panel 3* a completely ruptured liposome (**iv**) with a significant amount of the AMP visible on the surface area of the structure can be seen. The rupturing of this liposome was not captured in a series of images, but as a single image after scanning the slide to locate interesting objects. For this reason, it cannot be assumed the peptide caused the rupturing of the liposome, however it can be considered as a possibility.

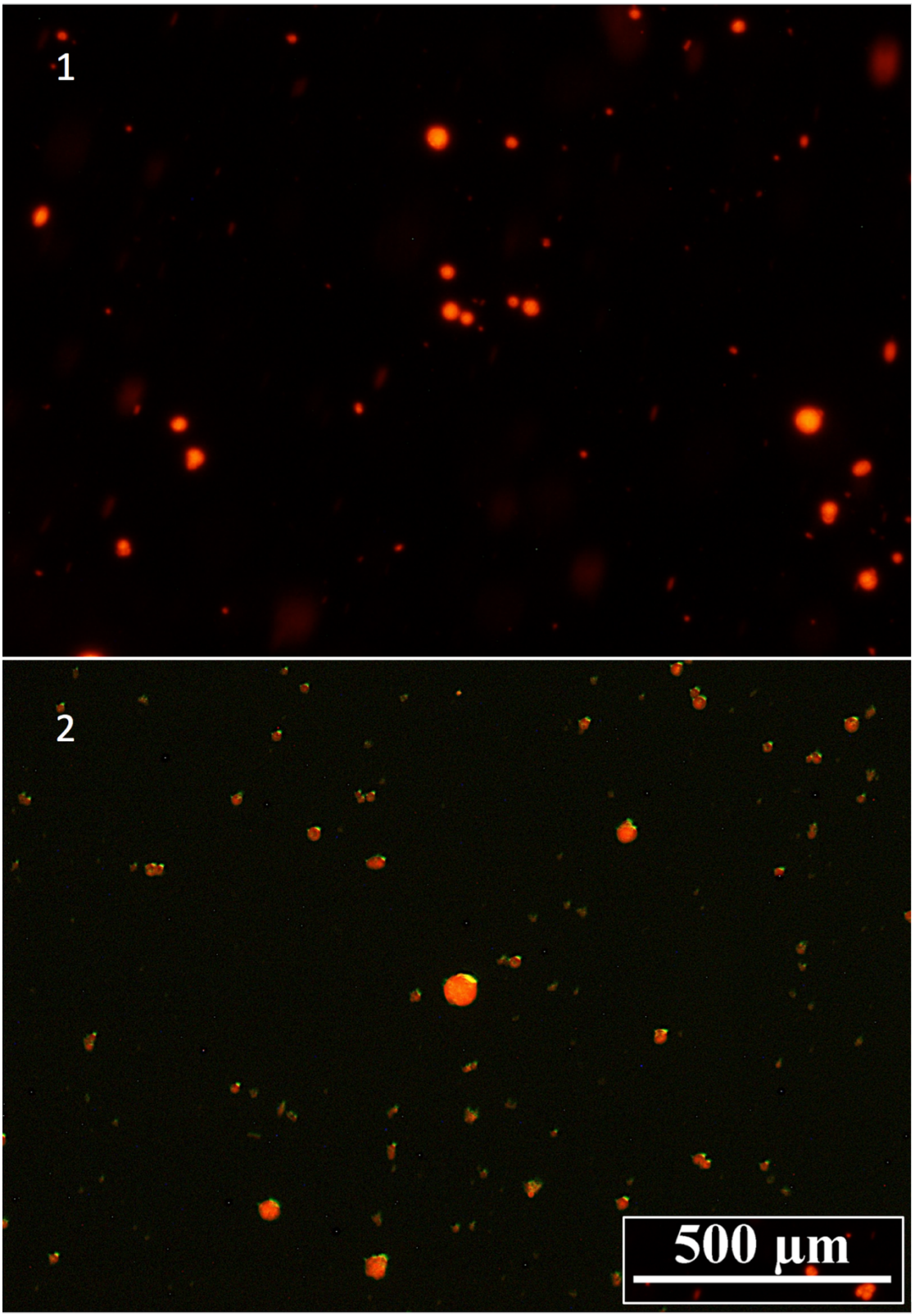

Figure 28 - Fluorescence microscopy image showing a comparison of labelled liposomes only (1) and labelled liposomes and labelled AMP (2) at 4x magnification.

Figure 28 – **1** shows an image of liposome only (without AMP) and in contrast *Figure 28* – ***2*** shows the liposomes after the labelled AMP was added to the microscope slide. This comparison demonstrates that when the AMP was added to the liposome solution, the AMP appears to be interacting with the liposome membrane in most cases. This effect as seen in *Figure 28* – ***2*** is

clearly not the result of simple diffusion of the AMP through the solution. The flux of liquid in *Figure 28 – **2*** appears to be traveling in a single direction, and this is due to adding a liquid containing the AMP to the microscope slide at a single point, and generating a flowing effect in the droplet on the surface of the microscope slide. This effect is quite normal and to be expected when mixing to liquids on the surface of a microscope slide.

In summary, the images show a spreading of the AMP across the liposome membrane and support the expected observations for a carpet binding mechanism, however a more thorough study using a confocal microscope is necessary to obtain higher quality images that could further support this hypothesis.

Chapter 3. Preparation of Hydroxamic Amino Acid

Synthetic Strategy

The preparation of a SPPS ready synthetic amino acid that contains a hydroxamic acid sidechain was planned due to the excellent chelating abilities of hydroxamate ligands toward hard metals.[44] To achieve this structure glutamic acid was selected as a framework to build the molecule upon due to its sidechain containing a carboxylic acid that is amendable to condensation with hydroxylamine to form the benzyl protected hydroxamic amino acid.

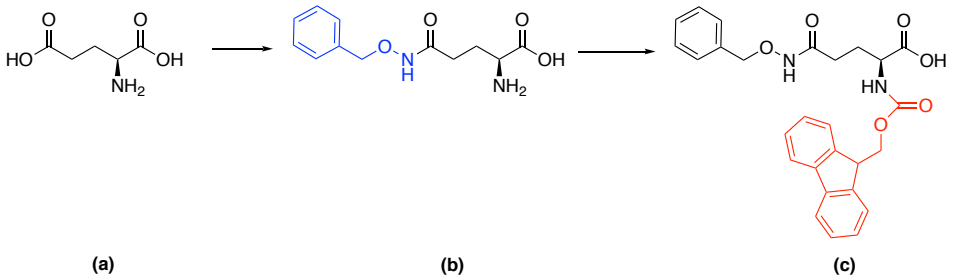

*Scheme 6 - Synthetic strategy outlining the construction of a SPPS ready unnatural amino acid bearing a benzyl protected hydroxamic acid unit (Glutamic acid – black, benzyl protected hydroxyl amine – blue, Fmoc protection group – red). Structure (**a**) glutamic acid, (**b**) benzyl protected hydroxamic amino acid, (**c**) Fmoc-ready hydroxamic amino acid*

The final step required to enable SPPS compatibility of the hydroxamic amino acid (*Scheme 6 – **b***) is installing an Fmoc protecting group to the α-amine nitrogen atom (*Scheme 6 – **c***). This final modification will allow the synthetic amino acid to be used on an automated peptide synthesiser using standard Fmoc SPPS chemistry. A further point to note is the hydroxylamine retains its benzyl protection group (*Scheme 6 – **b, c***), this is required to restrict unwanted reactivity during the SPPS process and can be removed under standard hydrogenation conditions upon completion of the peptide synthesis.

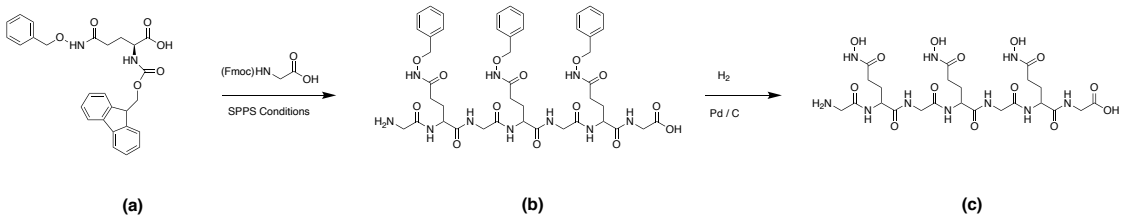

*Scheme 7 - Reaction scheme for the preparation of a peptide segment with three bidentate hydroxamic acid ligands that will act as a chelator for octahedral metal cations. (**a**) Hydroxamic amino acid monomer, (**b**) Tripeptide consisting of three hydroxamic amino acid monomers retaining benzyl protection, (**c**) Final hexadentate peptide segment*

The first step in the synthesis of the peptide segment is the elongation of the hydroxamic amino acid (HAA) monomer (*Scheme 7 – **a***). This occurs by programming the automated peptide synthesiser with the desired sequence, in this case *GLY-HAA-GLY-HAA-GLY-HAA-GLY* using standard SPPS conditions to afford the peptide segment as shown in (*Scheme 7 – **b***).

Once the segment is completed it can be liberated from the solid phase and subjected to standard hydrogenation conditions to yield the peptide segment containing the hexadentate hydroxamic acid chelator (*Scheme 7 – **c***). The peptide segment can then coordinate in an octahedral geometry with gallium(III). Due to the modular nature of peptides, the chelating segment can be attached to any complementary peptide or protein that can act as a targeting sequence, potentially leading to new and exciting imaging and therapeutic compounds.

Hydroxamic Acid Synthesis

Benzyl protection of the hydroxyl group of hydroxyl amine was installed to restrict reactivity to the nitrogen when undergoing further chemistry with **12**, **13** and **14**. The hydroxy group present on hydroxyl amine is capable of acting as a nucleophile, therefore the installation of a protection group is important to limit nucleophilic reactivity to the amine group.

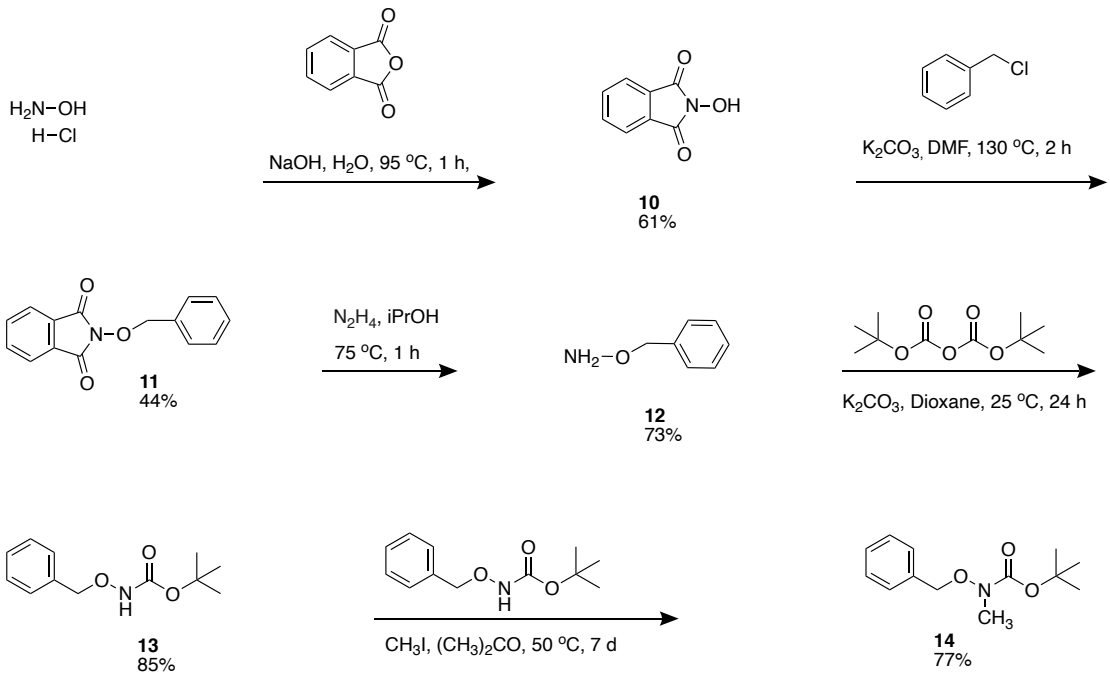

Scheme 8 – Reaction scheme showing the synthesis of the benzyl protected hydroxylamine and the N-methylated hydroxylamine

The reaction pathway for installing the benzyl protection is shown in *Scheme 8*. Compound **10** was prepared by the reaction of hydroxylamine and phthalic anhydride to synthesise *N*-hydroxyphthalimide **10**.

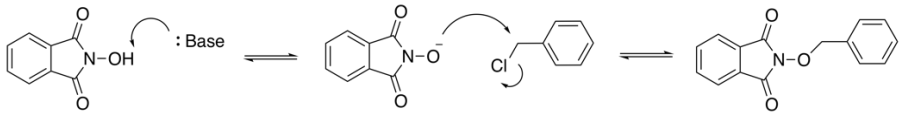

Scheme 9 – Nucleophilic substitution where N-hydroxyphthimide is acting as the nucleophile

In the following reaction, to form **11**, the hydroxyl proton of **10** was removed by the addition of the base K_2CO_3 and the reaction proceeds via an nucleophilic substitution mechanism as shown in *Scheme 9*. The following step utilises hydrazine to liberate the benzyl protected hydroxylamine **12** from the phthalimide structure of **11**. Further reactions **13** and **14** were carried out to install an *N*-methyl group on the amine of **12**. The addition of the methyl group can enhance the nucleophilic nature of the amine and therefore may improve reactivity in further steps of the synthetic protocol if necessary.

Hydroxamic Amino Acid Synthesis

The total synthetic pathway to obtain the Fmoc protected hydroxamic acid utilises glutamic acid as a framework to build upon. To allow the successful condensation between **12** and glutamic acid, several protection and deprotection steps were required to limit the reactivity to the γ-carboxylic acid (R-group) of the amino acid.

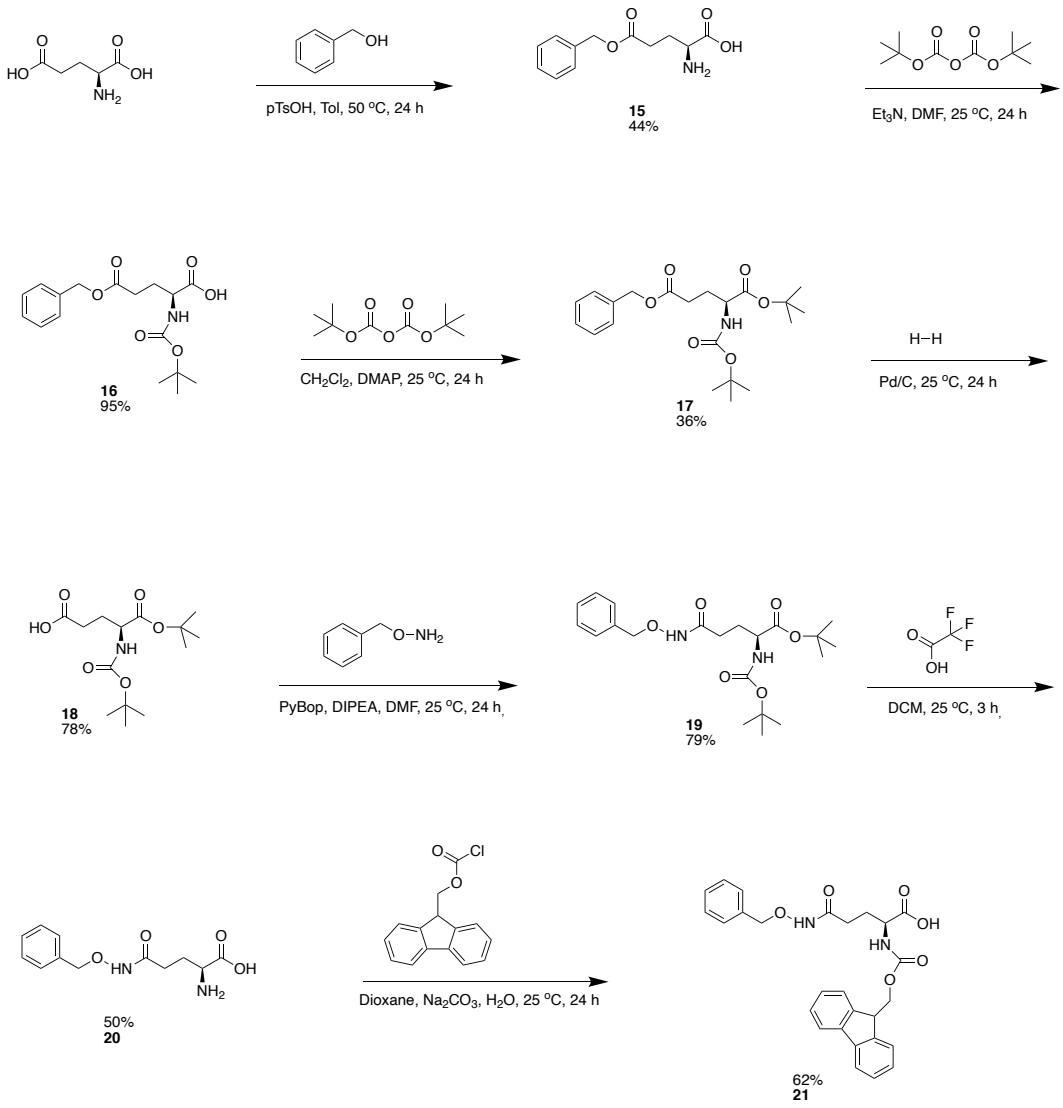

Scheme 10 – Reaction scheme showing the synthesis of the SPPS ready hydroxamic amino acid

The two carboxylic groups in glutamic acid are referred to as the α-carboxylic acid, as found in all amino acids, and the γ-carboxylic acid located on the sidechain of glutamic acid. The sidechain in glutamic acid is attached to the α-carbon of the amino acid via two methylene groups allowing free rotation about their bonds, generating flexibility that is well known to be beneficial for effective chelation.[40, 44]

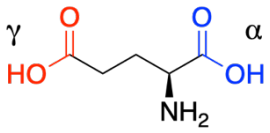

Figure 29 – Glutamic acid showing the α-carboxylic acid in blue and the γ-carboxylic acid in red

In order to form the hydroxamic acid moiety exclusively on the γ-position as shown in *Figure 29* - **γ**, the α-carboxylic acid and α-amine groups must be protected to avoid any unwanted reactivity occurring during the condensation of the γ-carboxylic acid and the hydroxyl amine **12** as seen in *Scheme 10* - ***19***. Central to the success of this synthetic strategy is the ability to selectively protect each carboxylic acid group in glutamic acid.

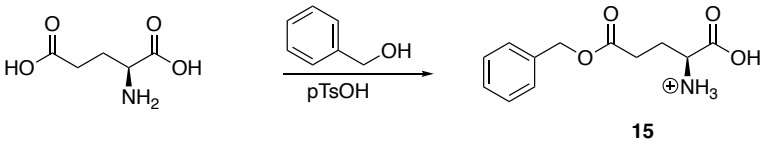

15

Scheme 11 – The selective benzyl ester protection of the γ-carboxylic acid in glutamic acid

An acid catalysed esterification was utilised for the selective protection of the γ-carboxylic acid that was made possible due to the protonation of the α-amine nitrogen resulting cationic charge rendering the α-carboxylic acid less reactive than the γ-carboxylic acid (*Scheme 11*).[82, 83] The selective protection of the γ-carboxylic acid group then allows the installation of a Boc protecting group at the α-amine position as seen in *Scheme 10* - **16.** In the following reaction, a t-butyl ester protecting group is installed on the α-carboxylic acid of **16** resulting in compound **17**. The order of these reactions appears to have no impact on the overall success of the synthetic pathway, however in the case of this synthesis the α-amine was protected first.

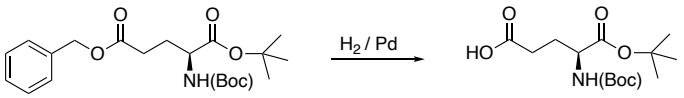

17 **18**

Scheme 12 – Removal of the benzyl ester from the γ-carboxylic acid group on glutamic acid after hydrogenation, with the α-amine and α-carboxylic acid groups retaining their protective groups

Due to the Boc and t-butyl ester protecting groups being acid labile, they are orthogonal toward the benzyl ester protection that was initially installed on the γ-carboxylic acid, and therefore the two acid labile groups can removed under different chemical conditions to that of the benzyl ester. Standard hydrogenation conditions can be used to remove the benzyl ester from the γ-

carboxylic liberating the free γ-carboxylic acid for further chemical reactivity as seen in *Scheme 12*. The liberated γ-carboxylic acid can be condensed with the previously synthesised benzyl protected hydroxylamine **12** to form the hydroxamic acid.

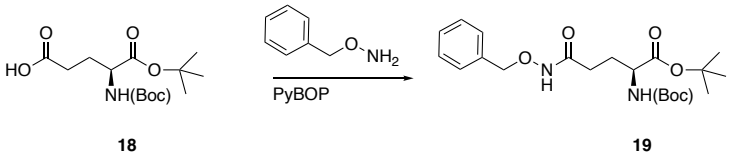

18 **19**

Scheme 13 – Condensation reaction between glutamic acid and hydroxylamine to form a hydroxamic amino acid

There are several strategies and numerous coupling reagents available to form amide bonds, however in this case PyBOP was initially selected and yielded positive results (*Scheme 13*), however in future studies other coupling reagents could be investigated to attempt to improve yields. The selective deprotection of **19** is carried out under acidic conditions due to Boc and t-butyl ester groups being acid labile. The benzyl protecting group is stable in the presence of TFA and therefore persists under these conditions.

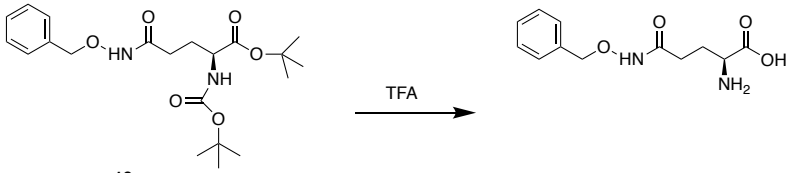

19 **20**

Scheme 14 – Selective deprotection of the acid labile t-butyl ester and Boc groups using TFA

After treatment with TFA, the α-carboxylic acid and α-amino nitrogen are liberated while the hydroxyl amine moiety retains its protecting group as shown in *Scheme 14*. Upon the formation of **20**, the amine group can be Fmoc-protected, to produce the appropriately protected amino acid that is ready for use on an automated Biotage peptide synthesiser.

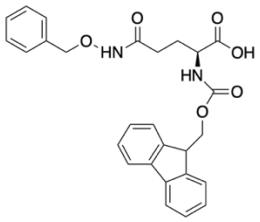

Figure 30 – Target Molecule: Synthetic amino acid equipped with a hydroxamic acid moiety and Fmoc protected amine group designed for automated solid phase peptide synthesis compatibility

The synthetic amino acid (*Figure 30)* can then be incorporated into a peptide sequence using standard SPPS conditions while the hydroxyl moiety retains benzyl protection to eliminate the potential for unwanted reactivity. Once prepared, hydrogenolysis of the peptide segment will be used to remove the benzyl acid protecting group, thereby liberating the free hydroxamic acid moiety within the peptide segment. The hydroxamic amino acid is bidentate by nature, and

therefore the peptide segment requires three subunits in its structure to form a hexadentate chelator. This will allow the peptide segment to chelate hard octahedral metals, such as gallium(III) and potentially lead to the development of novel peptide-based radiopharmaceutical agents.[42] Due to restricted access to the laboratory throughout the year, **21** was unable to be integrated into a peptide, however computational modelling was carried out on the proposed peptide segment.

Computational Modelling

Initially when considering the design of a peptide sequence containing three hydroxamic amino acid residues (monomers referred to as HAA), it became apparent that molecular spacing groups separating each subunit were required.

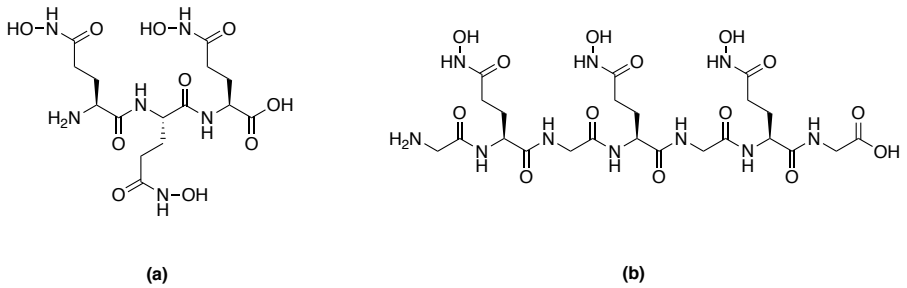

*Figure 31 – (**a**) Tripeptide composed of three hydroxamic acid bearing amino acids, (**b**) Revised structure of the peptide containing three hydroxamic acid moieties separated by glycine residues*

This became evident when computational studies using density functional theory (DFT) to optimise the geometry of the proposed tri-hydroxamic acid amino acid peptide (*Figure 31 – **a***) chelated to gallium(III) failed to produce a reasonable octahedral geometry about the metal, instead a highly distorted structure was obtained. This suggested there may be a problem with the limited flexibility in the structure shown in *Figure 31 – **a*** that was inhibiting the formation of the correct octahedral geometry characteristic of a Ga(III) complex.[42] In an attempt to remedy the problem glycine residues were added in an alternating fashion into the peptide segment (*Figure 31 - **b***) and geometry optimisation calculations were repeated, subsequentially succeeding in producing an octahedral coordination geometry about the metal cation.

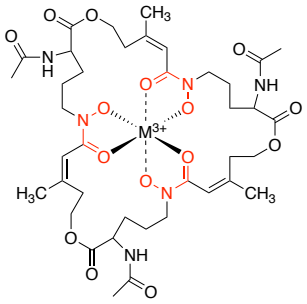

Figure 32 – The natural siderophore triacetylfusarinine: An excellent hexadentate chelator for hard metals, secreted by various fungus species. Hydroxamate moieties are highlighted in red

Natural siderophores utilise molecular spacings between their chelating groups facilitating an increase in flexibility within their structures, allowing the chelator molecules to assume the appropriate geometry needed to form a stable complex with a metal cation.[23, 24] The hexadentate siderophore triacetylfusarinine as shown in *Figure 32* is known to be an excellent chelator of hard metals such as iron(III) and gallium(III). The selectivity for these hard metals is partially due to the high degree of flexibility within the structure.[26, 41, 84] Therefore the molecular structures of siderophores such as triacetylfusarinine can serve as an inspiration into the potential design requirements of a synthetic peptide segment that has a high affinity for chelating hard metals such as ^{68}gallium.

Geometry Optimisation

a

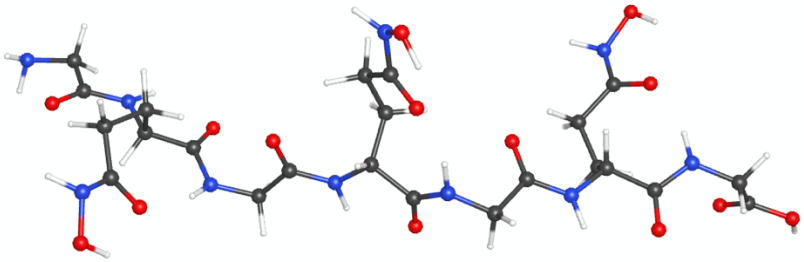

b

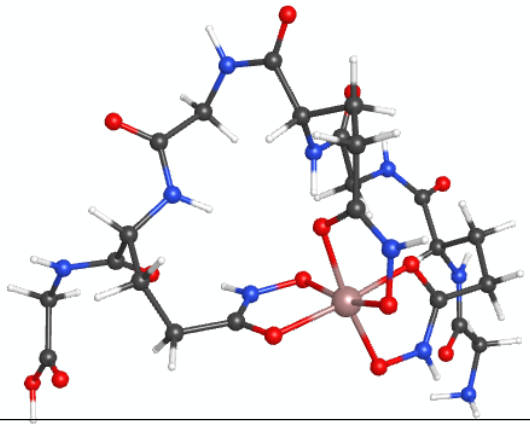

*Figure 33 – Computationally generated 3D structures of (**a**) linear peptide sequence (GLY-HAA-GLY-HAA-GLY-HAA-GLY), (**b**) peptide segment chelated to gallium, both structures obtained following geometry optimisation DFT calculations using B3LYP level of theory and Routine: 6-31G(d) basis set and WebMO Enterprise software*

Computational modelling was undertaken on the revised structure of the peptide segment as shown in *Figure 31* - ***b***. The peptide in its linear form (*Figure 33 – **a**)* was compared to the peptide-gallium complex (*Figure 33 – **b**)* using various DFT calculations with WebMO Enterprise software.[85] Initially geometry optimisations were run on both structures, followed by vibrational frequency calculations.

Geometry optimisation DFT calculations were carried out using a B3LYP level of theory and Routine: 6-31G(d) basis set on both molecules shown in *Figure 33* – (***a***, ***b***).[85] These calculations rendered the linear peptide segment (*Figure 33* – ***a***) and the complex (*Figure 33* – ***b***) successfully with the expected octahedral geometry of the peptide-gallium complex.[42] The optimised geometries were then used for vibrational frequency calculations using the previously calculated optimised geometry.[85] The successful completion of the geometry optimisation calculation of the peptide shown in *Figure 33* – ***b*** offered an excellent insight into the design requirements for the proposed structure. The glycine spacing groups and subsequent additional flexibility appear to be critical in forming the correct geometry about the metal ion and therefore the function of the peptide segment as an effective hexadentate chelator of gallium(III).

Energetics

Vibrational frequency DFT calculations were carried out on the structures seen in *Figure 33* (***a***, ***b***) and additionally on gallium(III) and the H^+ cation using a B3LYP level of theory and Routine: 6-31G(d) basis set.[85]

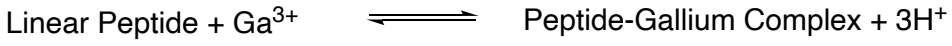

Scheme 15 – Basic reaction showing the formation of the hydroxamic amino acid peptide gallium(III) complex

The free energies of each species were calculated to determine the energy change of the reaction as shown in *Scheme 15.* Metal ions in a solvent rich environment form complexes with ligands, counter ions or solvent molecules. For the peptide chelator to form a complex with gallium(III), the previously bound ligands must be displaced from the metal cation, and as a consequence there is an intrinsic energetic cost for that dissociation to take place.[86]

Table 5 – DFT computational gas phase calculation of free energy values generated by WebMO Enterprise software using B3LYP level of theory and Routine: 6-31G(d) basis set

Compound	Free Energy (Hartree)	Total	ΔG° KJ / mol
Linear Peptide	-2499.38	-2499.38	
Gallium(III)	-1920.79	-1920.79	
Peptide-Gallium Complex	-4420.69	-4420.69	
Proton	-0.01	-0.03	
			-1458.2

The direct comparison of the free energy of gallium(III) and the peptide-gallium complex (*Table 5*) in the gas phase without considering solvent effects and the displacement of original ligands is less accurate, however can provide an indication that the chelation of the gallium(III) ion with the hexadentate peptide segment (*Figure 33)* will be favourable, as to be expected with chelating molecules.[87]

Chapter 4. Conclusion and Future Work

Preliminary studies were undertaken to optimise several processes that were critical to the successful synthesis of the antimicrobial peptides. This work included optimising the configuration and reaction conditions on an automated Biotage peptide synthesiser and optimising the purification method using HPLC.

Aurein 1.2 and Citropin 1.1 were successfully synthesised using automated solid phase peptide synthesis and then purified using reverse phase HPLC. The Aurein 1.2 microwave – room temperature comparison study showed the reaction time was significantly lowered and the purity of the crude peptide was increased when utilising microwave heating for the coupling steps during automated SPPS on a Biotage peptide synthesiser. Aurein 1.2 was used in a series of reactions to form conjugates with luminescent iridium complexes. Three conjugates were successfully prepared **7**, **8** and **9** and their spectroscopic properties examined and compared to those of the iridium complexes **4**, **5** and **6**. The yields obtained for the peptide conjugates were relatively low and therefore further work is necessary to develop a more effective coupling reaction condition to enhance the efficiency of conjugate formation. The attempts at coupling Citropin 1.1 with the iridium complexes failed in all cases, however further method development using Aurein 1.2 as a model may solve this problem in the future. The luminescent AMP **7** was then used to investigate the interactions of this molecule with membranes in the form of liposomes using fluorescent microscopy. These studies showed visible binding interaction between the peptide and the liposomes.

A synthetic scheme was developed for the preparation of a hydroxamic acid bearing amino acid and the desired Fmoc-protected compound was prepared. Unfortunately however, due to highly limiting time restrictions on laboratory access during 2020, this component of the project remains ongoing. Computational studies were carried out on the proposed metal chelating peptide structure and showed favourable energetics.

Future work developing the method for the efficient coupling of the luminescent carboxylic acid functionalised iridium complexes and peptides is necessary to improve yields. A series of careful experiments that comparing yields using different coupling reagents would be an effective way to determine whether there are inefficiencies in using HCTU for conjugating iridium complexes to AMPs.

Investigating microwave heating for the peptide-iridium complex conjugate formation would be an interesting study, as it is possible the peptides undergo internal aggregation as they are elongated on the resin surface that may inhibit their reactivity. Microwave heating may provide a mechanism to promote de-aggregation and enhance the coupling efficiency.

Investigating interactions of the labelled AMP with the liposome over time would be useful to attempt to capture a series of images of a liposome being lysed in the presence of an AMP.

Additionally, investigating the effect of increasing concentrations of AMP would assist in determining the threshold concentration for liposome membrane lysis. Additionally, using confocal microscopy would be beneficial to increase the resolution and clarity of the images during the fluorescence microscopy studies.

Studies to investigate the level of internal aggregation of the AMP peptides while held on the resin would be beneficial. These studies will aid in understanding the possible improvements of using microwave heating for the preparation of AMP peptide sequences and labelled AMPs. Additionally an investigation into the optical purity of the finished peptides would be an important aspect of future microwave synthesis studies to fully understand whether microwave heating can cause an increase in racemisation during the synthesis, and if so, to what extent.

Synthesis of metal chelating peptide segments using the new unnatural peptide bearing an hydroxamic acid group will be an important future study. This peptide synthesis once complete will allow metal chelating functionality to be directly incorporated into a peptide to facilitate the binding of metals that have useful radioisotopes such as gallium-68.

Chapter 5. Experimental

Instrumentation and Equipment

NMR spectra were recorded on a Bruker 400 MHz NMR Avance III spectrometer with a 5 mm BBFO probe, (^{1}H at 400.13 MHz and ^{13}C at 100.62 MHz) at standard conditions. NMR chemical shift values were denoted as δ in parts per million (ppm) and referenced to the solvent signal (d_6-DMSO: ^{1}H at 2.50 ppm, ^{13}C at 39.51 ppm; $CDCl_3$: ^{1}H at 7.27 ppm, ^{13}C at 77.25 ppm. Coupling constants (J) were recorded in Hz. Abbreviations ^{1}H-NMR data: singlet (s), doublet (d), triplet (t), quartet (q), multiplet (m).

Mass spectra were obtained using an Agilent 6530 Accurate-Mass Q-TOF LC/MS with a 1260 Infinity II vial sampler. All Peptide and peptide-complex samples were acidified with formic acid to a pH of 4 and run in a solvent system of ACN and H_2O (50:50).

SPPS was carried out on a Biotage® Initiator+ Alstra automated peptide synthesiser

Peptide purification was carried out using a Shimadzu reverse phase HPLC with a SPD-M20A (Photodiode Array Detector) using a gradient method. The solvent systems used were: A (0.1% TFA in H_2O) and B (0.1% TFA in CH_3CN). Analytical studies were undertaken using an Onyx Monolythic C_{18}, 100 × 4.6 mm, 1 mL min^{-1} flow rate. Semi-prep work was done using an Onyx Monolythic C_{18}, 100 × 10 mm, 5 mL min^{-1} flow rate. Fractions were collected using a FRC-10A automatic fraction collector using a 200 µL delay.

UV-visible absorbance spectra were recorded with an Agilent Carey Fluorescence Spectrophotometer. Excitation, emission spectra were collected using a HORIBA Scientific Nanolog (HORIBA Jobin Yvon IBH) and iridium complexes and peptide-iridium-complexes were dissolved in ACN and measured at 10 uM concentrations. All UV-vis and absorbance measurements were taken by Pria Ramkissoon.

Centrifuge work was carried out on an Eppendorf Centrifuge 5804-R equipped with a 4 × 100 mL Eppendorf tube (A-4-44) rotor at 4300 RCF for 10 minutes.

All lyophilising was carried out on a Labconco FreeZone Freeze Drier.

Fluorescence Microscopy was undertaken using a Nikon Eclipse TS-100 fluorescence microscope using a UV lamp excitation source.

Rendered Chemical Images (*Figure 33*) were created with WebMO software, www.webmo.net

Peptide Chemistry

General Procedure

Peptide Synthesis

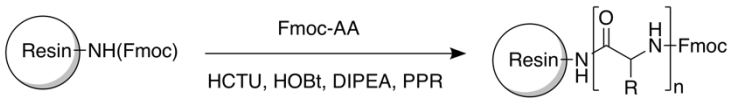

Scheme 16 – General conditions for solid phase peptide synthesis (SPPS)

Solid phase peptide synthesis was carried out using a Biotage® Initiator+ Alstra automated peptide synthesiser. 30 mL Biotage synthesis vials were used in all cases. The solid phase was Chem-Impex International Rink Amide resin (0.47 mmol g^{-1} loading) that was used at various scales. The resin was swollen for 2 hours with either DMF or NMP before commencing synthesis in all cases. Chem-Impex Fmoc-(L)-amino acids were used in all cases at a concentration of 0.5 M in 4 eq. to resin loading. Coupling reagents HCTU (0.5 M) and HOBt (2.0 M) were used in 4 eq. to resin loading. DIPEA in DMF solution was used at a concentration of 0.2 M in 6 eq. to resin loading. The Fmoc-cleavage cocktail (20% Piperidine in DMF) was used in 72 eq. to resin loading for Fmoc group cleavage. The solvent system for the synthesis was DMF in all Fmoc-amino acids excluding phenylalanine where NMP was used. Initial coupling of the first Fmoc-amino acid to the resin was reacted for 10 hours, all remaining monomers were reacted for 1 hour. All reactions were carried out at room temperature. Fmoc deprotection was 15 minutes in all cases. Cleavage of the peptide from the resin and amino acid sidechain protection was carried out with 10 mL TFA (9 5%) / TIPS (0.5%) for 45 minutes in all cases.

A 30 mL Biotage reactor vial containing swollen resin was placed in the reactor of the Biotage Initiator+ Alstra. Fmoc-amino acids, coupling reagents, 20% piperidine solution and DIPEA solution were placed in the manifold of the synthesiser according to the programming layout. The resin was treated with Fmoc-cleavage cocktail (15 mins). The first Fmoc-amino acid in the sequence was reacted overnight (10 hours), then treated with Fmoc-cleavage cocktail (15 min). The process was repeated for each coupling step (1 hour) and deprotection steps (15 mins). The resin was then washed with DCM (3 mL × 5), ether (3 mL × 5) and dried under reduced pressure.

Cleavage / Deprotection

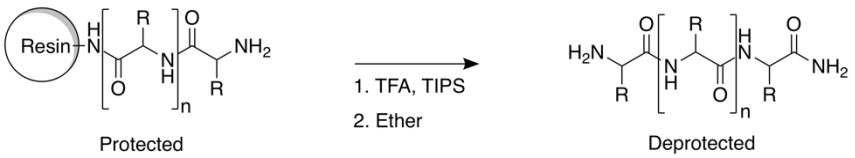

Scheme 17 – General conditions for the cleavage of the peptide from the solid resin and deprotection of amino acid sidechain protection groups, followed by a precipitation using ether

The resin was treated with TFA/TIPS cleavage cocktail and placed on an agitator or spinning wheel for 45 minutes. The filtrate was collected and the resin washed with cleavage cocktail twice (2 × 1 mL). The acidic aqueous filtrate was subjected to a slow stream of N_2 reducing the volume to ~ 1 mL. Ether was added (10 mL). The suspension was centrifuged at 4300 RCF for 10 mins. The ether was decanted and the pellet resuspended in CH_3CN and H_2O (50:50, 2 mL). The solution was snap frozen in liquid nitrogen and lyophilised.

Purification

Analytical: The crude peptide (1 mg) was dissolved in (1 mL) of CH_3CN and H_2O (50:50) and filtered using a 0.45 µm HPLC syringe wheel filter. The peptide solution was analysed using Reverse phase HPLC with a gradient method (**A** - 0.1% TFA in H_2O) and (**B** - 0.1% TFA in CH_3CN) 10-90% over 20 minutes. Each fraction was analysed using mass spectroscopy to identify product containing fractions. Semi-Preparative: The crude peptide was dissolved in minimal CH_3CN and H_2O (50:50) and filtered. Semi-preparative reverse phase HPLC was carried out with a gradient method (**A** - 0.1% TFA in H_2O) and (**B** - 0.1% TFA in CH_3CN) over 30 minutes to obtain the pure peptide.

Peptide Labelling with Luminescent Iridium Complexes

Aurein 1.2 (**2**), (300 mg) and Citropin 1.1 (**3**), (200 mg) were prepared according to the general procedure for peptide synthesis, and retained on the Rink Amide resin. The Fmoc group at the *N*-terminus was cleaved by treating the peptide on the resin with 20% Piperidine in DMF. The resin was dried thoroughly and weighed to calculate a scaling factor to determine portion size for further reactions. Resin calculation for (**2**): Theory yield 300 mg, dried resin weight 0.7451 g, ∴ scaling factor is 2.48. Resin calculation for (**3**): Theory yield 200 mg, dried resin weight 0.4471 g, ∴ scaling factor is 2.24. Rink amide resin with attached peptide was measured with consideration of the conversion factor and placed in a 10 mL Biotage reaction container with DMF (~ 2 mL) and the resin was left to swell for an hour. The DMF was removed under reduced pressure to afford the swollen resin. The iridium complex of choice (4 eq.) was weighed in a 10 mL sample vial equipped with magnetic stir bar and charged with minimal DMF and DIPEA (8 eq.) and left to stir until fully dissolved. HOBt (4 eq.) and HCTU (4 eq.) were added to the stirring solution and generally dissolved instantly. The solution was added to the swollen resin and the 10 mL Biotage container sealed and placed on a rotating wheel for ~ 2 days. The resin was treated as per the general procedure for cleavage and purification to afford the pure peptide.

Liposome Preparation

Labelled AMP (**7**) was prepared by dissolving 0.1 mg in 1 mL of milliQ water for use as a stock solution 46 µM which was used to further dilute to 10 µM solution for experimentation.

Labelled liposome solutions were prepared by Ahmed Houri. 1,2-Dimyristoyl-sn-glycero-3-phosphocholine (DMPC), were dissolved in chloroform and 0.1% DMPE-Atto-597 labelled liposome was added to the 10 µmol DMPC solution. The solvent was evaporated under a gentle stream of N_2 and vacuum desiccated overnight. Liposomes were hydrated in a PBS phosphate-buffered saline solution (100 mM NaCl at pH 6.9) at 37 °C for 30 min, vortexed for 1 min and briefly sonicated for 1 min to yield a mixed population of labelled vesicles.[88]

Synthesis

(1): AGAG

AGAG (**1**) was synthesised (110 mg, 0.4 mmol scale) according to the general peptide synthesis procedure with the following modifications. Fmoc-AAs (0.7 M, 3 eq.), HCTU (0.5 M, 3 eq.), HOBt (0.5 M, 3 eq.), DIPEA (0.2 M, 6 eq.). (Crude yield 98%) **HRMS: (**Calcd. for $C_{10}H_{18}N_4O_5$: 274.1277) $[M]^+$ 274.1513, $[M\text{-}H+Na]^+$ 297.1335.

(2): Aurein 1.2

Aurein 1.2 (**2**) was synthesised (147 mg, 0.1 mmol scale) according to the general peptide synthesis procedure and purified according to the general purification procedure. (Purified yield 91.3 mg, 62%) **HRMS:** (Calcd. for $C_{71}H_{114}N_{16}O_{18}$:1478.8497) $[M]^+$ 1478.8497, (Deconvoluted spectrum).

(3): Citropin 1.1

Citropin 1.1 (**3**) was synthesised (200 mg, 0.1 mmol scale) according to the general peptide synthesis procedure. (No yield available) **HRMS:** (Calcd. for $C_{76}H_{131}N_{19}O_{19}$:1613.9869) $[M]^+$ 1613.99, (Deconvoluted spectrum).

(7): Aurein 1.2 + (4)

Aurein 1.2-iridium complex (**7**) was synthesised (25 mg, 0.017 mmol scale) according to the general peptide labelling procedure and purified according to the general purification procedure. (Purified yield 2.8 mg, 8%) **HRMS:** (Calcd. $C_{103}H_{137}IrN_{21}O_{19}$+:2166.0057) $[M\text{-}H]^+$ 2165.00, (Deconvoluted spectrum).

(8): Aurein 1.2 + (5)

Aurein 1.2-iridium complex (**8**) was synthesised (25 mg, 0.017 mmol scale) according to the general peptide labelling procedure and purified according to the general purification procedure. (Purified yield 2.0 mg, 5%) **HRMS:** (Calcd. $C_{104}H_{139}IrN_{21}O_{19}$+ :2180.0213) $[M\text{-}H]^+$ 2179.01, (Deconvoluted spectrum).

(9): Aurein 1.2 + (6)

Aurein 1.2-iridium complex (**9**) was synthesised (25 mg, 0.0169 mmol) according to the general peptide labelling procedure and purified according to the general purification procedure. (Purified yield 1.0 mg, 4%) **HRMS:** (Calcd. $C_{103}H_{133}F_4IrN_{21}O_{19}$+:2237.9680) $[M-H]^+$ 2236.96, (Deconvoluted spectrum).

Organic Synthesis

Preparation of Benzyl Protected Hydroxamic Acid

(10): 2-hydroxyisoindoline-1,3-dione

10

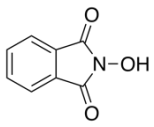

A 2 L single neck round bottom flask was charged with NaOH (24 g, 0.6 mol). The NaOH was dissolved in 400 mL of water and the flask was cooled. slowly, hydroxylamine (42 g, 0.6 mol) was added in small portions until dissolved. Phthalic anhydride (82 g, 0.55 mol) was added with vigorous stirring. The flask was heated to 95 °C and the solution became homogeneous. The reaction allowed to cool to RT and the solid was then collected washed with cold water and dried in a desiccator giving the product as a pale yellow solid. (Yield 55.4 g, 61%).[89] **^{1}H-NMR:** (400 MHz, d_6-DMSO) δ:10.80 (s, ^{1}H), 7.83 (s, 4H). **^{13}C-NMR:** (d_6-DMSO) δ:164.6, 135.0, 129.2, 123.4 **HRMS:** (Calcd. $C_8H_4O_3$:163.0269) $[M-H]^+$ 164.0347

(11): 2-(benzyloxy)isoindoline-1,3-dione

11

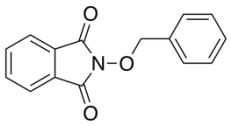

A 1 L 3 neck round bottom flask was charged with (**10**) (55.4 g, 0.339 mol) benzyl chloride (45.8 g, 0.36 mol) and 200 mL of DMF. The flask was heated to 130 °C. K_2CO_3 (27.6 g, 0.2 mol) was then added in small portions, over 10 minutes. After one hour, the reaction was cooled to RT and left to stir overnight. Water (200 mL) was added and a yellow precipitate formed and was collected. The solid was washed with water and dried under vacuum. The solid was purified by recrystallization in ethanol (600 mL) to yield the product as a yellow crystalline solid (38.2 g, 44% yield).[89] **^{1}H-NMR:** (400 MHz, d_6-DMSO) δ: 7.86 (s, 4H), 7.52 – 7.51 (m, 2H), 7.43 - 7.39 (m, 3H), 5.18 (s, 2H). **^{13}C-NMR:** (d_6-DMSO) δ: 163.0, 134.7, 134.0, 129.5, 129.0, 128.4, 128.4, 123.4, 79.1 **HRMS:** (Calcd. $C_{15}H_{11}NO_3$:253.0739) $[M+Na]^+$ 276.0644

(12): O-benzylhydroxylamine

12

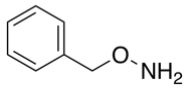

A 1 L 3 neck round bottom flask was charged with (**11**) (39.1 g 0.154 mol) and 294 mL of isopropyl alcohol. The reaction was heated to 75 °C and hydrazine monohydrate (8.8 mL, 0.176 mol) was added dropwise over 30 minutes. The solution was stirred overnight at 75-80 °C. The reaction mixture was cooled to RT and the solid was removed. The filtrate was then concentrated in vacuum to yield a yellow oil. The oil was then distilled at reduced pressure and a single fraction was collected at 75-80° C to yield (**12**) as colourless oil (Yield 13.82 g 73%).[89] **^{1}H-NMR:** (400 MHz, d_6-DMSO) δ: 7.32 - 7.26 (m, 5H), 6.04 (s, 2H), 4.57 (s, 2H) **^{13}C-NMR:** (d_6-DMSO) δ: 138.8, 128.6, 128.4, 127.9, 77.4.

(13): tert-butyl (benzyloxy)carbamate

13

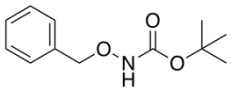

A 3 neck 250 mL round bottom flask was charged with tetrahydrofuran (30 mL), water (30 mL), (**12**) (2.0 g, 16.2 mmol), K_2CO_3 (6.73 g, 48.7 mmol). The reaction was cooled to 0 °C and Boc_2O (3.72 g, 17.1 mmol) dissolved in THF (20 mL) was added dropwise. The reaction was warmed to RT and stirred overnight. The reaction was monitored by TLC and was completed the following day. The solvent was removed under reduced pressure and the remaining oily residue was dissolved in ethyl acetate. The organic layer was then washed with water (3x20 mL), 10% aqueous citric acid (3 × 20 mL) and brine (1 × 10 mL). The organic layer was dried over $MgSO_4$ and concentrated to give a yellow oil. (Yield 3.62g, 85%).[89] **^{1}H-NMR:** (400 MHz, d_6-DMSO) δ: 7.38 - 7.36 (m, 5H), 4.73 (s, 2H), 1.41 (s, 9H). **^{13}C-NMR:** (d_6-DMSO) δ: 156.7, 136.7, 129.2, 128.7, 128.5, 80.1, 77.6, 28.5 **HRMS: (**Calcd. $C_{12}H_{17}NO_3$:223.2108) $[M+Na]^+$ 246.1110

(14): tert-butyl (benzyloxy)(methyl)carbamate

14

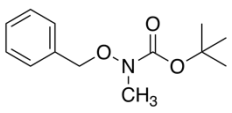

A 100 mL 3 neck RBF was charged with (**13**) (2.86 g, 12.3 mmol), K_2CO_3 (2.2 g, 15.3 mmol), Iodomethane (4.8 mL, 10.9 g) and 30 mL of acetone. The mixture was heated to 50 °C and stirred for 7 days with monitoring by TLC to determine completion. The reaction mixture was filtered and concentrated. The residue was then dissolved in 30 mL of ether and washed with saturated $NaHCO_3$ (15 mL × 3) and brine (20 mL × 1). The organic layer was then dried over $MgSO_4$ and then concentrated to give a pale-yellow oil (Yield 2.68 g, yield 77%).[90] **^{1}H-NMR:** (400 MHz, d_6-DMSO) δ: 7.41 - 7.36 (m, 5H), 4.80 (s, 2H), 3.01 (s, 3H), 1.42 (s, 9H). **^{13}C-NMR:** (d_6-DMSO) δ: 155.8, 135.5, 129.2, 128.2, 128.1, 80.2, 75.2, 36.0, 27.7. **HRMS: (**Calcd. $C_{13}H_{19}NO_3$:237.1365) $[M+Na]^+$ 260.1268

Preparation of Hydroxamic Acid Functionalised Glutamic Acid

(15): (S)-2-amino-5-(benzyloxy)-5-oxopentanoic acid

15

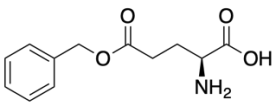

A 100 mL RBF was charged with toluene (30 mL), glutamic acid (5.00 g, 34.0 mmol) and benzyl alcohol (3.74 g, 34.58 mmol). The reaction was heated to 50 °C and pTsOH (7.27 g, 38.22 mmol) was added in portions. The reaction was stirred for two hours at 50 °C and then cooled to RT and stirred overnight. Water (20 mL) and ethanol (10 mL) was added to the reaction pH adjusted to 6. The white precipitate was collected and washed with cold ethanol. (Yield 3.57 g, 44%)[82, 83] **^{1}H-NMR:** (400 MHz, D_2O) δ: 7.47 (s, 5H), 5.21 (s, 2H), 3.79 (t, J = 4 Hz, 1H), 2.65 - 2.61 (m, 2H), 2.22 - 2.16 (m, 2H) **^{13}C-NMR:** (D_2O) δ: 174.46, 128.82, 128.65, 128.35, 67.20, 53.93, 29.91, 25.44 **HRMS: (**Calcd. $C_{12}H_{15}NO_4$: 237.1001) $[M+H]^+$ 238.1052

(16): (S)-5-(benzyloxy)-2-((tert-butoxycarbonyl)amino)-5-oxopentanoic acid

16

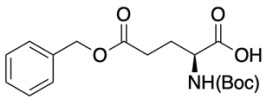

A 100 mL RBF was charged with (**15**) (2.51 g, 10.6 mmol), DMF (60 mL), TEA (1.18 g, 11.6 mmol) and stirred at RT for 30 minutes. The reaction was cooled in an ice bath and Boc_2O (2.54 g, 11.6 mmol) warmed to RT and added dropwise. The reaction was warmed to RT and stirred overnight. The organics were removed under reduced pressure and the oily residue was dissolved

in water (15 mL) and saturated $NaHCO_3$ (10 mL). The aqueous portion was washed with ether (15 mL × 3) and acidified with HCl (conc.) to ~ pH 2, extracted with EtOAc and dried over $MgSO_4$. The organics were removed under reduced pressure to afford a yellow oil (Yield 2.73 g, 77%)[91] **^{1}H-NMR:** (400 MHz, $CDCl_3$) δ: 7.34 (s, 5H), 5.20 - 5.17 (m, 1H), 5.12 (s, 2H), 4.38 - 4.32 (m, 1H), 2.59 - 2.42 (m, 2H), 2.27 - 2.21 (m, 1H), 1.97 - 1.93 (m, 1H), 1.43 (s, 9H). **^{13}C-NMR:** (d_6-DMSO) δ: 173.84, 171.94, 155.38, 136.00, 128.23, 127.78, 127.64, 77.89, 65.26, 52.38, 29.92, 27.99, 25.88 **HRMS: (**Calcd. $C_{17}H_{23}NO_6$: 337.1525) $[M+Na]^+$ 360.1420

(17): 5-benzyl 1-(tert-butyl) (tert-butoxycarbonyl)-L-glutamate

17

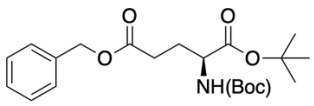

A 100 mL RBF was charged with (**16**) (2.59 g, 7.68 mmol), DMAP (0.94 g, 7.68 mmol) and DCM (10 mL) and stirred at RT for one hour. Boc_2O (2.01 g, 9.21 mmol) was warmed to RT and added dropwise. The reaction was stirred overnight at RT. The reaction was diluted with DCM (30 mL) and washed with water (15 mL × 2) and brine (15 mL × 1), dried over $MgSO_4$ and concentrated to a residue that was purified by silica gel chromatography (DCM:MeOH, 95:5) to afford an oil. (Yield 1.10 g, 36% yield).[92] **^{1}H-NMR:** (400 MHz, d_6-DMSO) δ: 7.36 (s, 5H), 7.16 (d, J = 8 Hz, 1H) 5.10 (s, 2H) 3.88 - 3.82 (m, 1H), 2.43 (q, J = 8 Hz, 2H) 1.98 - 1.91 (m, 2H) 1.83 - 1.76 (m, 2H) 1.39 (s, 9H), 1.38 (s, 9H). **^{13}C-NMR:** (d_6-DMSO) δ: 172.04, 171.33, 155.50, 136.15, 128.38, 127.94, 127.78, 80.39, 78.09, 65.42, 53.39, 29.95, 28.13, 27.59, 25.84 **HRMS: (**Calcd. $C_{17}H_{23}NO_6$: 393.2151) $[M+Na]^+$ 416.2047

(18): (S)-5-(tert-butoxy)-4-((tert-butoxycarbonyl)amino)-5-oxopentanoic acid

18

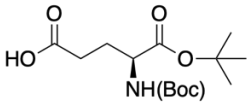

A 100 mL 2 N RBF was charged with (**17**) (2.0 g, 5.08 mmol), MeOH (40 mL) and 10% Pd/C. H_2 was applied using modest pressure and the reaction was stirred overnight at RT. The reaction mixture was filtered through celite and concentrated. The residue was purified by silica gel chromatography (DCM:MeOH, 9:1) to afford an oil (Yield 1.63 g, 78%). **^{1}H-NMR:** (400 MHz, d_6-DMSO) δ: 7.13 (d, J = 8 Hz, 1H), 4.08 - 4.07 (m, 1H), 3.82 - 3.79 (m, 1H), 2.29 - 2.24 (m, 2H), 1.90 - 1.85 (m, 1H), 1.74 - 1.72 (m, 1H), 1.39 (s, 9H), 1.38 (s, 9H). **^{13}C-NMR:** (d_6-DMSO) δ: 173.70, 171.46, 155.47, 80.27, 78.01, 53.52, 30.03, 28.11, 27.57, 25.89 **HRMS: (**Calcd. $C_{14}H_{25}NO_6$: 303.1682) $[M+Na]^+$ 326.1512, $[M+K]^+$ 342.1251

(19): tert-butyl N5-(benzyloxy)-N2-(tert-butoxycarbonyl)-L-glutaminate

19

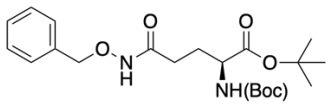

A 100 mL RBF was charged with (**18**) (1.25 g, 4.12 mmol), (**12**) (0.56 g, 4.53 mmol), DIPEA (0.59 g, 4.53 mmol) and DMF (30 mL). The reaction was cooled on an ice bath and a solution of PyBOP (2.36 g, 4.53 mmol) in DCM (12 mL) was added dropwise. The reaction was warmed to RT and stirred overnight. The organics were removed under reduced pressure and the residue was dissolved in water (60 mL) and extracted with EtOAc (25 mL × 3). The organics were washed with HCl (25 mL × 1, 0.1 M) and dried over $MgSO_4$, and concentrated. The residue was purified by silica gel chromatography (DCM:MeOH, 9:1) to afford the yellow oil (Yield 1.32 g, 79%).[93] **^{1}H-NMR:** (400 MHz, d_6-DMSO) δ: 7.38 (s, 5H), 7.10 (d, J = 8 Hz, 1H), 4.77 (s, 2H), 3.81 - 3.76 (m, 1H), 2.05 - 2.01 (m, 2H), 1.92-1.87 (m, 1H), 1.77 - 1.69 (m, 1H), 1.39 (s, 9), 1.38 (s, 9H) **^{13}C-NMR:** (d_6-DMSO) δ: 171.43, 168.61, 155.48, 136.02, 128.73, 128.26, 127.63, 80.31, 78.04, 76.81, 53.77, 28.64, 28.15, 27.61, 26.25 **HRMS: (**Calcd. $C_{21}H_{32}N_2O_6$: 408.2260) $[M+Na]^+$ 431.2065

(20): N5-(benzyloxy)-L-glutamine

20

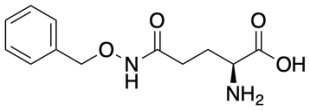

A 100 mL RBF was charged with (**19**) (392.8 mg, 0.96 mmol), DCM (4 mL) and TFA (2.18 g, 19.22 mmol). The reaction was stirred for 3 hours at RT and the volatiles removed with a stream of N_2. The residue was dissolved in minimal MeOH and excess ether (40 mL) was added. The precipitate was washed with ether (30 mL × 3) to afford a white solid. (Yield 122.2 mg, 50%)[65, 94] **^{1}H-NMR:** (400 MHz, D_2O) δ: 7.49 (s, 5H), 4.93 (s, 2H), 3.73 - 3.67 (m, 1H), 2.31 -2.26 (m, 2H), 2.10 - 2.04 (m, 2H) **^{13}C-NMR:** (D_2O) δ: 173.42, 170.83, 134.57, 129.86, 129.21, 128.70, 78.20, 53.74, 28.28, 26.04 **HRMS: (**Calcd. $C_{12}H_{16}N_2O_4$: 252.1110) $[M+H]^+$ 253.1359

(21): N2-(((9H-fluoren-9-yl)methoxy)carbonyl)-N5-(benzyloxy)-L-glutamine

21

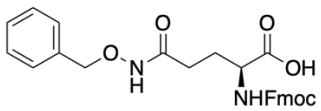

A 100 mL RBF was charged with (**20**) (72mg, 0.0285 mmol), Na_2CO_3 (aq.) 10% w/w (151 mg, 1.42 mmol). Fmoc-Cl (82 mg, 0.316 mmol) in a solution of dioxane was added dropwise over 30 minutes. The reaction was stirred at RT overnight. Water (18 mL) was added and extracted with ether (10 mL × 3). The aqueous portion was acidified to pH 2 and refrigerated overnight. The solid was collected and washed with ether (3 mL × 2) (Yield 68.3 mg, 55%).[95, 96] **^{1}H-NMR:** (400 MHz, d_6-DMSO) δ: 11.01 (s, 1H), 7.90 (d, J = 8 Hz, 2H), 7.73 (d, J = 8 Hz, 2H), 7.43 (d, J = 8 Hz, 1H), 7.44 - 7.32 (m, 9H), 4.78 (s, 2H) 4.29 - 4.26 (m, 1H), 4.24 - 4.20 (m, 2H), 3.98 - 3.93 (m, 1H), 2.09 - 2.07 (m, 2H), 2.01 - 1.98 (m, 1H), 1.81 - 1.76 (m, 1H).**^{13}C-NMR:** (500 Mhz CD_3OD) δ: 175.10, 171.67, 158.61, 145.22, 145.09, 142.49, 136.85, 130.26, 129.53, 129.38, 128.70, 128.09, 126.21, 126.17, 120.82, 78.97, 67.98, 30.11, 28.32, 15.34 **HRMS: (**Calcd. $C_{27}H_{26}N_2O_6$: 474.1791) $[M+H]^+$ 475.1874

References

1. X. Xu and R. Lai, *Chem. Rev.*, 2015, **115**, 1760-1846.

2. Y. Shai, *Biochim. Biophys. Acta Biomembr.*, 1999, **1462**, 55-70.

3. H. Sato and J. B. Feix, *Biochim. Biophys. Acta Biomembr.*, 2006, **1758**, 1245-1256.

4. D. L. Nelson, *Lehninger Principles of Biochemistry*, W.H. Freeman, New York, 6th edn., 2013.

5. T. Rozek, K. L. Wegener, J. H. Bowie, I. N. Olver, J. A. Carver, J. C. Wallace and M. J. Tyler, *Eur. J. Biochem.*, 2000, **267**, 5330-5341.

6. J. Li, J.-J. Koh, S. Liu, R. Lakshminarayanan, C. S. Verma and R. W. Beuerman, *Front. Neurosci.*, 2017, **11**, 73-73.

7. M.-D. Seo, H.-S. Won, J.-H. Kim, T. Mishig-Ochir and B.-J. Lee, *Molecules*, 2012, **17**, 12276-12286.

8. K. L. Wegener, P. A. Wabnitz, J. A. Carver, J. H. Bowie, B. C. S. Chia, J. C. Wallace and M. J. Tyler, *Eur. J. Biochem.*, 1999, **265**, 627-637.

9. M. Shahmiri, B. Cornell and A. Mechler, *Biointerphases*, 2017, **12**, 05G6051-6005G6058.

10. M. Shahmiri, M. Enciso and A. Mechler, *Sci. Rep.*, 2015, **5**, 16378-16391.

11. Y. Shai, *BBA - Biomembranes*, 1999, **1462**, 55-70.

12. B. Valeur, *Molecular Fluorescence Principles and Applications*, Wiley, Weinheim, 2nd edn., 2013.

13. M. A. Bopp, Y. Jia, L. Li, R. J. Cogdell and R. M. Hochstrasser, *Proc. Natl. Acad. Sci.*, 1997, **94**, 10630-10635.

14. Z. Liu, Z. Bian and C. Huang, *Luminescent Iridium Complexes and Their Applications*, Springer, Berlin, 1st edn., 2009.

15. D. L. Taylor and Y.-L. Wang, *Nature*, 1980, **284**, 405-410.

16. M. S. T. Goncalves, *Chem. Rev.*, 2009, **109**, 190-212.

17. K. K.-W. Lo, A. W.-T. Choi and W. H.-T. Law, *Dalton Trans.*, 2012, **41**, 6021-6047.

18. V. I. Martynov, A. A. Pakhomov, N. V. Popova, I. E. Deyev and A. G. Petrenko, *Acta Naturae*, 2016, **8**, 33-46.

19. X. Bossuyt, S. Cooreman, H. De Baere, P. Verschueren, R. Westhovens, D. Blockmans and G. Marien, *Clin. Chim. Acta*, 2013, **415**, 101-106.

20. C. S. Nathan, A. S. Paul and Y. T. Roger, *Nat. Methods*, 2005, **2**, 905-909.

21. M. Zimmer, *Chem. Rev.*, 2002, **102**, 759.

22. F. De Angelis, S. Fantacci, N. Evans, C. Klein, S. M. Zakeeruddin, J.-E. Moser, K. Kalyanasundaram, H. J. Bolink, M. Gratzel and M. K. Nazeeruddin, *Inorg. Chem.*, 2007, **46**, 5989-6001.

23. J. Neilands, *J. Biol. Chem.*, 1995, **270**, 26723-26726.

24. R. Saha, N. Saha, R. S. Donofrio and L. L. Bestervelt, *J. Basic Microbiol.*, 2013, **53**, 303-317.

25. G. Cairo, F. Bernuzzi and S. Recalcati, *Genes Nutr.*, 2006, **1**, 25-39.

26. H. Haas, *Nat. Prod. Rep.*, 2014, **31**, 1266-1276.

27. J. Brandel, N. Humbert, M. Elhabiri, I. J. Schalk, G. L. A. Mislin and A.-M. Albrecht-Gary, *Dalton Trans.*, 2012, **41**, 2820-2834.

28. S. Dev and J. L. Babitt, *Hemodial. Int.*, 2017, **21**, 6-20.

29. H. H. Malluche, A. J. Smith, K. Abreo and M. C. Faugere, *N. Engl. J. Med.*, 1984, **311**, 140-144.

30. L. Tauchenová, B. Krizova, M. s. Kubánek, S. Franková, V. e. Meluskova, J. Tintera, D. Kautznerová, J. Malusková, M. Jirsa and J. Kautzner, *Can. J. Cardiol.*, 2016, **32**, 1574.e1571-1574.e1573.

31. N. B. Bhatt, D. N. Pandya and T. J. Wadas, *Molecules*, 2018, **23**, 638-661.

32. I. Velikyan, *Molecules*, 2015, **20**, 12913-12943.

33. S. M. Moerlein and M. J. Welch, *Int. J. Nucl. Med. Biol.*, 1981, **8**, 277-287.

34. M. S. Hofman and R. J. Hicks, *Semin. Nucl. Med.*, 2016, **46**, 448-461.

35. O. Jacobson, D. O. Kiesewetter and X. Chen, *Bioconjug. Chem.*, 2015, **26**, 1-18.

36. H. Goodfellow, Z. Viney, P. Hughes, S. Rankin, G. Rottenberg, S. Hughes, F. Evison, P. Dasgupta, T. O' Brien and M. S. Khan, *BJU Int.*, 2014, **114**, 389-395.

37. U. Yararbas, N. C. Avci, L. Yeniay and A. M. Argon, *Bosn. J. Basic Med. Sci*, 2018, **18**, 72-79.

38. A. B. Kinupe Abrahao, Y. Ung, Y.-J. Ko and S. R. Berry, *J. Clin. Oncol.*, 2017, **35**, 464-464.

39. M. D. Bartholomä, A. S. Louie, J. F. Valliant and J. Zubieta, *Chem. Rev.*, 2010, **110**, 2903-2920.

40. T. W. Price, J. Gallo, V. Kubek, Z. Bhmov, T. J. Prior, J. Greenman, P. Hermann and G. J. Stasiuk, *Dalton Trans.*, 2017, **46**, 16973-16982.

41. C. Zhai, D. Summer, C. Rangger, H. Haas, R. Haubner and C. Decristoforo, *J. Labelled Compd. Radiopharm.*, 2015, **58**, 209-214.

42. I. Gosse, K. Robeyns, C. Bougault, A. Martinez, B. Tinant and J.-P. Dutasta, *Inorg. Chem.*, 2016, **55**, 1011-1013.

43. A. Sengupta, A. Seitz and K. M. Merz, *J. Am. Chem. Soc.*, 2018, **140**, 15166-15169.

44. P. Spang, C. Herrmann and F. Roesch, *Semin. Nucl. Med.*, 2016, **46**, 373-394.

45. N. Viola-Villegas and R. P. Doyle, *Coord. Chem. Rev.*, 2009, **253**, 1906-1925.

46. W. C. Cole, S. J. Denardo, C. F. Meares, M. J. McCall, G. L. Denardo, A. L. Epstein, H. A. O'Brien and M. K. Moi, *J. Nucl. Med.*, 1987, **28**, 83-90.

47. S. V. Deshpande, S. J. Denardo, D. L. Kukis, M. K. Moi, M. J. McCall, G. L. Denardo and C. F. Meares, *J. Nucl. Med.*, 1990, **31**, 473-479.

48. M. Eiblmaier, L. A. Meyer and C. J. Anderson, *Cancer Biol. Ther.*, 2008, **7**, 63-69.

49. R. P. Junghans, D. Dobbs, M. W. Brechbiel, S. Mirzadeh, A. A. Raubitschek, O. A. Gansow and T. A. Waldmann, *Cancer Res.*, 1993, **53**, 5683-5689.

50. C. F. Meares, M. K. Moi, H. Diril, D. L. Kukis, M. J. McCall, S. V. Deshpande, S. J. Denardo, D. Snook and A. A. Epenetos, *Br. J. Cancer*, 1990, **10**, 21-26.

51. P. Pellegrini, N. Howell, R. Shepherd, N. Lengkeek, E. Oehlke, A. Katsifis and I. Greguric, *Molecules*, 2013, **18**, 7160-7178.

52. H. Mohsin, F. Jia, G. Sivaguru, M. Hudson, T. Shelton, T. Hoffman, C. Cutler, A. Ketring, P. Athey, J. Simon, R. Frank, S. Jurisson and M. Lewis, *Bioconjug. Chem.*, 2006, **17**, 485-492.

53. M. Petrik, C. Zhai, Z. Novy, L. Urbanek, H. Haas and C. Decristoforo, *Mol. Imaging Biol.*, 2016, **18**, 344-352.

54. E. L. Robert, *The Sigma-Aldrich Library of Chemical Safety Data*, Sigma-Aldrich Corp., Milwaukee, Wis., USA, 2nd edn., 1988.

55. F. Albericio and A. El-Faham, *Org. Process Res. Dev.*, 2018, **22**, 760-772.

56. G. Sabatino, B. Mulinacci, M. C. Alcaro, M. Chelli, P. Rovero and A. M. Papini, *Lett. Pept. Sci.*, 2002, **9**, 119-123.

57. B. Dhayalan, K. Mandal, N. Rege, M. A. Weiss, S. H. Eitel, T. Meier, R. O. Schoenleber and S. B. H. Kent, *Chem. Eur. J.*, 2017, **23**, 1709-1716.

58. R. Behrendt, P. White and J. Offer, *J. Pept. Sci.*, 2016, **22**, 4-27.

59. S. L. Pedersen, A. P. Tofteng, L. Malik and K. J. Jensen, *Chem. Soc. Rev.*, 2012, **41**, 1826-1844.

60. M. Brandt, S. Gammeltoft and K. J. Jensen, *Int. J. Pept. Res. Ther.*, 2006, **12**, 349-357.

61. B. Bacsa, B. Desai, G. Dibó and C. O. Kappe, *J. Pept. Sci.*, 2006, **12**, 633-638.

62. B. Bacsa, K. Horváti, S. Bõsze, F. Andreae and C. O. Kappe, *J. Org. Chem*, 2008, **73**, 7532-7542.

63. S. Kojo, H. Uchino, M. Yoshimura and K. Tanaka, *Chem. Commun.*, 2004, **19**, 2146-2147.

64. E. Schreiner, L. G. Trabuco, P. L. Freddolino and K. Schulten, *BMC Bioinform.*, 2011, **12**, 190-190.

65. D. Kadereit, P. Deck, I. Heinemann and H. Waldmann, *Chem. Eur. J.*, 2001, **7**, 1184-1193.

66. Y. Han, F. Albericio and G. Barany, *J. Org. Chem*, 1997, **62**, 4307-4312.

67. K. Neumann, J. Farnung, S. Baldauf and J. W. Bode, *Nat. Commun*, 2020, **11**, 982-992.

68. E. Atherton, N. L. Benoiton, E. Brown, R. C. Sheppard and B. J. Williams, *J. Chem. Soc., Chem. Commun.*, 1981, **7**, 336-337.

69. E. D. Stroud, D. J. Fife and G. G. Smith, *J. Org. Chem*, 1983, **48**, 5368-5369.

70. R. Behrendt, M. Schenk, H. J. r. Musiol and L. Moroder, *J. Pept. Sci.*, 1999, **5**, 519-529.

71. H.-J. Musiol, F. Siedler, D. Quarzago and L. Moroder, *Biopolymers*, 1994, **34**, 1553-1562.

72. O. F. Luna, J. Gomez, C. Cárdenas, F. Albericio, S. H. Marshall and F. Guzmán, *Molecules*, 2016, **21**, 1542-1554.

73. P. Sieber, *Tetrahedron Lett.*, 1987, **28**, 6147-6150.

74. G. B. Fields, *Peptide Synthesis Protocols*, Humana Press, Totowa, NJ, 1st edn., 1995.

75. R. R. Becklin and D. M. Desiderio, *Anal. Lett.*, 1995, **28**, 2175-2190.

76. A. R. Goldfarb, L. J. Saidel and E. Mosovich, *J. Biol. Chem.*, 1951, **193**, 397-404.

77. M. Piacenza, F. Della Sala, G. M. Farinola, C. Martinelli and G. Gigli, *J. Phys. Chem. B*, 2008, **112**, 2996-3004.

78. B. D. Stringer, L. M. Quan, P. J. Barnard, D. J. D. Wilson and C. F. Hogan, *Organometallics*, 2014, **33**, 4860-4872.

79. J. N. Israelachvili, *Intermolecular and Surface Forces*, Elsevier Science, 3 edn., 2010.

80. A. C. Alves, D. Ribeiro, M. Horta, J. L. F. C. Lima, C. Nunes and S. Reis, *J. R. Soc. Interface*, 2017, **14**.

81. C. Matos, C. Moutinho and P. Lobão, *J. Membr. Biol*, 2012, **245**, 69-75.

82. A. A. Rana, M. Kamruzzaman and M. Takafuji, *Bangladesh J. Sci. Ind. Res.*, 2011, **46**, 271-276.

83. A. Martanez de Ilarduya, N. Ittobane, M. Bermadez, A. Alla, M. El Idrissi and S. Muaoz-Guerra, *Biomacromolecules*, 2002, **3**, 1078-1086.

84. X. Lin, Y. Yosaatmadja, M. Kalyukina, M. J. Middleditch, Z. Zhang, X. Lu, K. Ding, A. V. Patterson, J. B. Smaill and C. J. Squire, *ACS Med. Chem. Lett*, 2019, **10**, 1180-1186.

85. J. R. Schmidt and W. F. Polik, *WebMO Enterprise*, 2016, WebMO LLC.

86. J. Smid, *Angew. Chem., Int. Ed. Engl.*, 1972, **11**, 112-127.

87. C.-S. Chung, *J. Chem. Educ.*, 1984, **61**, 1062-1064.

88. M. Shahmiri, M. Enciso, C. G. Adda, B. J. Smith, M. A. Perugini and A. Mechler, *Sci. Rep.*, 2016, **6**, 38184-38196.

89. E. Koverzanova, I. Levina and A. Gridnev, *J. Foc. Phy.*, 2018, **12**, 46-52.

90. A. Safavy, D. C. Smith, A. Bazooband and D. J. Buchsbaum, *Bioconjug. Chem.*, 2002, **13**, 327-332.

91. N. J. Manesis and M. Goodman, *J. Org. Chem*, 1987, **52**, 5342-5349.

92. X. Tian, J. Pai and I. Shin, *Chem. Asian J.*, 2012, **7**, 2052-2060.

93. A. J. d. M. Santos Oliveira, R. D. de Castro, H. d. L. F. Pessoa, A. Wadood and D. P. de Sousa, *Biomed Res. Int.*, 2019, **2019**, 9676-9676.

94. F. S. Gibson, S. C. Bergmeier and H. Rapoport, *J. Org. Chem*, 1994, **59**, 3216-3218.

95. M. Bodanszky and A. Bodanszky, *The Practice of Peptide Synthesis*, Springer Berlin Heidelberg, Berlin, Heidelberg, 2nd edn., 1994.

96. M. B. Gawande and P. S. Branco, *Green Chem.*, 2011, **13**, 3355-3359.

Appendices

(1): AGAG – HRMS

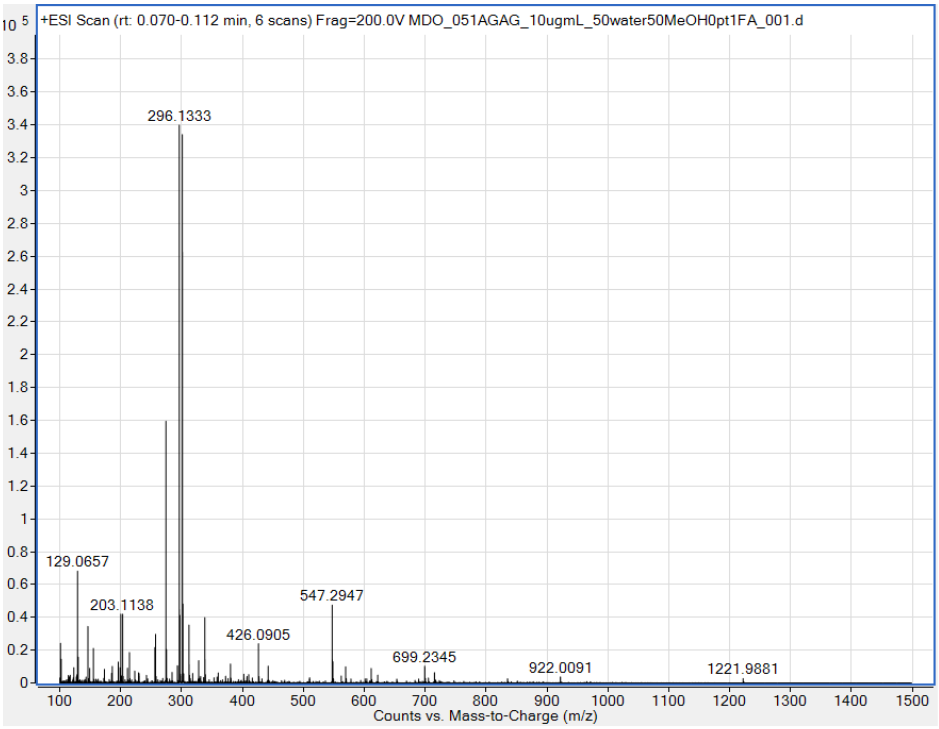

*Figure 34 – Compound (**1**) HRMS (positive mode) of AGAG peptide synthesised using TBTU as the coupling reagent. Calcd. for $C_{10}H_{18}N_4O_5$: 274.1277) $[M-H+Na]^+$ 297.1335*

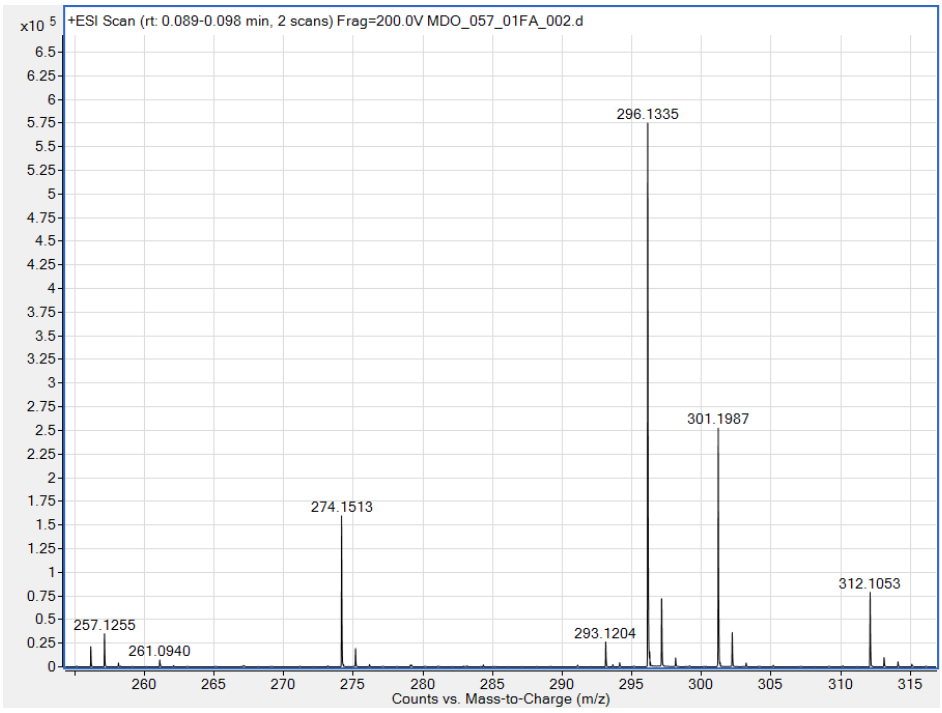

*Figure 35 – Compound (**1**) HRMS (positive mode) of AGAG peptide synthesised using HCTU as the coupling reagent. Calcd. for $C_{10}H_{18}N_4O_5$: 274.1277) $[M-H+Na]^+$ 297.1335*

(2): Aurein 1.2 – HRMS

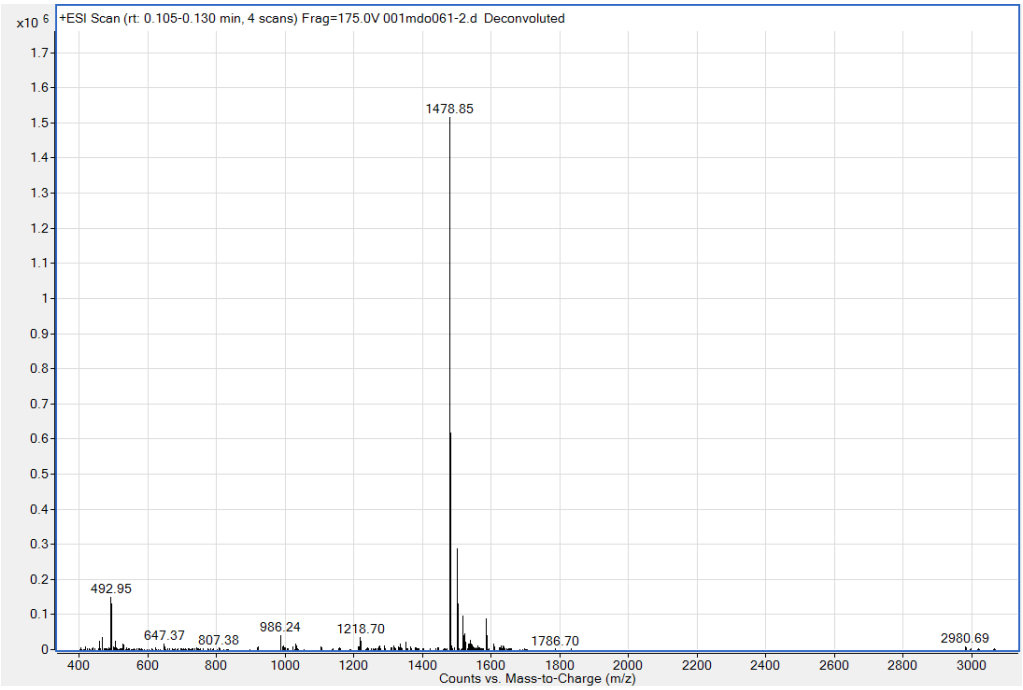

*Figure 36 – Compound (**2**) HRMS (positive mode) of Aurein 1.2, (Calcd. for $C_{71}H_{114}N_{16}O_{18}$: 1478.8497) $[M]^+$ 1478.8497, (Deconvoluted spectrum).*

(3): Citropin 1.1 – HRMS

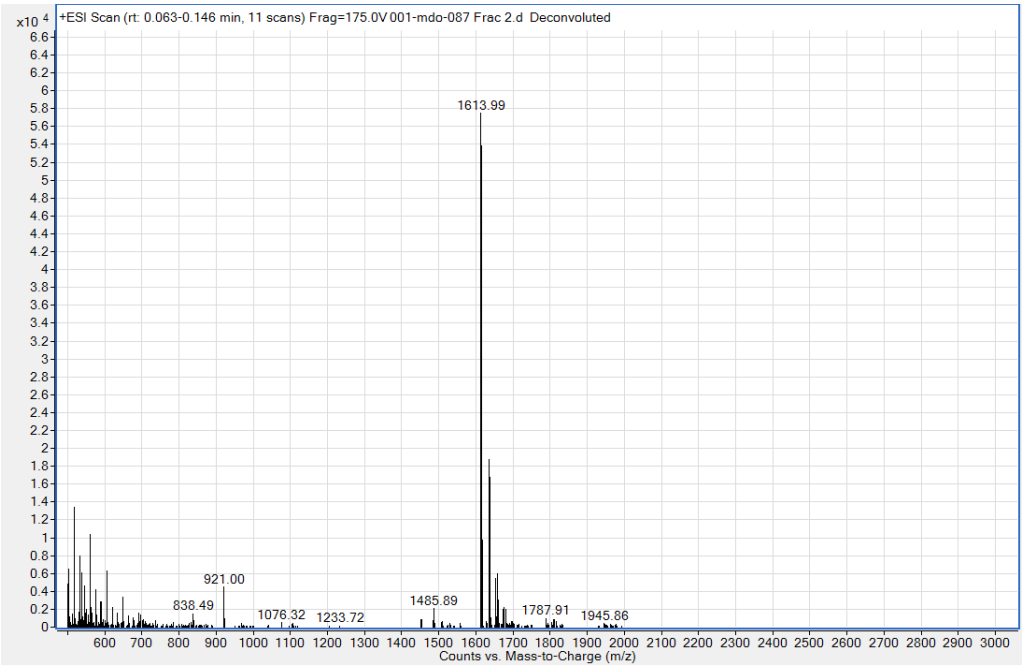

*Figure 37 – Compound (**3**) HRMS (positive mode) of Citropin 1.1 (Calcd. for $C_{76}H_{131}N_{19}O_{19}$: 1613.9869) $[M]^+$ 1613.99, (Deconvoluted spectrum).*

(4): Iridium Complex – HRMS

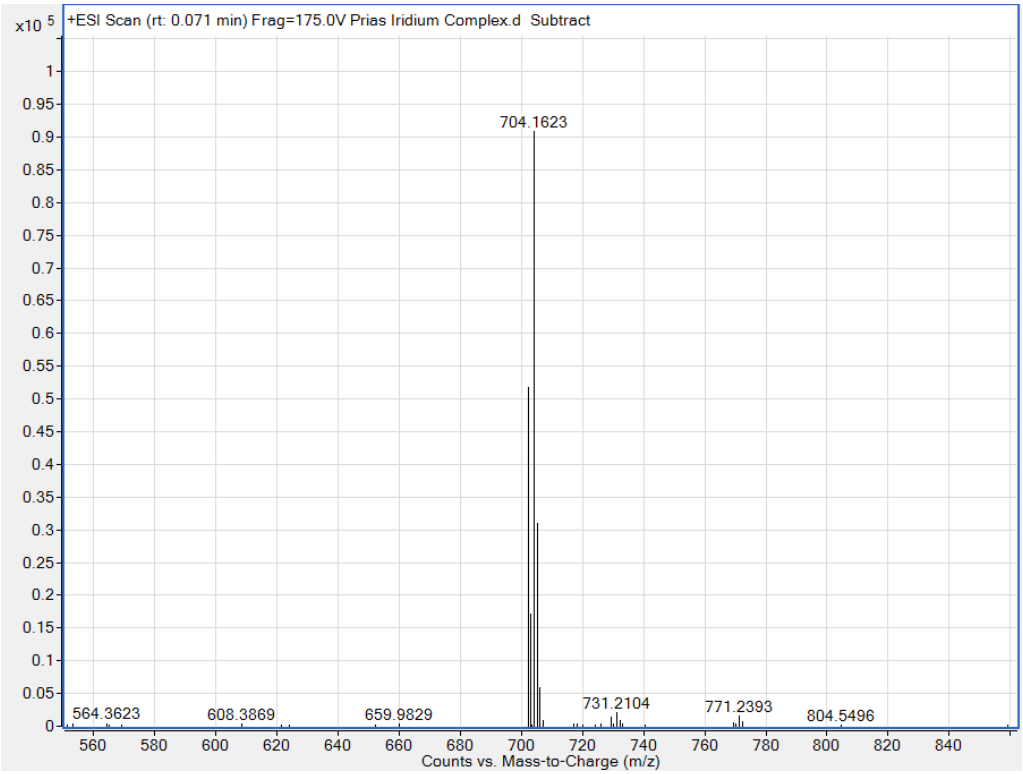

*Figure 38 – Compound (**4**) HRMS (Positive mode) of iridium Complex (Calcd. for $C_{32}H_{25}IrN_5O_2$: 704.1632) $[M]^+$ 704.1623.*

(5): Iridium Complex – HRMS

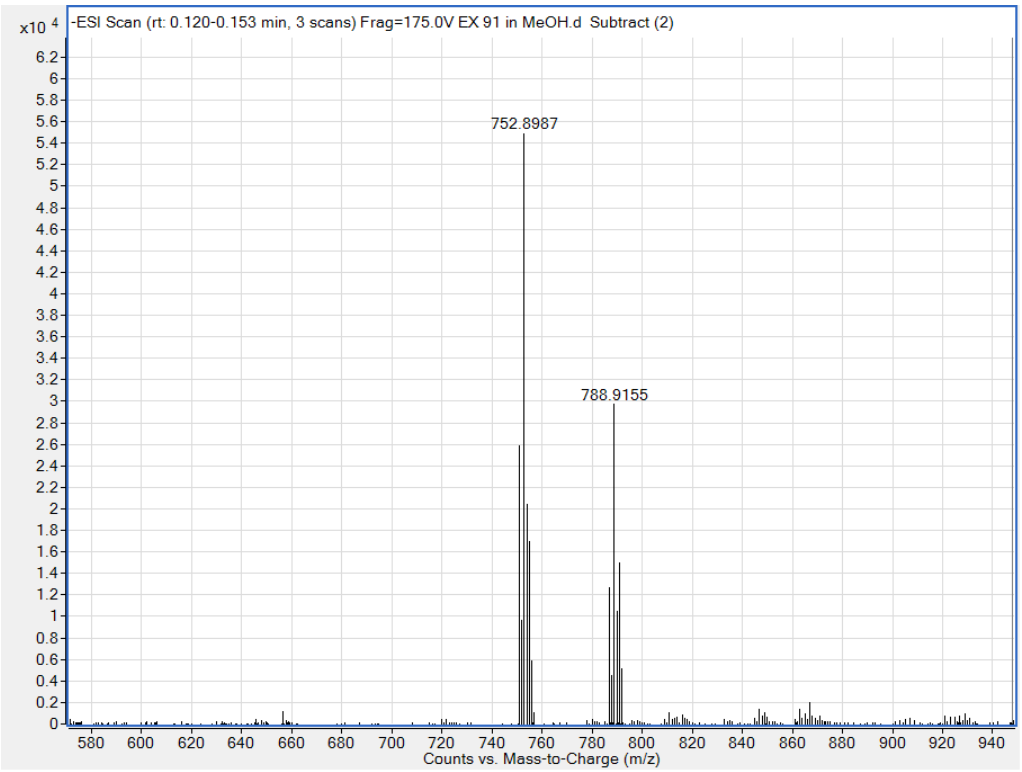

*Figure 39 – Compound (**5**) HRMS of iridium Complex, (Calcd. for $C_{33}H_{27}IrN_5O_2$: 718.1789) $[M+Cl]^+$ 752.8987, $[M+2Cl^-]^+$ 788.9155*

(6): Iridium Complex – HRMS

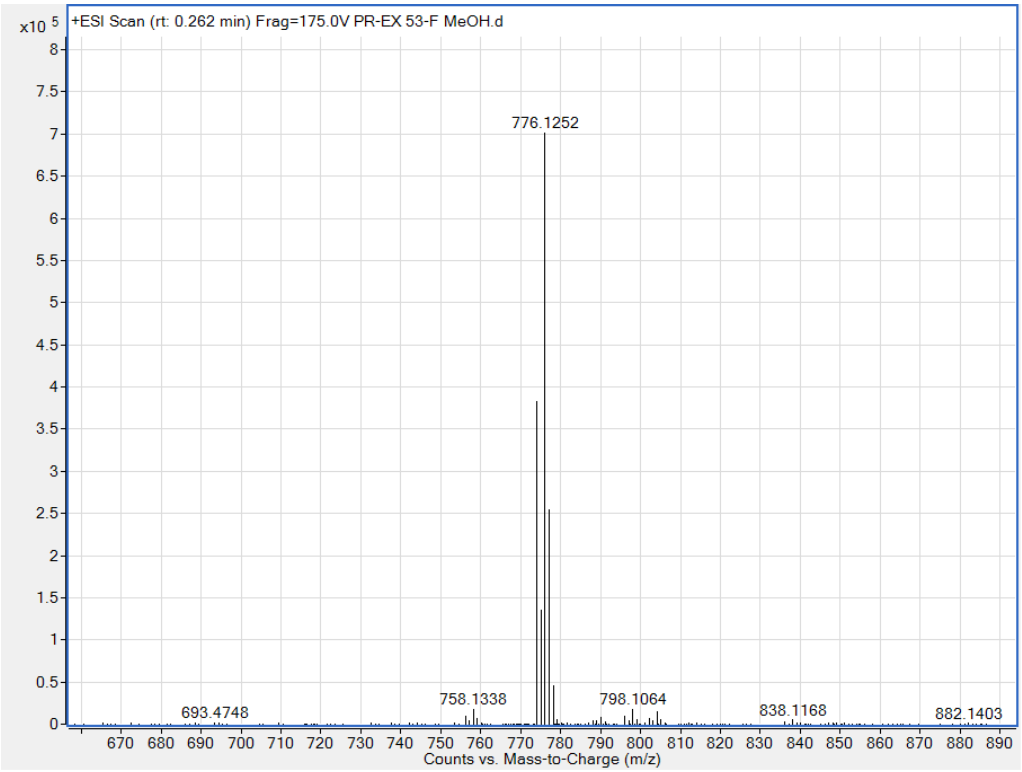

*Figure 40 – Compound (**6**) HRMS of iridium Complex (Calcd. for $C_{32}H_{21}F_4IrN_5O_2$: 776.1275) $[M]^+$ 776.1252*

(7): Aurein 1.2 + (4) HRMS, HPLC Chromatograph

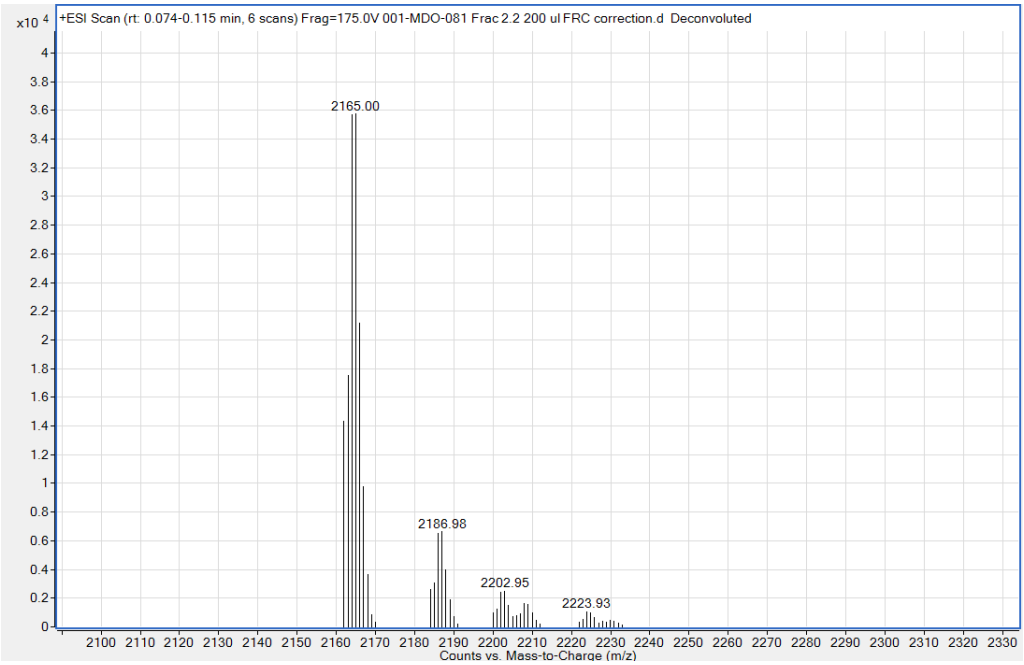

*Figure 41 – Compound (**7**) HRMS (positive mode) of Aurein 1.2-iridium Complex, (Calcd. $C_{103}H_{137}IrN_{21}O_{19}$+ : 2166.0057) $[M-H]^+$ 2165.00, (Deconvoluted spectrum).*

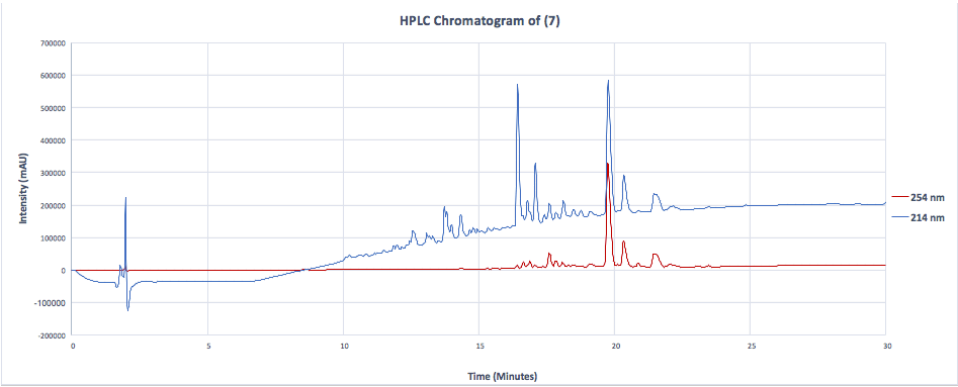

*Figure 42 – Compound (**7**) HPLC Chromatogram (retention time: 19.8 minutes) showing λ 254 nm (blue) and λ 214 (red).*

(8): Aurein 1.2 + (5) HRMS, HPLC Chromatogram

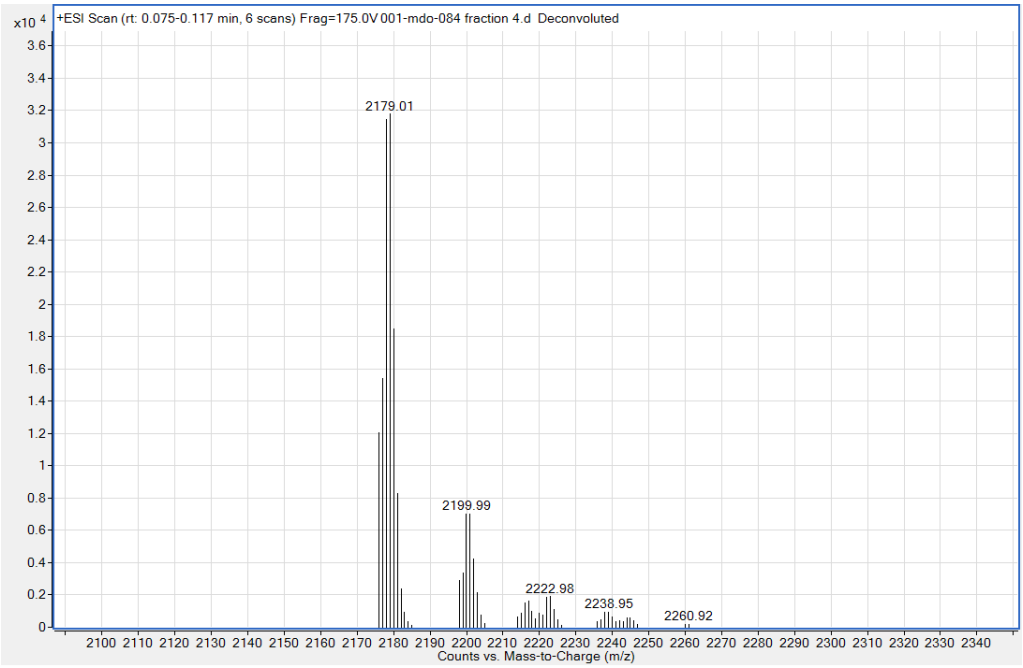

Figure 43 – Compound (8) HRMS (positive mode) of Aurein 1.2-iridium Complex (Calcd. $C_{104}H_{139}IrN_{21}O_{19}$+ : 2180.0213) [M-H]$^+$ 2179.01, (Deconvoluted spectrum).

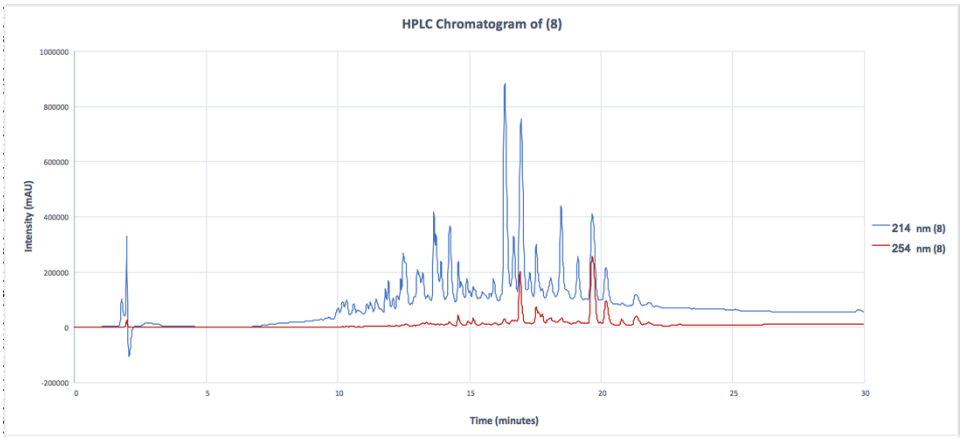

*Figure 44 HPLC Chromatogram of (**8**) (retention time: 19.8 minutes) showing λ 254 nm (blue) and λ 214 (red).*

(9): Aurein 1.2 + (6) HRMS, HPLC Chromatogram

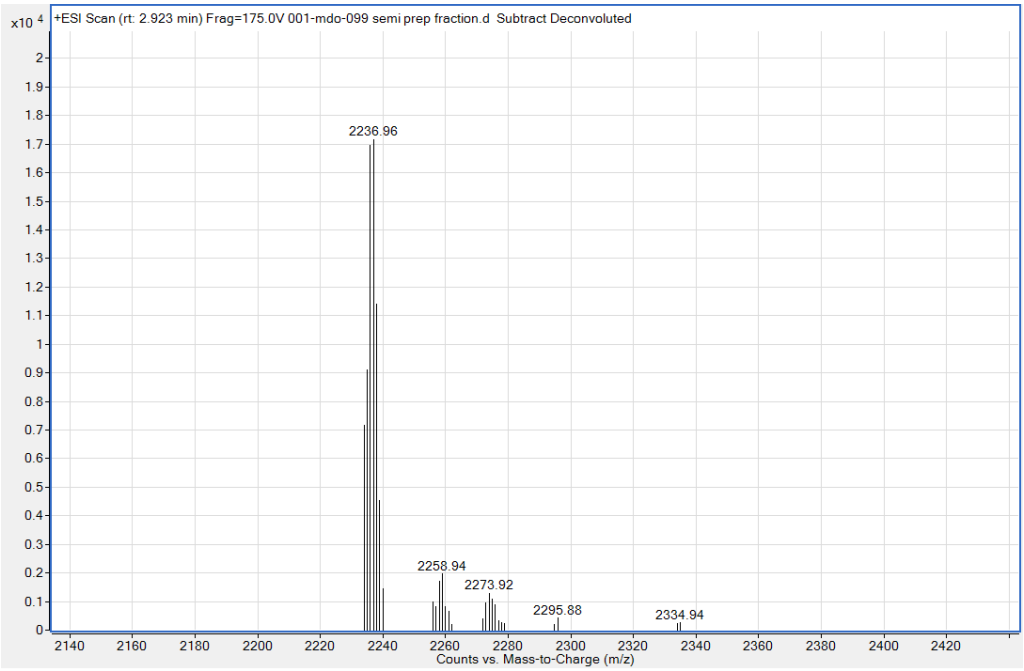

*Figure 45 – Compound (**9**) HRMS (positive mode) of Aurein 1.2-iridium Complex (Calcd. $C_{103}H_{133}F_4IrN_{21}O_{19}^+$: 2237.9680) $[M-H]^+$ 2236.96, (Deconvoluted spectrum).*

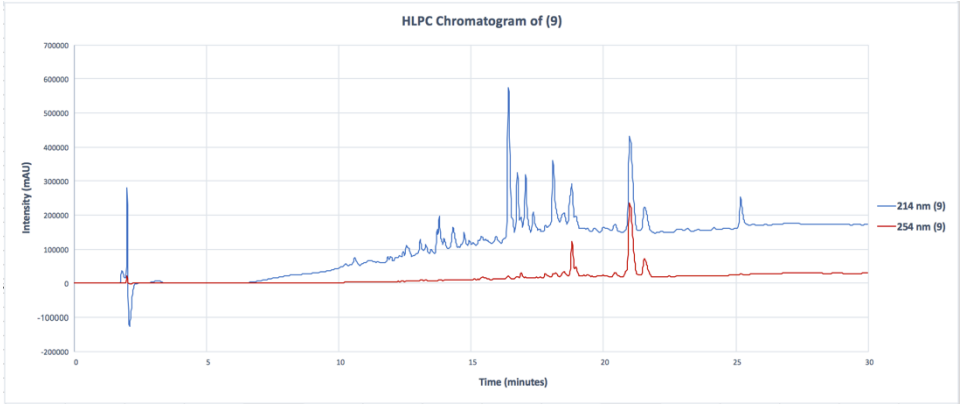

*Figure 46 – HPLC Chromatogram of (**9**) (retention time: 21.2 minutes) showing λ 254 nm (blue) and λ 214 (red).*

(10): Absorption of 7, 8 and 9

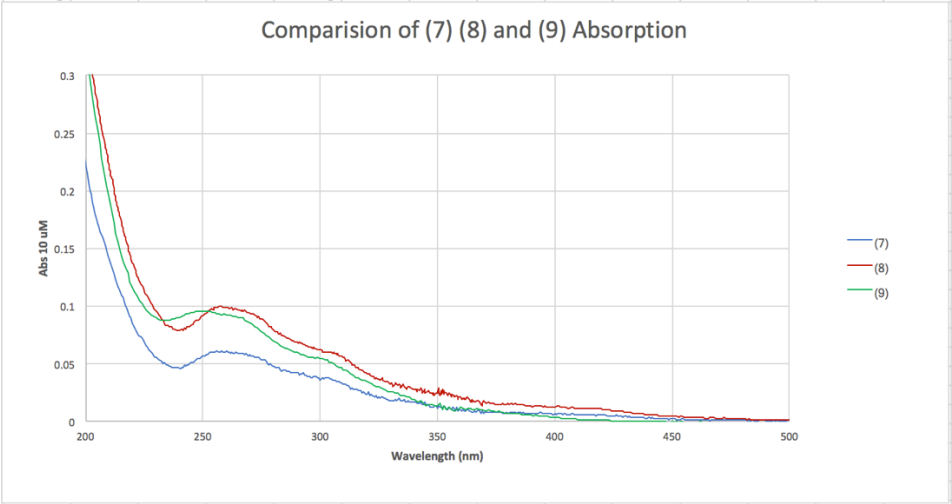

Figure 47 – Comparison of the absorbance of (7), (8) and (9)

(11): ^{1}H-NMR, ^{13}C-NMR, HRMS

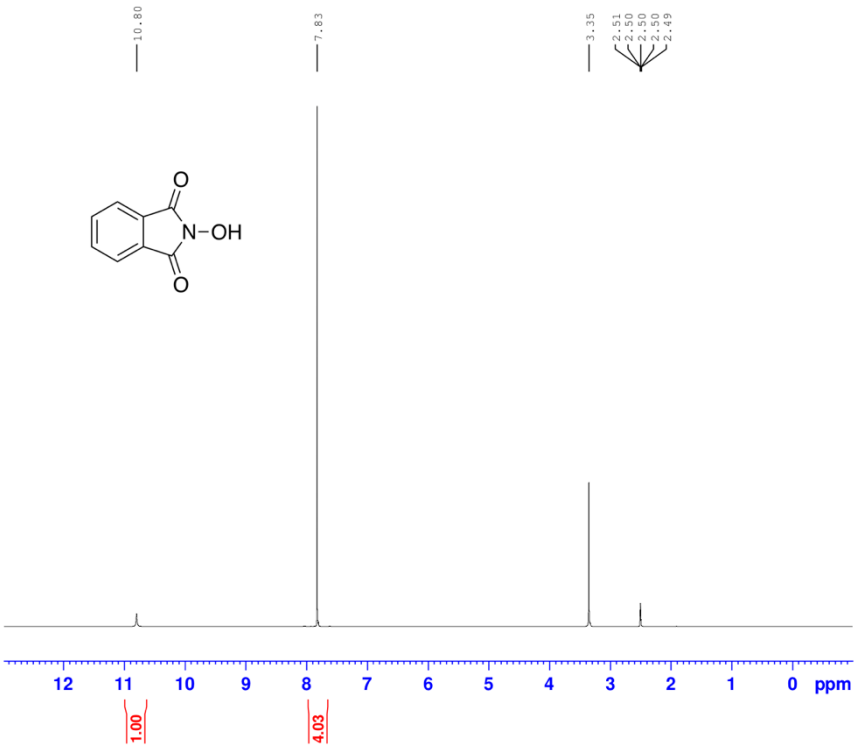

*Figure 48 – Compound (**10**) ^{1}H-NMR obtained using 400 MHz Bruker NMR spectrometer in d_6-DMSO*

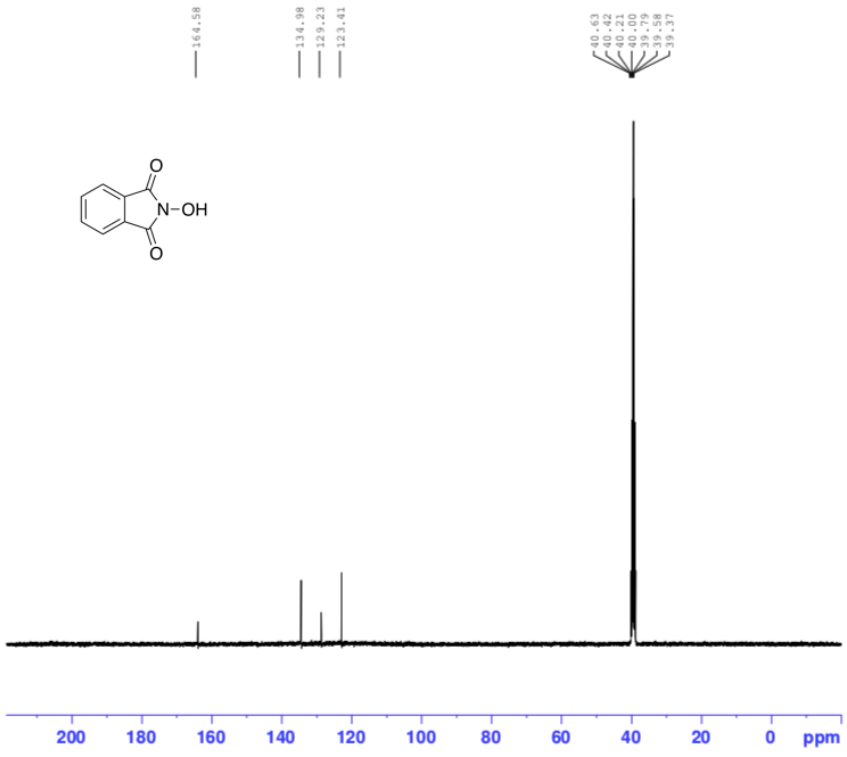

*Figure 49 – Compound (**10**) ^{13}C-NMR obtained using 400 MHz Bruker NMR spectrometer in d_6-DMSO*

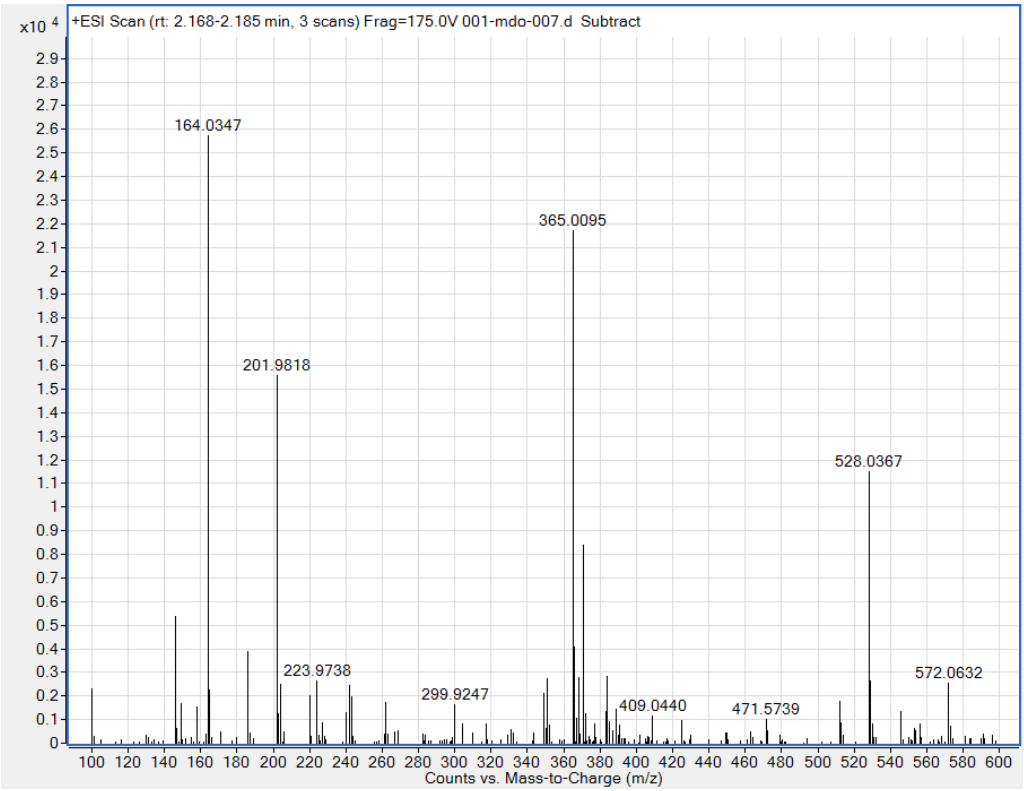

*Figure 50 – Compound (**10**) HRMS - Positive mode. (Calcd. $C_8H_4O_3$: 163.0269) $[M-H]^+$ 164.0347*

(12): ^{1}H-NMR, ^{13}C-NMR, HRMS

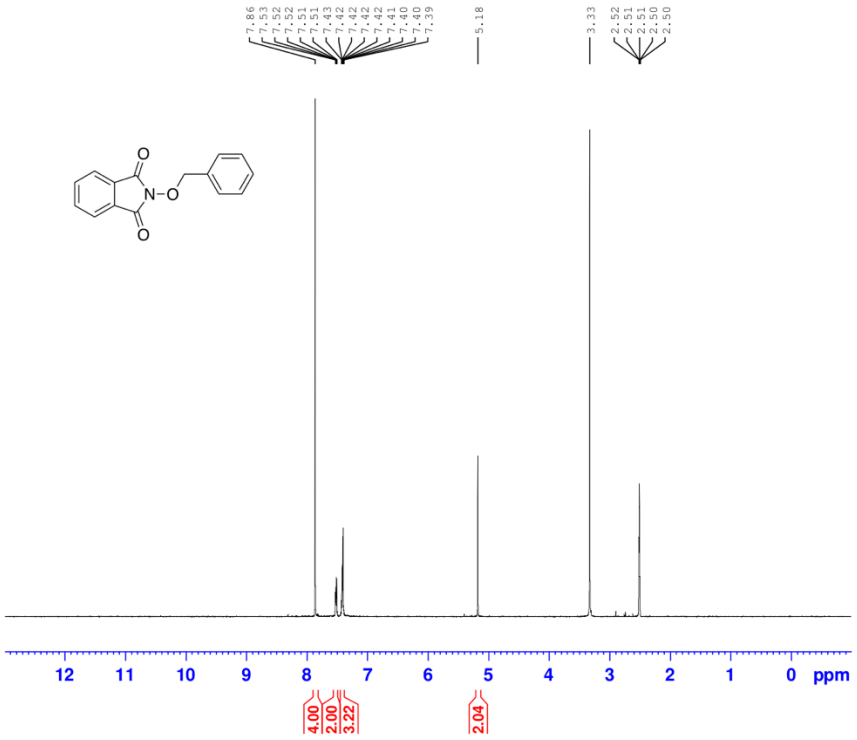

*Figure 51 – Compound (**11**) ^{1}H-NMR obtained using 400 MHz Bruker NMR spectrometer in d_6-DMSO*

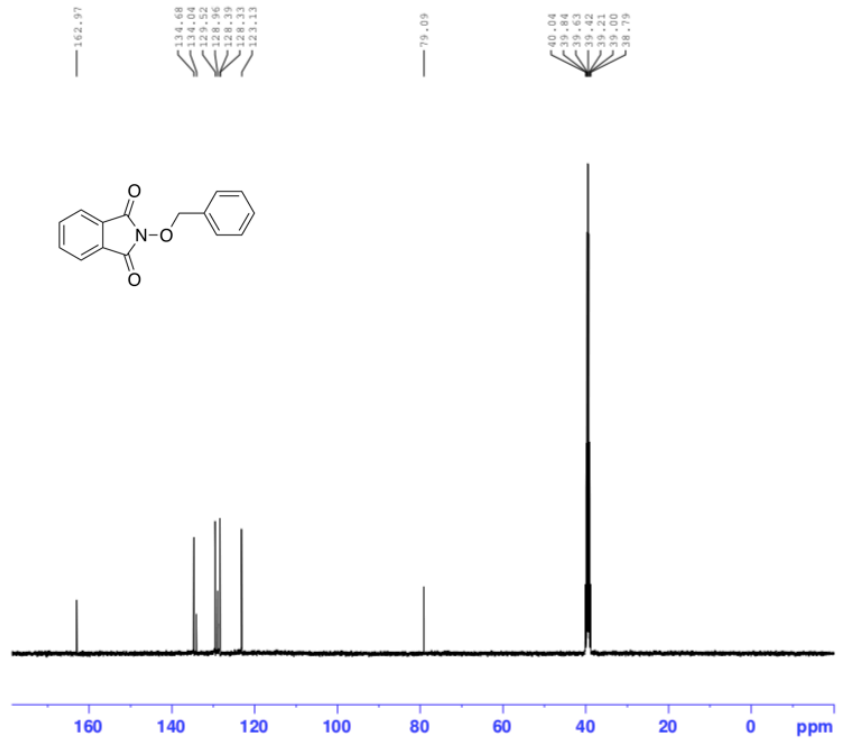

*Figure 52 – Compound (**11**) ^{13}C-NMR obtained using 400 MHz Bruker NMR spectrometer in d_6-DMSO*

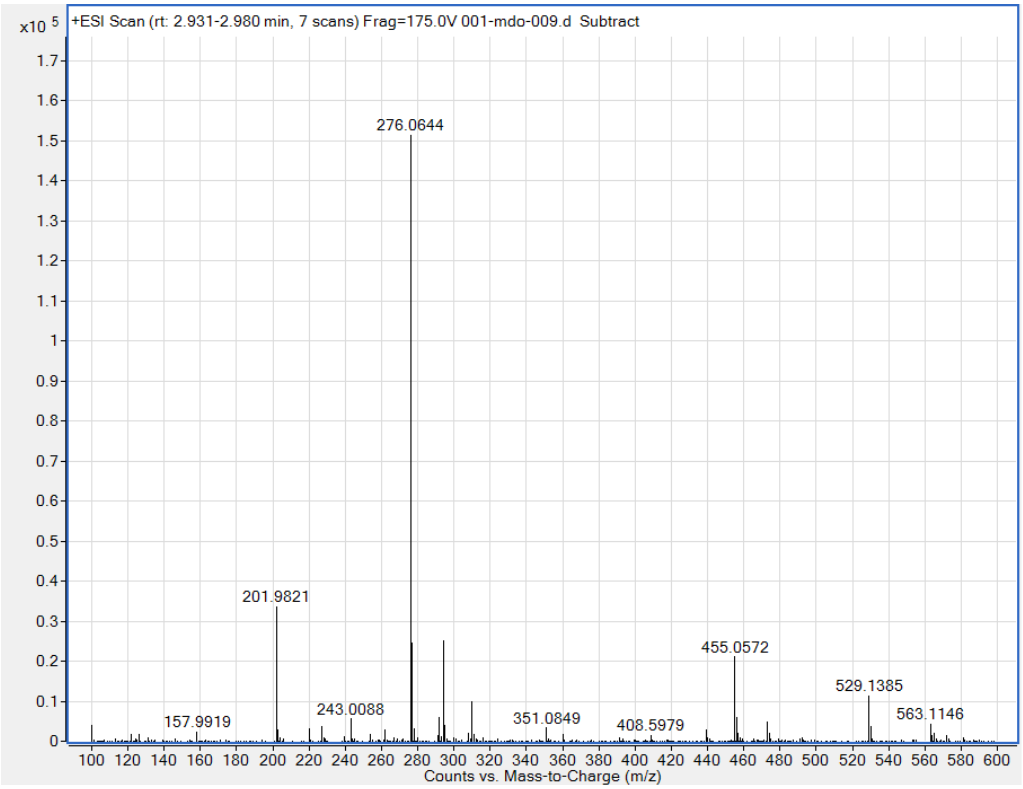

*Figure 53 – Compound (**11**) - HRMS - Positive mode. (Calcd. $C_{15}H_{11}NO_3$: 253.0739) $[M+Na]^+$ 276.0644*

(13): ^{1}H-NMR, ^{13}C-NMR

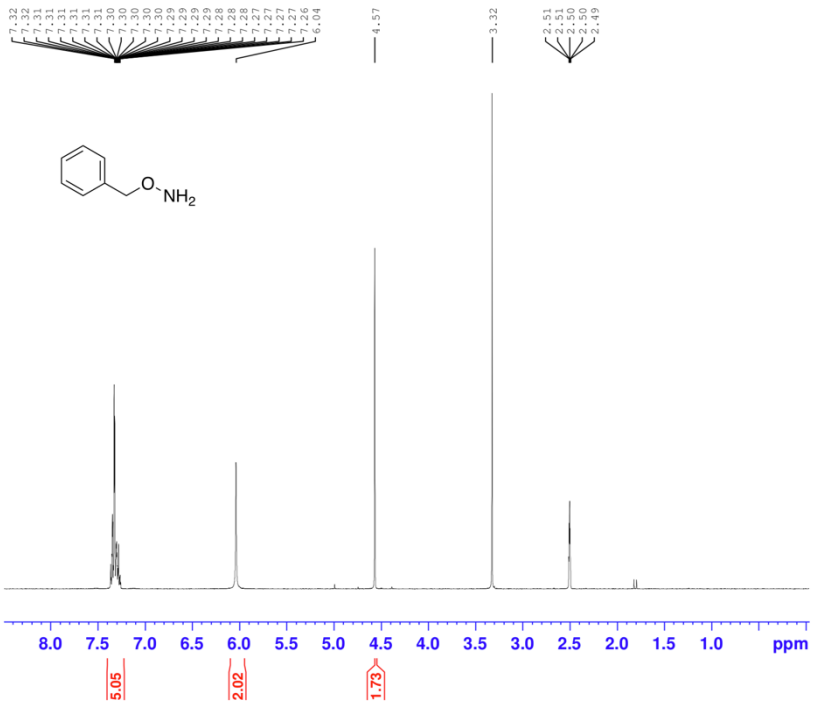

*Figure 54 – Compound (**12**) ^{1}H-NMR obtained using 400 MHz Bruker NMR spectrometer in d_6-DMSO*

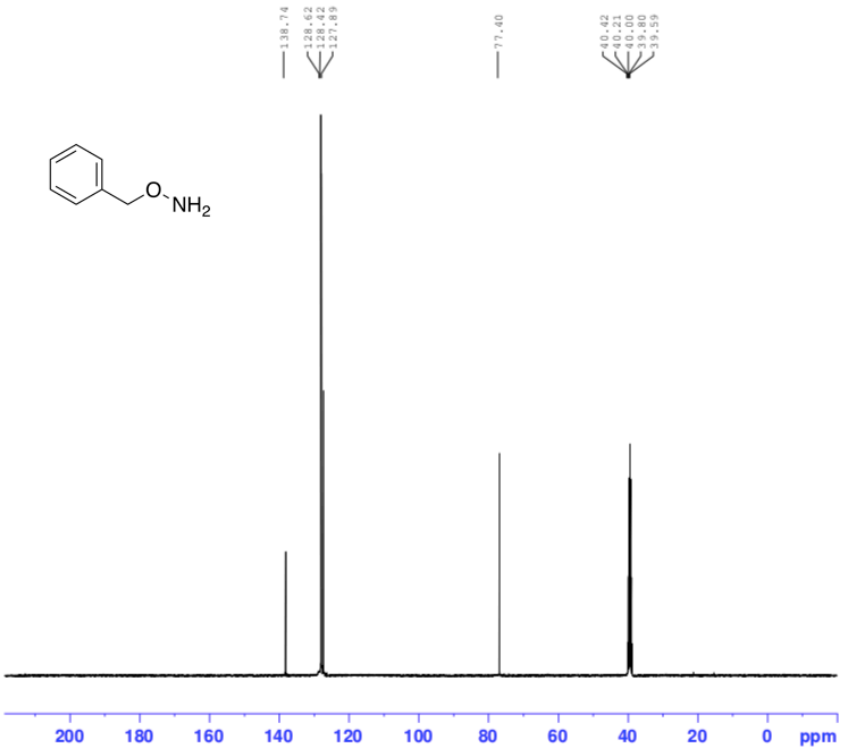

*Figure 55 – Compound (**12**) ^{13}C-NMR obtained using 400 MHz Bruker NMR spectrometer in d_6-DMSO*

(14): ^{1}H-NMR, ^{13}C-NMR, HRMS

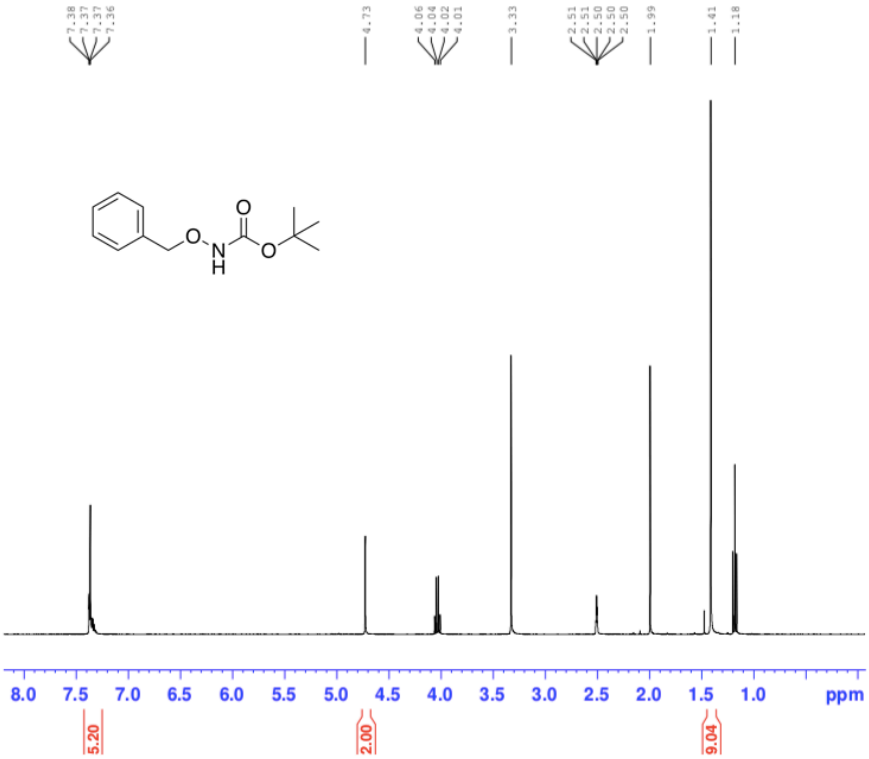

*Figure 56 – Compound (**13**) ^{1}H-NMR obtained using 400 MHz Bruker NMR spectrometer in d_6-DMSO*

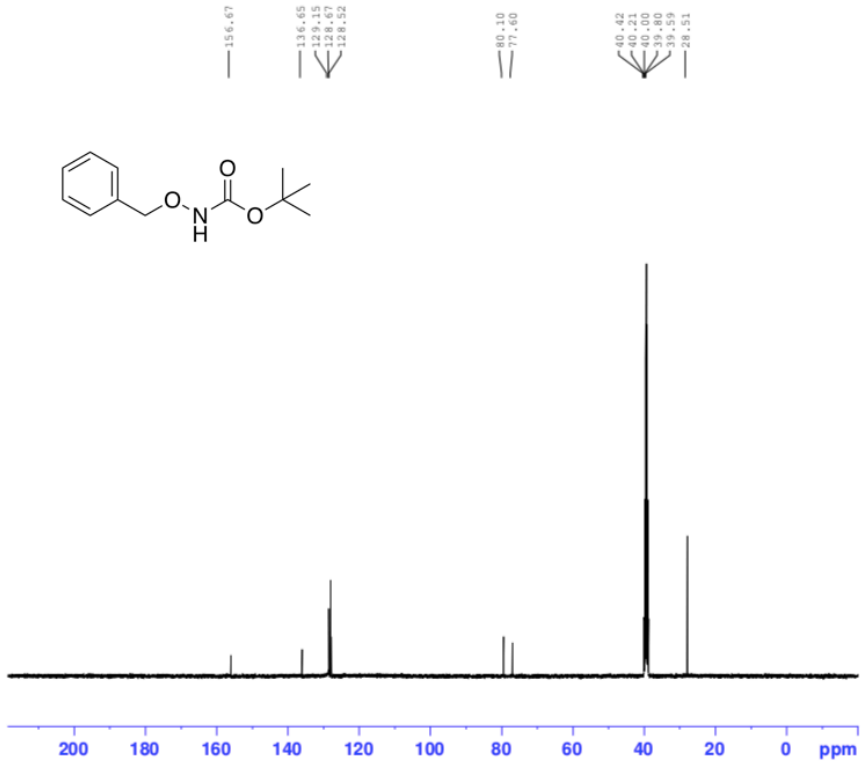

*Figure 57 – Compound (**13**) ^{13}C-NMR obtained using 400 MHz Bruker NMR spectrometer in d_6-DMSO*

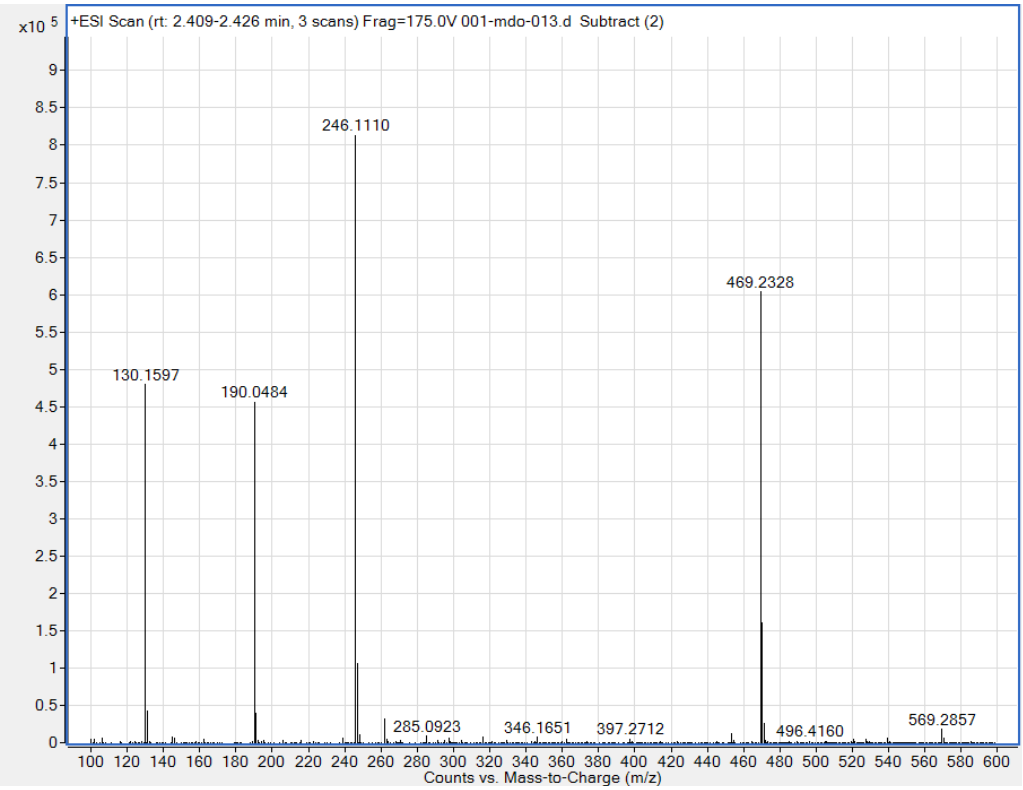

*Figure 58 – Compound (**13**) HRMS - Positive mode. (Calcd. $C_{12}H_{17}NO_3$: 223.2108) $[M+Na]^+$ 246.1110*

(15): ^{1}H-NMR, ^{13}C-NMR, HRMS

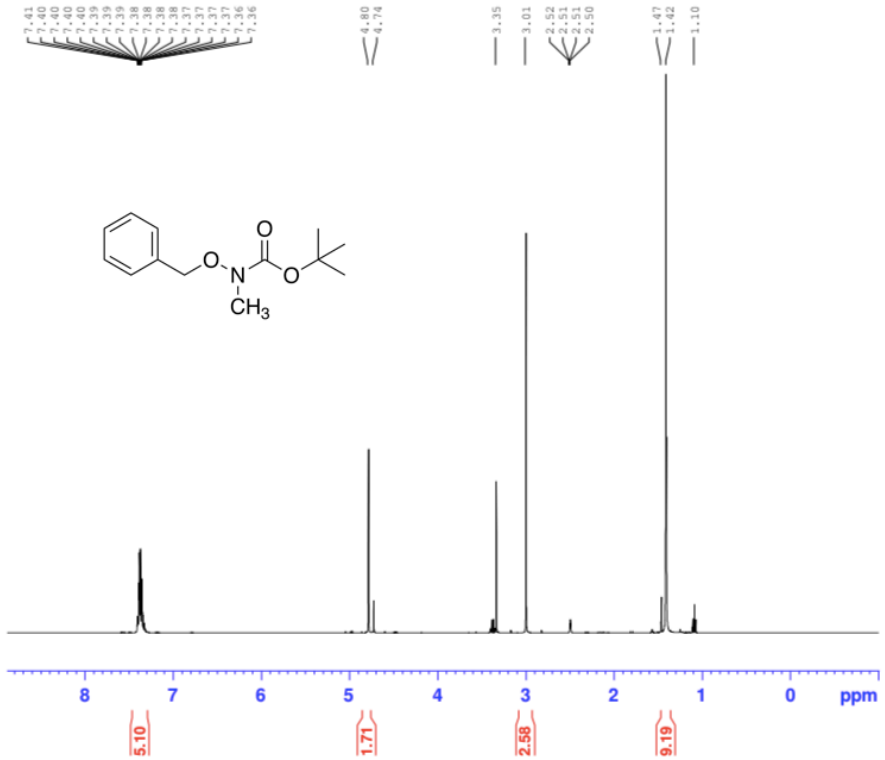

*Figure 59 – Compound (**14**) ^{1}H-NMR obtained using 400 MHz Bruker NMR spectrometer in d_6-DMSO*

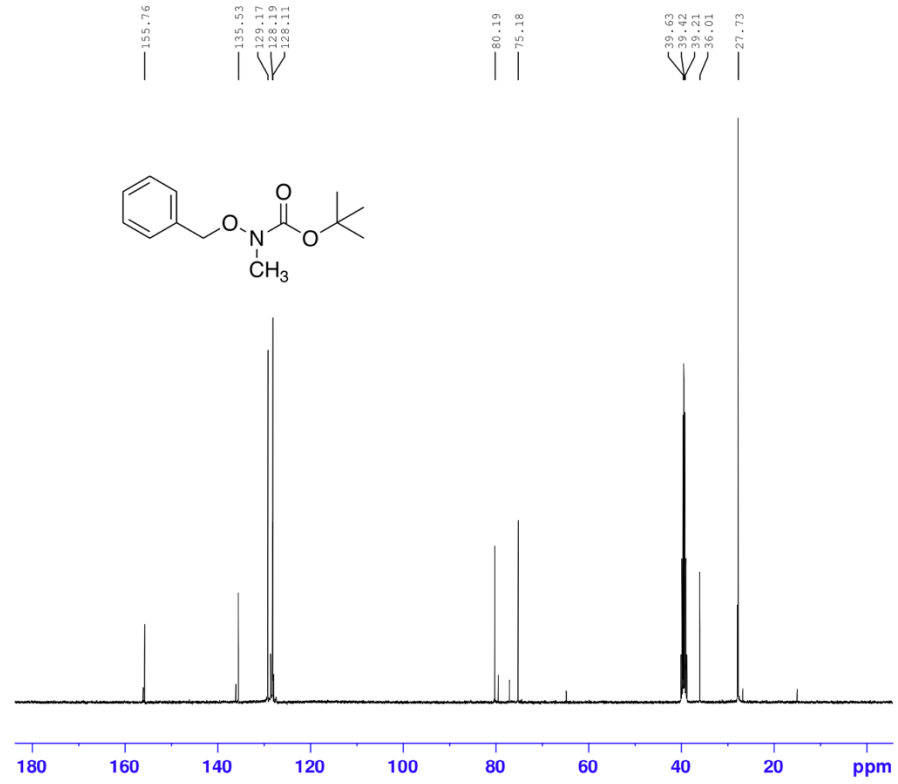

*Figure 60 – Compound (**14**) ^{13}C-NMR obtained using 400 MHz Bruker NMR spectrometer in d_6-DMSO*

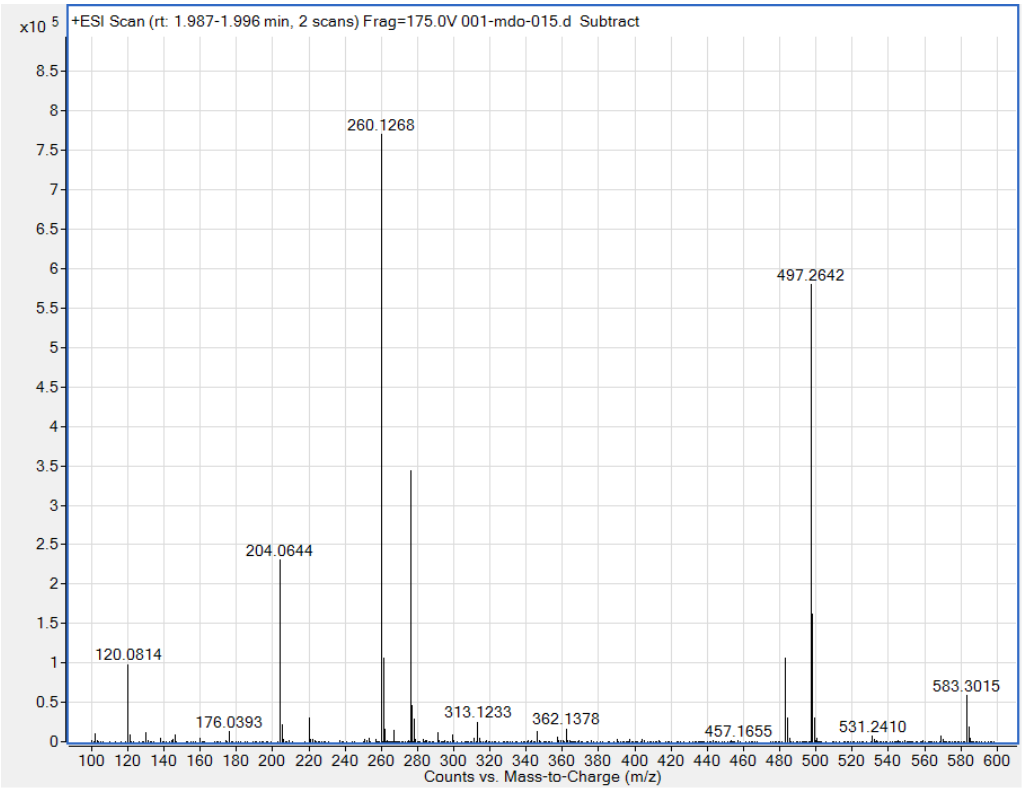

*Figure 61 – (**14**) HRMS - Positive mode. (Calcd. $C_{13}H_{19}NO_3$: 237.1365) $[M+Na]^+$ 260.1268*

(16): ^{1}H-NMR, HRMS, ^{13}C-NMR

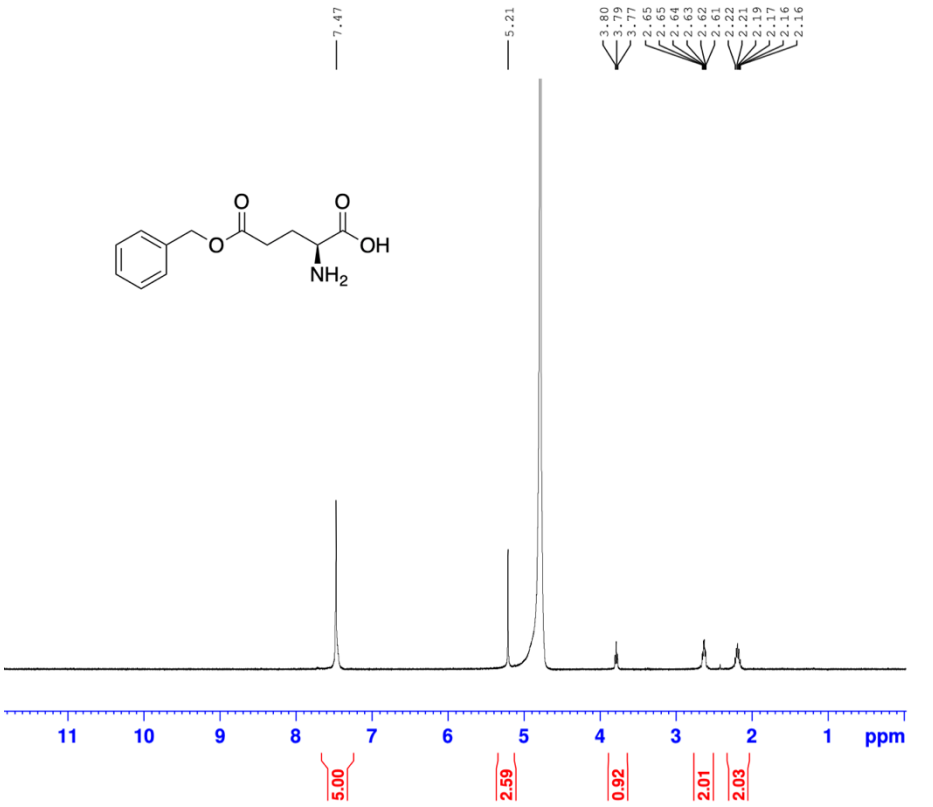

*Figure 62 – Compound (**15**) ^{1}H-NMR obtained using 400 MHz Bruker NMR spectrometer in D_2O*

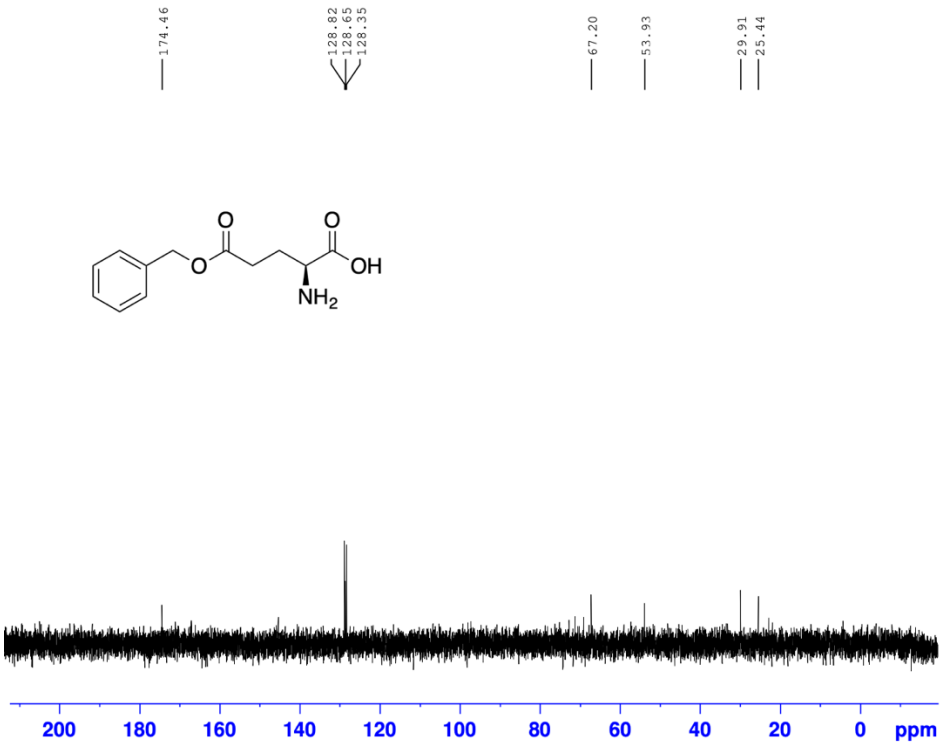

*Figure 63 – Compound (**15**) ^{13}C-NMR obtained using 400 MHz Bruker NMR spectrometer in D_2O*

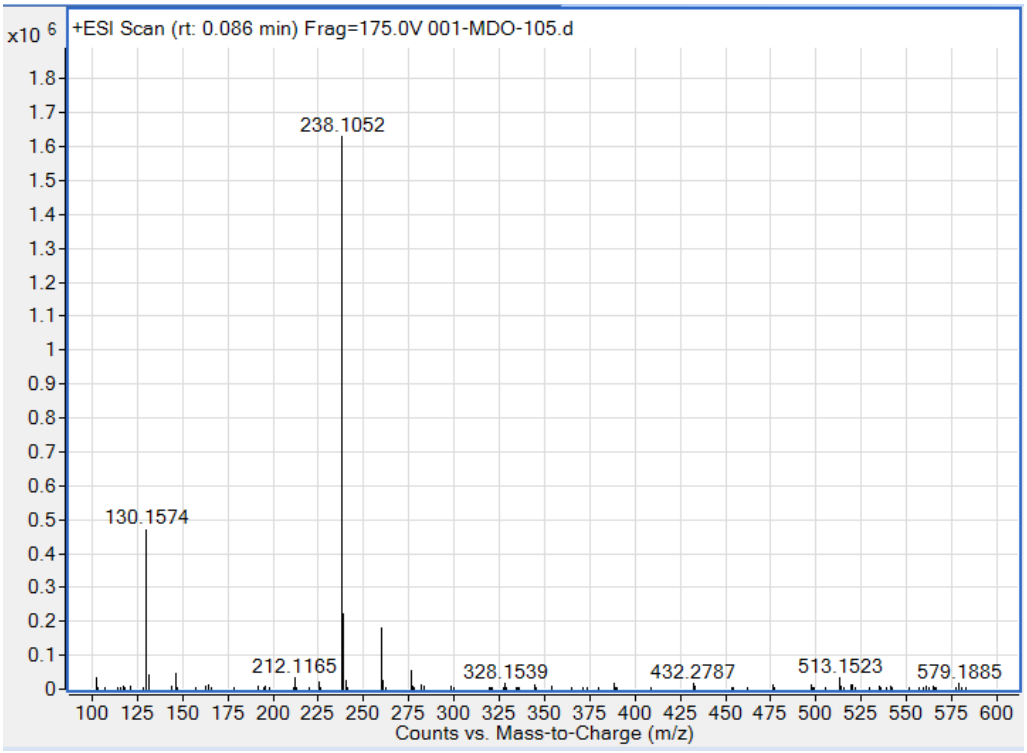

*Figure 64 – Compound (**15**) HRMS - Positive mode. (Calcd. $C_{12}H_{15}NO_4$: 237.1001) $[M+H]^+$ 238.1052*

(17): ^{1}H-NMR, ^{13}C-NMR, HRMS

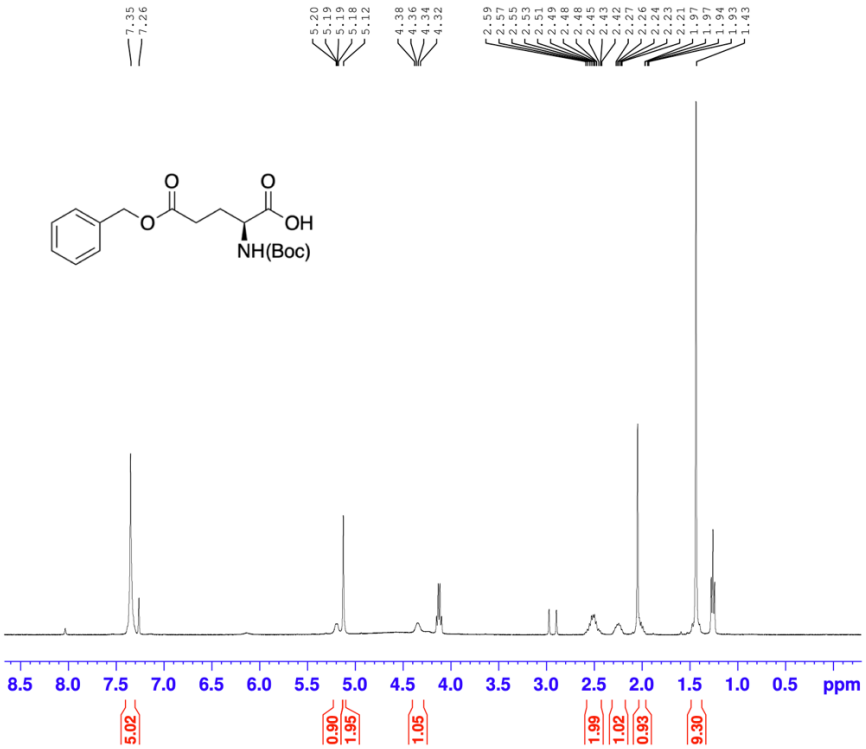

*Figure 65 – Compound (**16**) ^{1}H-NMR obtained using 400 MHz Bruker NMR spectrometer in $CDCl_3$*

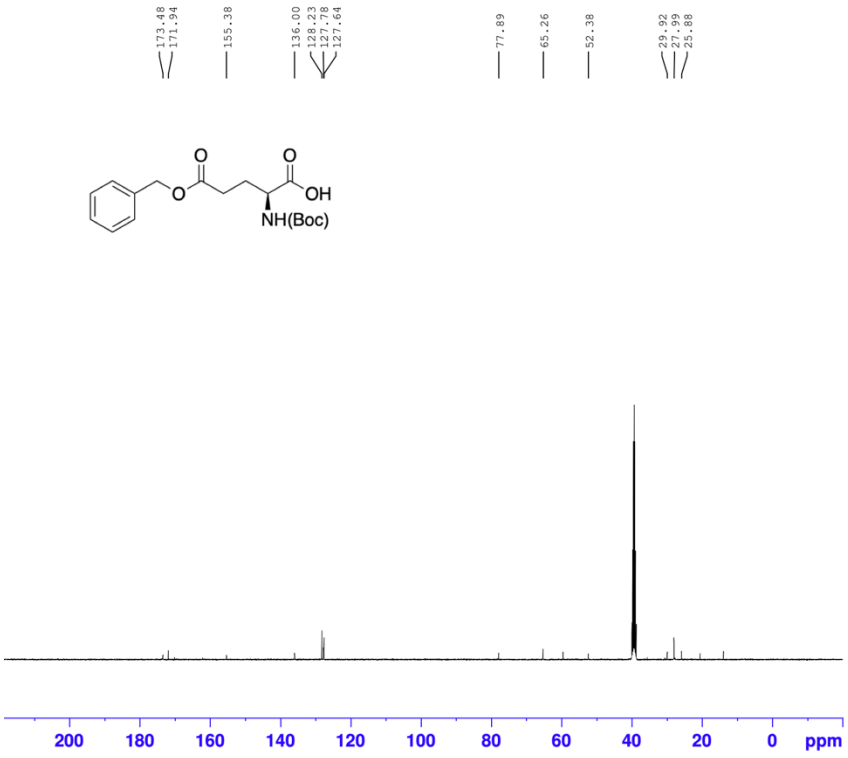

*Figure 66 – Compound (**16**) ^{13}C-NMR obtained using 400 MHz Bruker NMR spectrometer in d_6-DMSO*

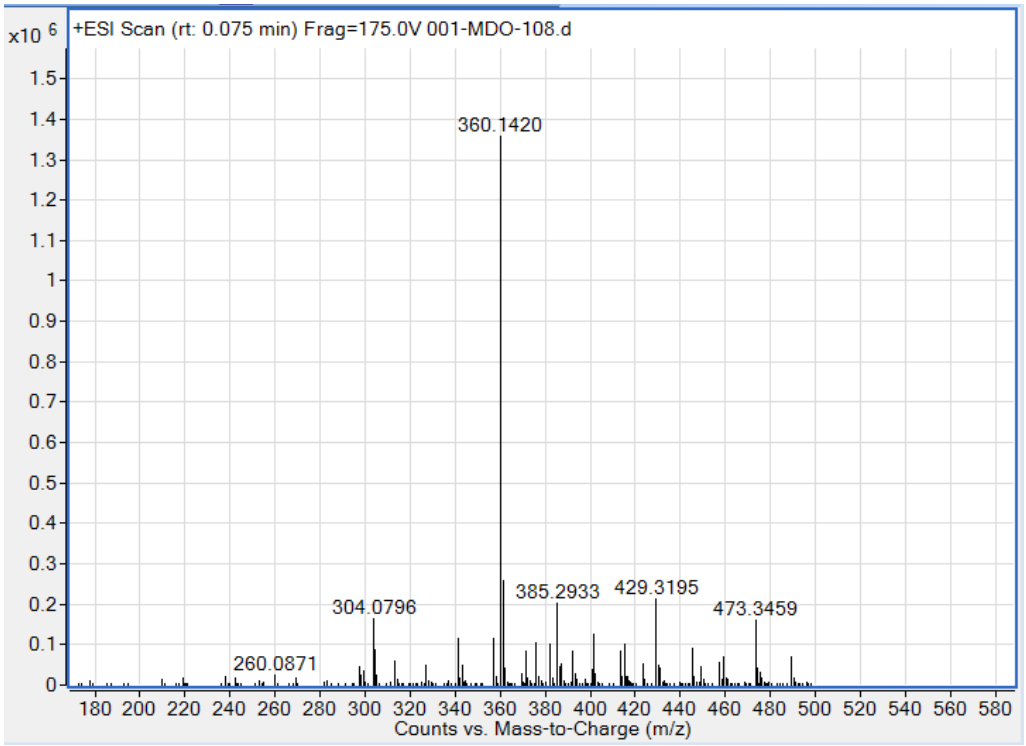

*Figure 67 – Compound (**16**) HRMS - Positive mode. (Calcd. $C_{17}H_{23}NO_6$: 337.1525) $[M+Na]^+$ 360.1420*

(18): ^{1}H-NMR, ^{13}C-NMR, HRMS

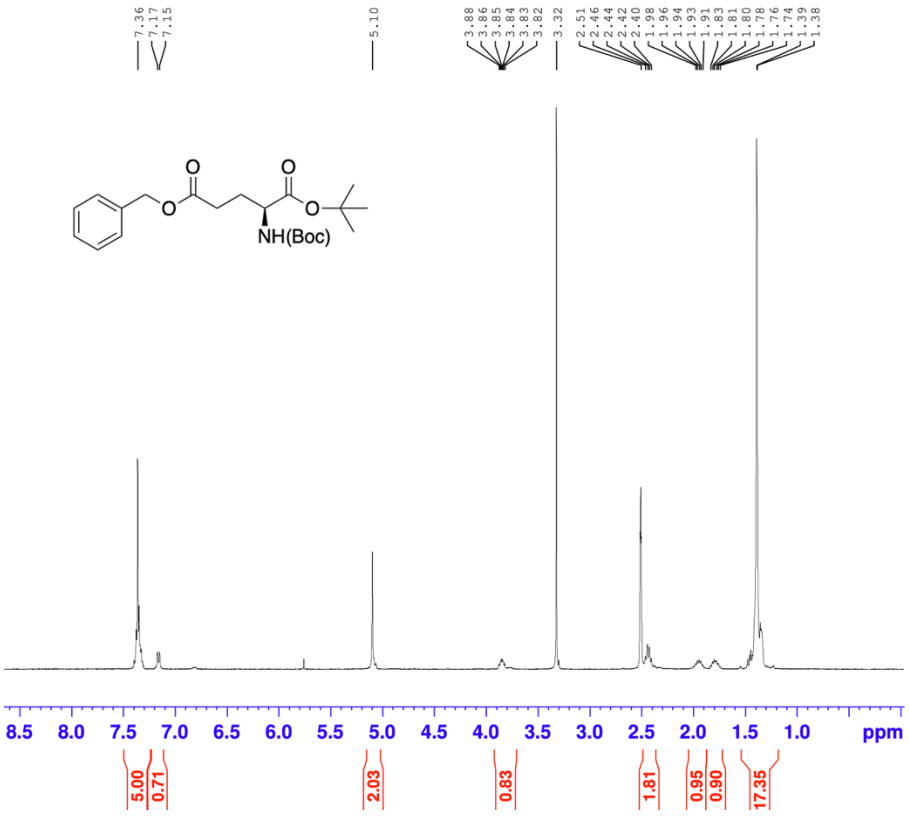

*Figure 68 – Compound (**17**) ^{1}H-NMR obtained using 400 MHz Bruker NMR spectrometer in d_6-DMSO*

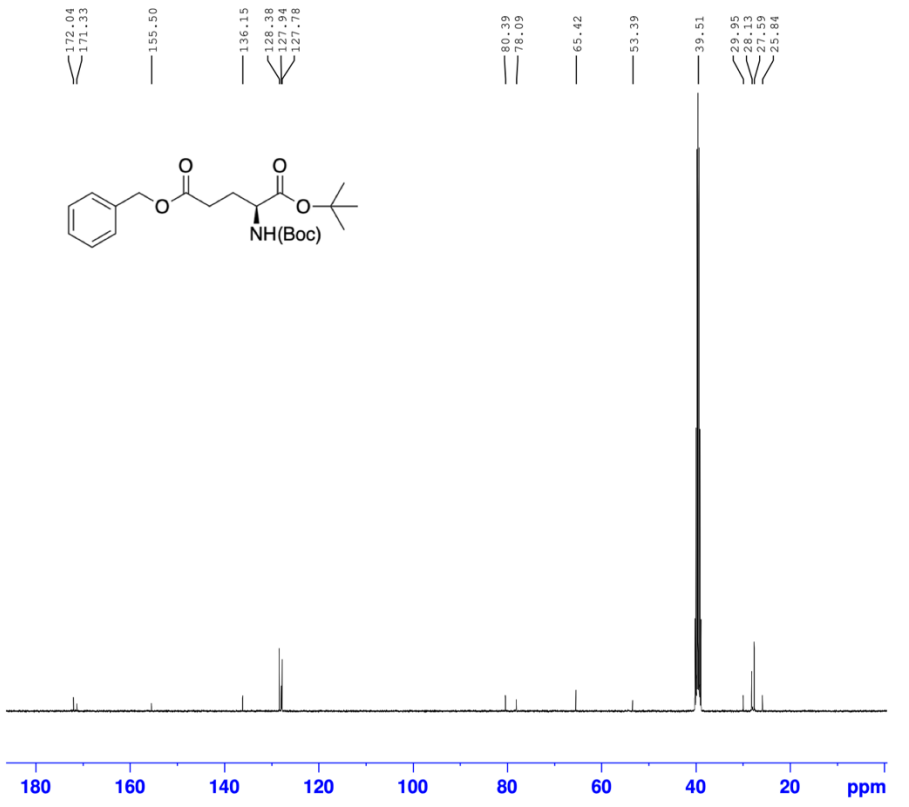

*Figure 69 – Compound (**17**) ^{13}C-NMR obtained using 400 MHz Bruker NMR spectrometer in d_6-DMSO*

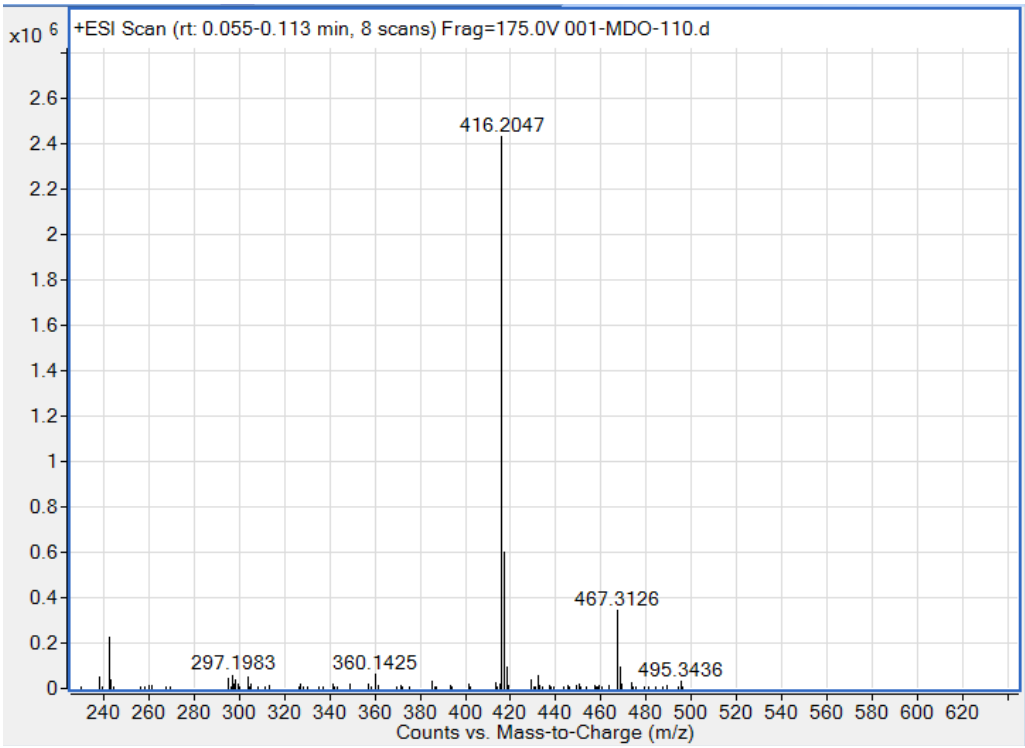

*Figure 70 – (**17**) HRMS - Positive mode (Calcd. $C_{21}H_{31}NO_6$: 393.2151) $[M+Na]^+$ 416.2047 $[M+K]^+$ 467.3126*

(19): ^{1}H-NMR, ^{13}C-NMR, HRMS

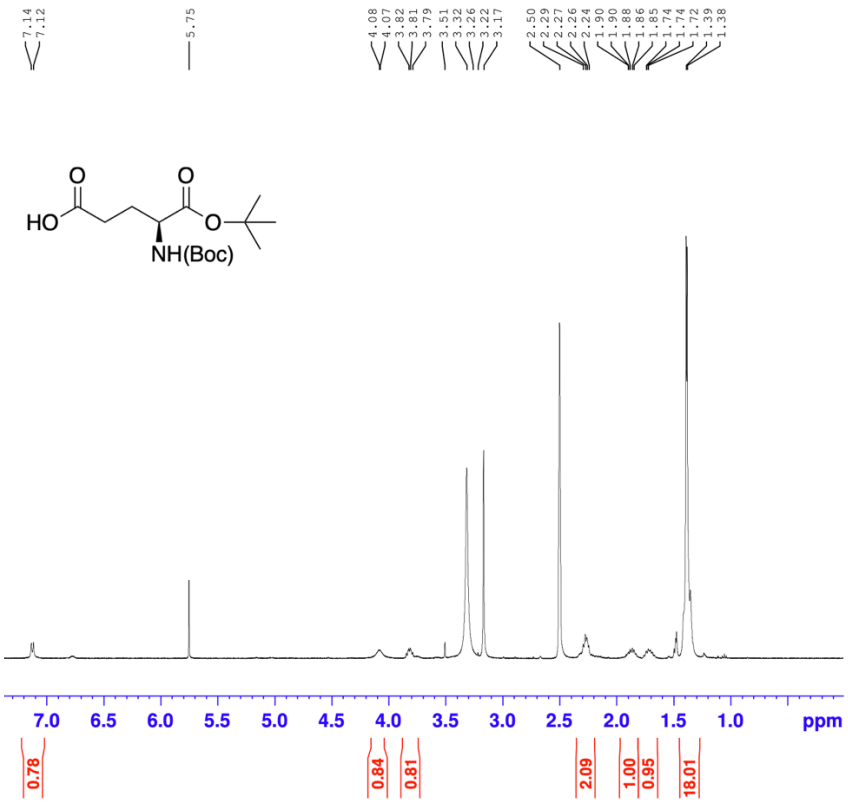

*Figure 71 – Compound (**18**) ^{1}H-NMR obtained using 400 MHz Bruker NMR spectrometer in d_6-DMSO*

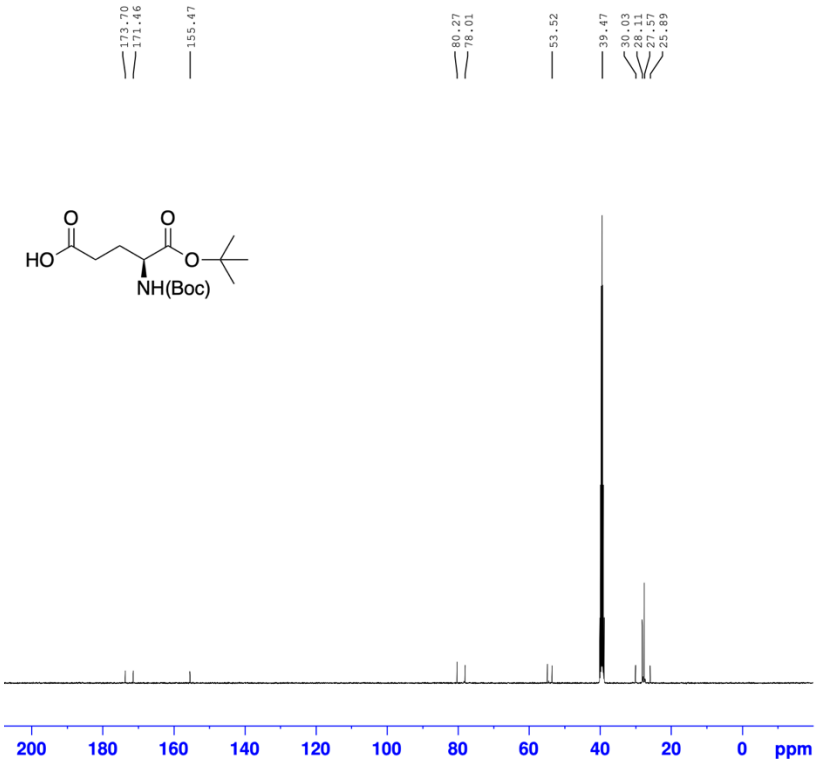

*Figure 72 – Compound (**18**) ^{13}C-NMR obtained using 400 MHz Bruker NMR spectrometer in d_6-DMSO*

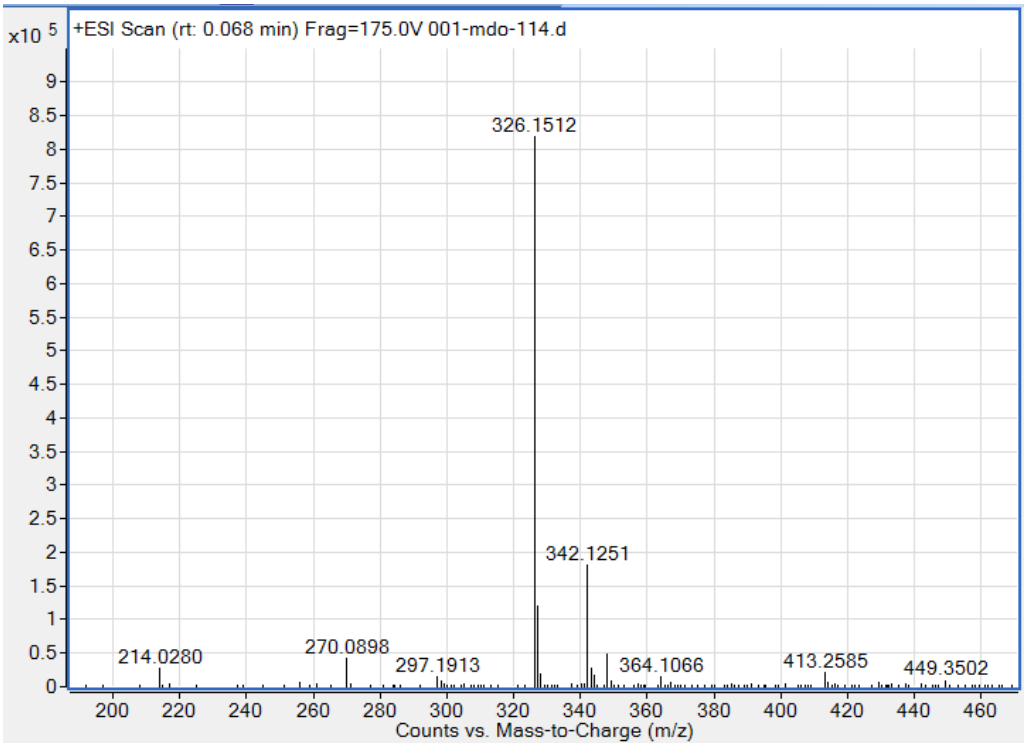

*Figure 73 – (**18**) HRMS - Positive mode (Calcd. $C_{14}H_{25}NO_6$: 303.1682) $[M+Na]^+$ 326.1512 $[M+K]^+$ 342.1251*

(20): ^{1}H-NMR, ^{13}C-NMR, HRMS

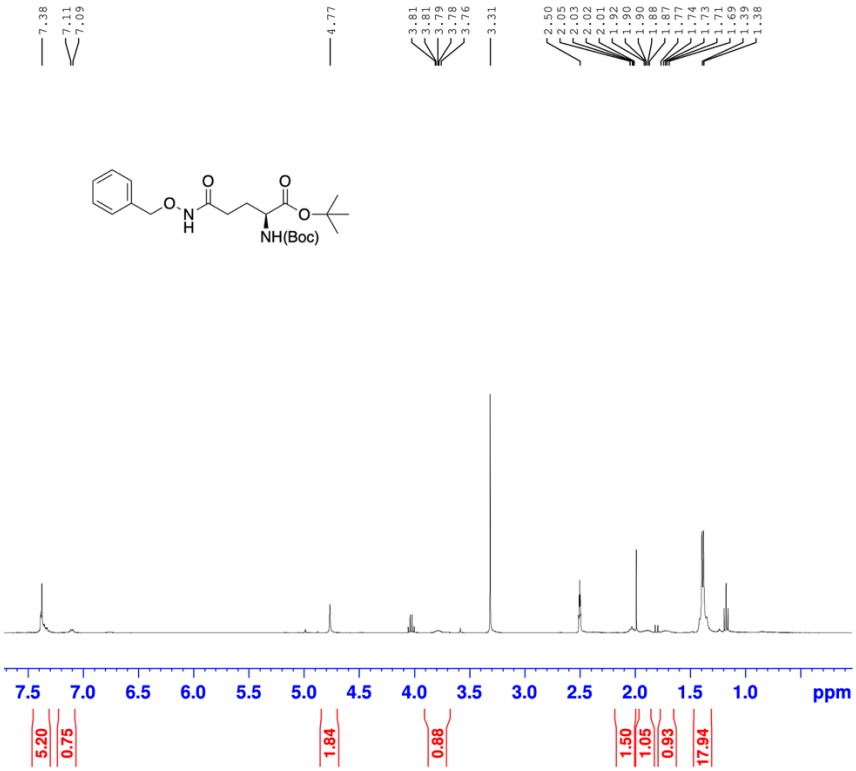

*Figure 74 – Compound (**19**) ^{1}H-NMR obtained using 400 MHz Bruker NMR spectrometer in d_6-DMSO*

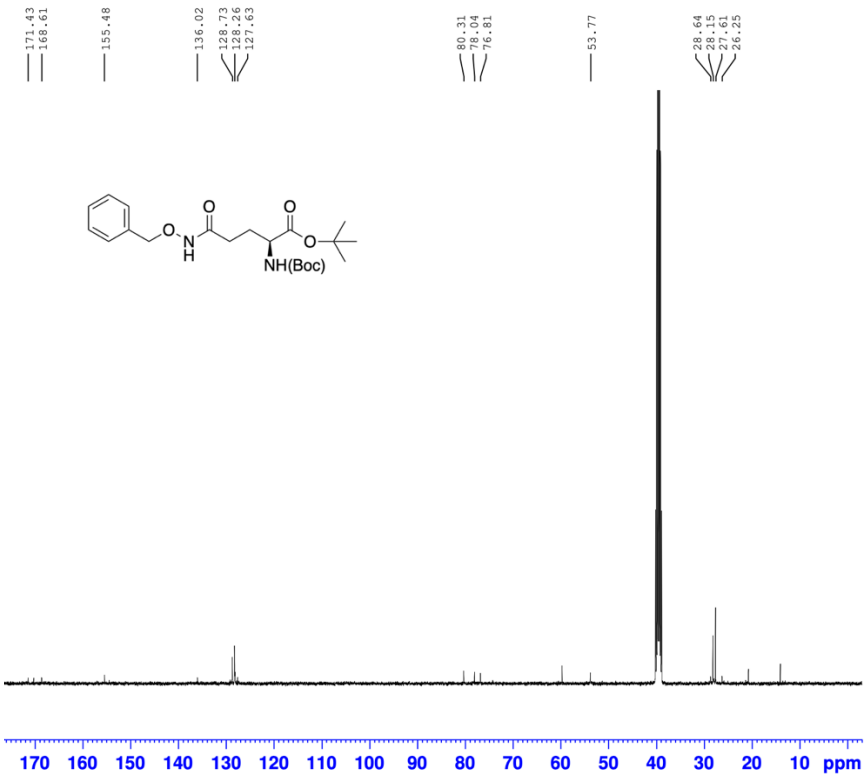

*Figure 75 – Compound (**19**) ^{13}C-NMR obtained using 400 MHz Bruker NMR spectrometer in d_6-DMSO*

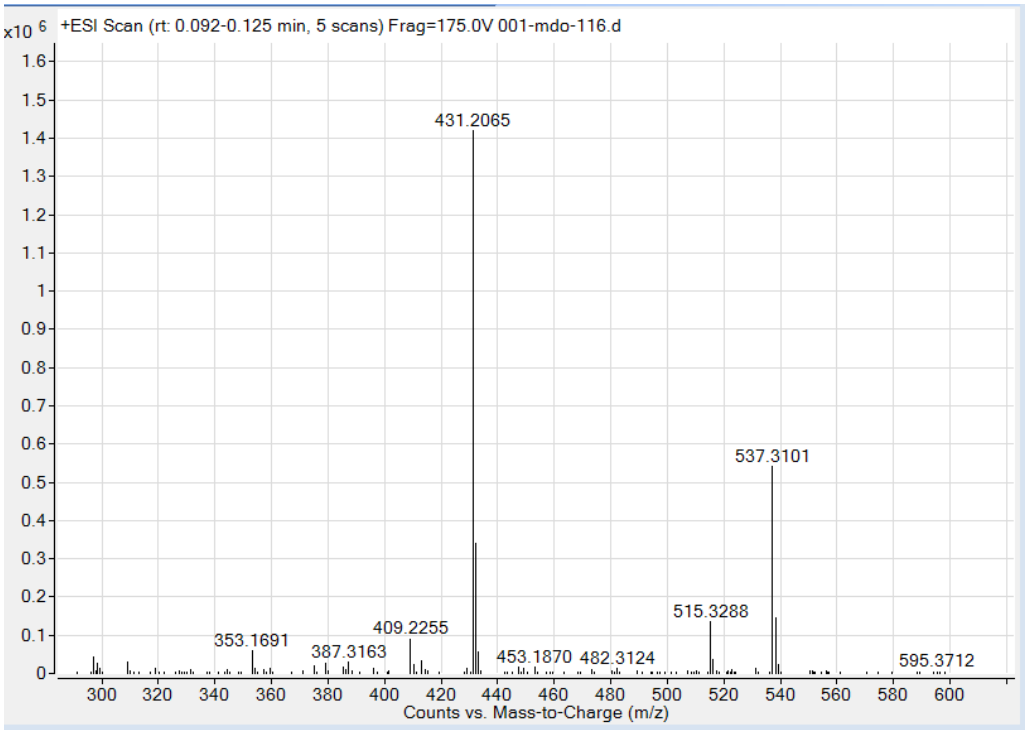

*Figure 76 – (**19**) HRMS - Positive mode (Calcd. $C_{21}H_{32}N_2O_6$: 408.2260) $[M+Na]^+$ 431.2065*

(21): ^{1}H-NMR, ^{13}C-NMR, HRMS

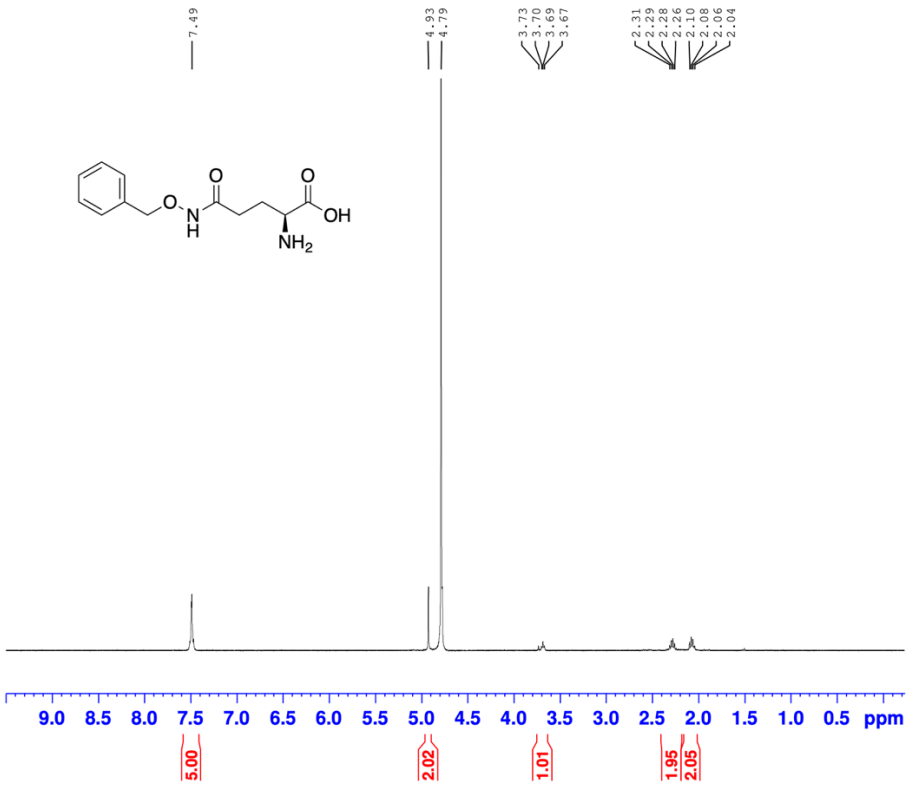

*Figure 77 – Compound (**20**) ^{1}H-NMR obtained using 400 MHz Bruker NMR spectrometer in D_2O*

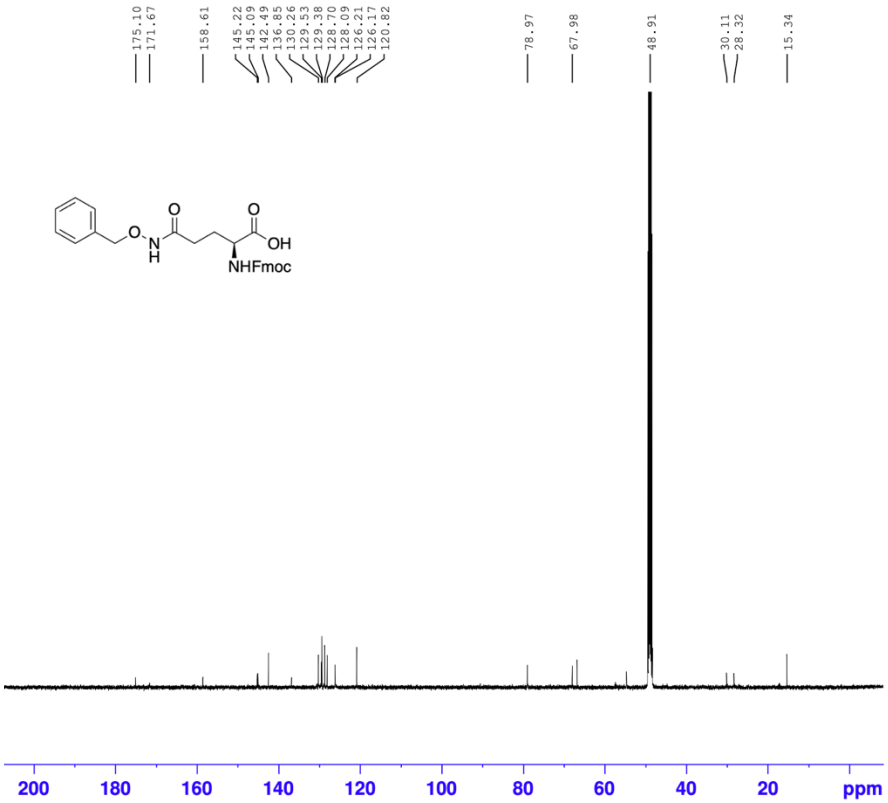

*Figure 78 – Compound (**20**) ^{13}C-NMR obtained using 500 MHz Bruker NMR spectrometer in CD_3OD*

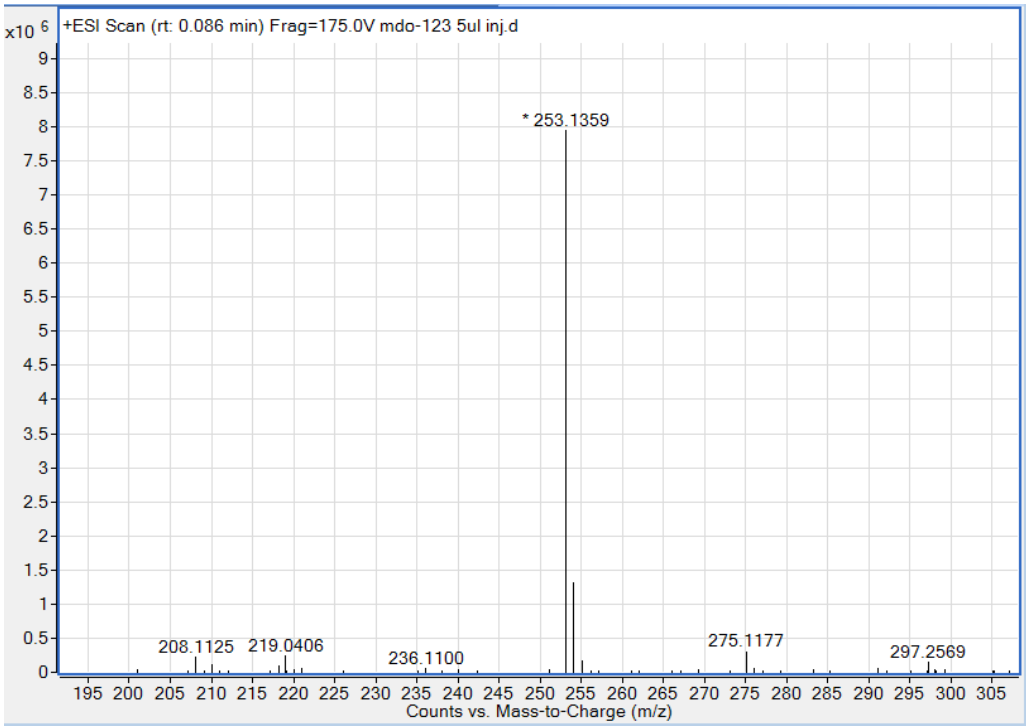

*Figure 79 – (**19**) HRMS - Positive mode (Calcd. $C_{12}H_{16}N_2O_4$: 252.1110) $[M+H]^+$ 253.1359*

(22): ^{1}H-NMR, ^{13}C-NMR, HRMS

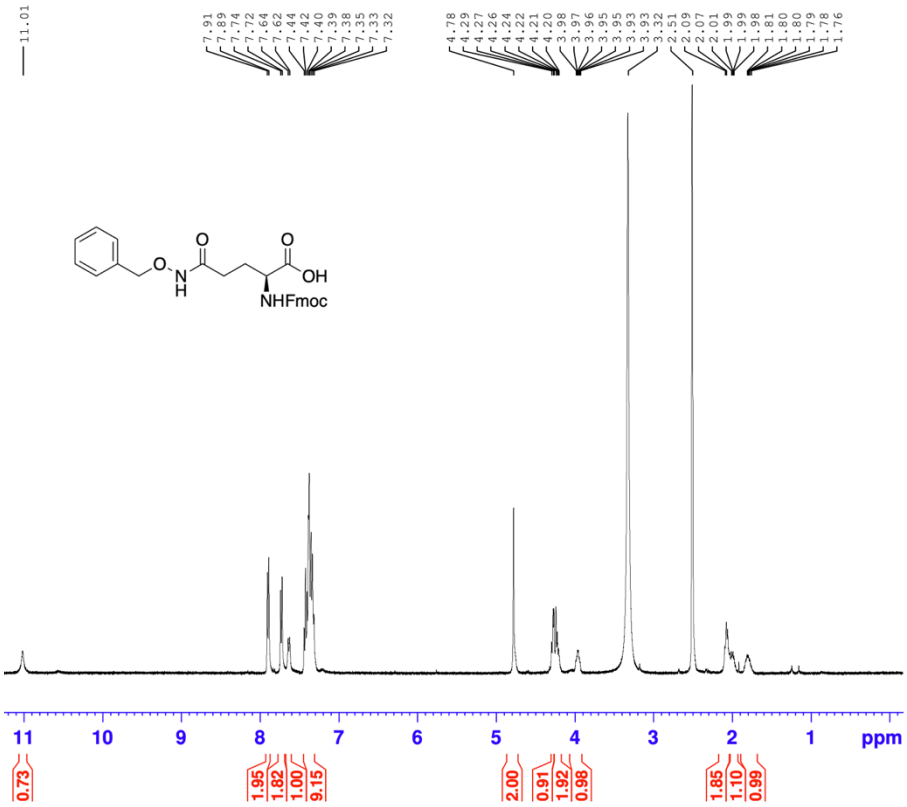

*Figure 80 – Compound (**21**) ^{1}H-NMR obtained using 400 MHz Bruker NMR spectrometer in CD_3OD*

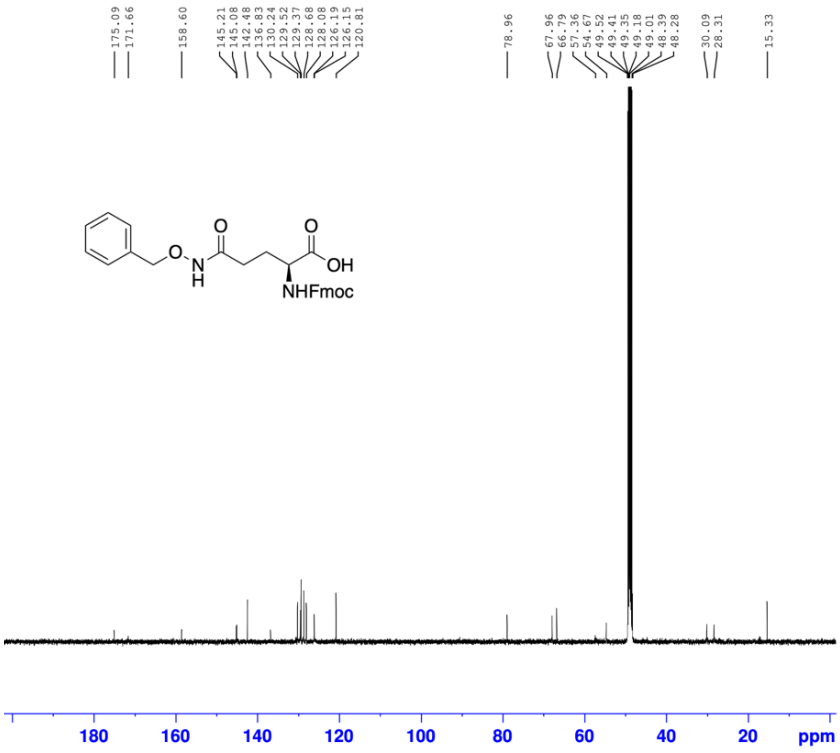

*Figure 81 – Compound (**21**) ^{13}C-NMR obtained using 400 MHz Bruker NMR spectrometer in CD_3OD*

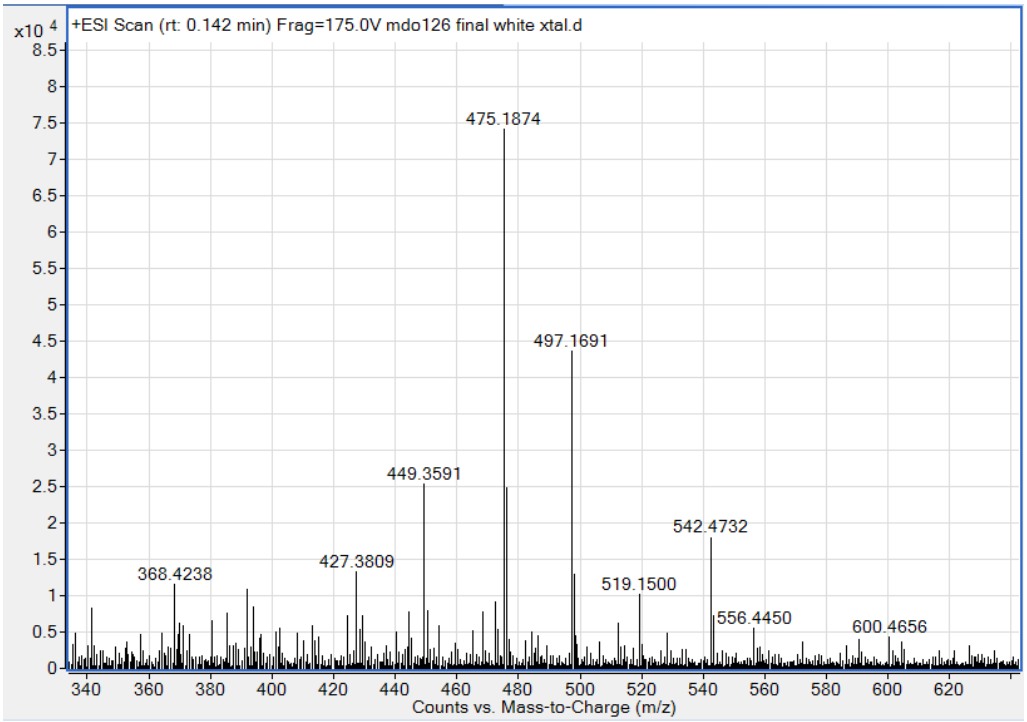

*Figure 82 – (**21**) HRMS - Positive mode (Calcd. $C_{27}H_{26}N_2O_6$: 474.1790) $[M+H]^+$ 475.1874 $[M+Na]^+$ 497.1691*